NONLINEAR ADAPTIVE CONTROLLER DESIGN FOR AIR-BREATHING HYPERSONIC VEHICLES

DISSERTATION

Presented in Partial Fulfillment of the Requirements for the Degree Doctor of Philosophy in the Graduate School of the Ohio State University

By

Lisa Fiorentini, M.S.

Graduate Program in Electrical and Computer Engineering

The Ohio State University

2010

Dissertation Committee:

Prof. Andrea Serrani, Advisor

Prof. Stephen Yurkovich

Prof. Kevin M. Passino

ABSTRACT

Air-breathing hypersonic vehicles represent such a reliable and cost-effective technology for access to space, that in the past few years a considerable effort has been made by the US Air Force and NASA to further their development and design. Notwithstanding the recent success of NASA's X-43A experimental vehicle, the design of robust guidance and control systems for hypersonic vehicles is still an open problem, due to the peculiarity of the vehicle dynamics. This dissertation presents the design of two nonlinear robust controllers for an air-breathing hypersonic vehicle model capable of providing stable tracking of velocity and altitude (or flight-path angle) reference trajectories. To overcome the analytical intractability of a dynamical model derived from first principles, a simplified control-oriented model is used for control design. The control-oriented model retains the most important features of the model from which it was derived, including the non-minimum phase characteristic of the flight-path angle dynamics and strong couplings between the engine and flight dynamics.

The first control design considers as control inputs the fuel equivalence ratio and the elevator and canard deflections. A combination of nonlinear sequential loop-closure and adaptive dynamic inversion has been adopted for the design of a dynamic state-feedback controller. An important contribution given by this work is the complete characterization of the internal dynamics of the model has been derived for Lyapunov-based stability analysis of the closed-loop system, which includes the structural dynamics. The results obtained address the issue of stability robustness

with respect to both parametric model uncertainty, which naturally arises in adopting reduced-complexity models for control design, and dynamic perturbations due to the flexible dynamics.

In the second control design a first step has been taken in extending those results in the case in which only two control inputs are available, namely the fuel equivalence ratio and the elevator deflection. The extension of these results to this new framework is not trivial since several issues arise. First of all, the vehicle dynamics are characterized by exponentially unstable zero-dynamics when longitudinal velocity and flight-path angle are selected as regulated output. This non-minimum phase behavior arises as a consequence of elevator-to-lift coupling. In the previous design the canard was strategically used to adaptively decouple lift from elevator command, thus rendering the system minimum phase. Moreover, the canard input was also employed to enforce the equilibrium at the desired trim condition and to provide a supplementary stabilizing action. As a result, when this control input is not assumed to be available, the fact that the system needs to be augmented with an integrator (to reconstruct the desired equilibrium) and the non-minimum phase behavior have a strong impact on the control design. In these preliminary results the flexible effects are not taken into account in the stability analysis but are considered as a perturbation and included in the simulation model. The approach considered utilizes a combination of adaptive and robust design methods based on both classical and recently developed nonlinear design tools. As a result, the issue of robustness with respect to parameter uncertainties is addressed also in this control design.

Simulation results on the full nonlinear model show the effectiveness of both controllers.

For Maria Rosa and Loris.

ACKNOWLEDGMENTS

First of all I want to thank my parents, who have always supported my choices, being really understanding even when these choices brought me 6000 miles away from them. Their constant encouragement means really a lot to me and even though we are apart, feeling them always so close, give me the strength to go through every bad moment and makes me enjoy thoroughly every little success. Thank you.

Then I want to thank my adviser, Prof. Andrea Serrani, for several reasons: for being an irreplaceable and invaluable guide in my research topic; for being such a great teacher, so competent in many different areas; for showing interest in my personal growth, suggesting me readings, courses to take and encouraging me to do my best; for teaching me so many things and being able to provide me always different and new insights of theoretical concepts; for being patient every time I do not understand something or I do something not the way it was supposed to be done; for being so enthusiast of the things we do even though it has been a long day or a tough week; for being understanding, available and very friendly. Thanks.

I also want to thank all the members of the hypersonics research group (Prof. Yurkovich, the team at Wright Patterson Air Force Base – Dave, Mike and Mike –, David, Mohammad and Alicia) and the Professors of the ECE Department who really helped me a lot during all these years. Thanks.

VITA

1979	Born - Lugo (RA), Italy
1998-2003	B.S.- M.S. Electrical Engineering, Universita' Politecnica delle Marche Ancona, Italy
2004-2005	Analyst - Accenture Rome Office, Italy
2005-2007	Master of Science Electrical and Computer Engineering The Ohio State University
2007-2009	Graduate Research Assistant Graduate Teaching Assistant The Ohio State University
2009-Present	Presidential Fellowship The Ohio State University

FIELDS OF STUDY

Major Field: Electrical & Computer Engineering

TABLE OF CONTENTS

LIST OF FIGURES

LIST OF TABLES

NOMENCLATURE

CDM1	=	control-design model, controller with full control authority
CDM2	=	control-design model, controller with reduced control authority
SM	=	simulation model
FPA	=	flight-path angle
$\bar{c}$	=	mean aerodynamic chord
D	=	drag
g	=	acceleration due to gravity
h	=	altitude
h_0	=	nominal altitude
h_r	=	altitude reference trajectory
h_s	=	inverse of the air density approximation exponential decay rate
I_{yy}	=	moment of inertia
L	=	lift
M	=	pitching moment
m	=	vehicle mass

m_0 = vehicle nominal mass

$\tilde{m}$ = multiplicative uncertainty of the vehicle mass $m = \tilde{m}(t) \cdot m_0$

N_i = ith generalized force

$\mathcal{P}$ = vector of all uncertain parameters that enter the COM

$\mathcal{P}$ = vector of all uncertain parameters that enter the COM

$\mathcal{P}_i$ = ith element of $\mathcal{P}$

$\mathcal{P}^0$ = nominal value of $\mathcal{P}$

$\mathcal{P}_i^0$ = ith element of $\mathcal{P}^0$

Q = pitch rate

$\bar{q}$ = dynamic pressure

S = reference area

T = thrust

V = velocity

V_r = velocity reference trajectory

z_T = thrust-to-moment coupling coefficient

x = state of the control oriented model

x^* = state trim condition

α = angle of attack

α_d = desired reference trajectory for α

γ = flight path angle

δ_c	=	canard angular deflection
δ_e	=	elevator angular deflection
η_i	=	ith generalized elastic coordinate
$\dot{\eta}_i$	=	time derivative of η_i
θ	=	pitch angle
ϑ_i	=	vectors of unknown parameters
Ξ_0	=	compact set of admissible initial conditions for x
$\Xi_{\mathcal{P}}$	=	compact set in which $\mathcal{P}$ is assumed to range
ρ	=	air density
Φ	=	stoichiometrically normalized fuel to air ratio
ω_i	=	natural frequency for elastic mode η_i
ζ_i	=	damping ratio for elastic mode η_i
$\dot{\bullet}$	=	time derivative
$\tilde{\bullet}$	=	error
$\|\bullet\|$	=	Euclidean norm
$\mathbb{P}_X(\mathcal{S})$	=	projection of the set $\mathcal{S}$ onto the subspace X

CHAPTER 1

INTRODUCTION

Air-breathing hypersonic vehicles are intended to be a reliable and cost-effective technology for access to space. In the past few years, a considerable effort has been made by the US Air Force and NASA to further their development and design. Notwithstanding the recent success of NASA's X-43A experimental vehicle, the design of robust guidance and control systems for hypersonic vehicles is still an open problem, due to the peculiarity of the vehicle dynamics. The slender geometries and light structural weights required for these aircraft cause significant flexible effects, and a strong coupling between propulsive and aerodynamic forces results from the integration of the scramjet engine. In addition, because of the variability of the vehicle characteristics with flight conditions (for example, thermal effects on the structure), significant uncertainties affect the vehicle model [4, 5, 2]. A thorough survey of difficulties encountered in modeling and control of hypersonic vehicles, with a focus on aero-thermo-elasticity, is given in McNamara and Friedmann[24].

For the design of guidance and control systems for hypersonic vehicles based on linearized dynamical models, several results are available in the literature, which consider control solutions of various complexity. The pivotal early work of Schmidt et al.[30, 31, 7] employed classic and multivariable linear control for the longitudinal model of the vehicle dynamics developed in Chavez and Schmidt[4, 5]. Active

structural damping based on Kalman filtering was proposed in Heeg el al.[14]. Subsequent research efforts have considered, for generic vehicle models, the application of $\mathcal{H}_\infty$ and μ-synthesis methods[3], gain-scheduling and linear parameter-varying (LPV) control[21, 20], and model reference adaptive control[27]. Implicit model-following control methods have been considered in Refs. [13, 12, 33] for linearized versions of the first-principles model developed by Bolender and Doman[2], and adaptive control techniques have been considered in Kuipers et al.[18] for the CFD-based model of Mirmirani et al.[26]. Finally, some aspects of the control systems design for NASA's Hyper-X vehicle[6, 8] are presented in Davidson et al.[7]

As far as nonlinear control design is concerned, conventional and adaptive sliding-mode control [35, 38] and robust inversion-based design [23, 36] have been proposed in the literature for simpler vehicle models than the one considered in this paper, which is based on Reference [2]. In particular, the specific plant models employed in the above-mentioned references include neither the structural dynamics, the elevator-to-lift coupling, nor the coupling between thrust and pitching moment due to the underslung location of the engine. Indeed, as discussed in Refs. [2, 1], it is the presence of these interactions that render many of the traditional design methodologies unsuitable or difficult to apply to this class of vehicle. For example, the elevator-to-lift coupling generates exponentially unstable zero-dynamics (with respect to either altitude or flight-path angle as a controlled output) which complicate the design of controllers based on dynamic inversion.

For the Bolender and Doman model, a nonlinear controller which resorts to approximate feedback linearization techniques was proposed in Parker et al. [28]. The approach pursued in that work considered the development of a simplified model for control design in which the flexible dynamics and certain dynamic couplings of

interest were strategically ignored in order for the standard assumptions for the applicability of dynamic inversion to hold. With the aid of an external control loop, the nonlinear controller was able to provide stable tracking for a sizable flight envelope, albeit without a formal proof of stability in presence of the flexible dynamics, which were regarded as dynamic perturbations. Furthermore, the fact that the controller was based on the inversion of a reduced-order model naturally prompted the issue of evaluating the robustness of the scheme with respect to parameter and dynamic model uncertainty. However, the complexity of the control law itself rendered such an assessment prohibitive from an analytical standpoint.

The two controllers presented in this dissertation are based on the assumed-modes version [37] of the model by Bolender and Doman. Similar to Parker et al.[28], simplified models derived from curve-fitted approximations of the aerodynamic and propulsive forces are used for control design.

In the first design, a nonlinear controller which employs as control inputs the fuel equivalence ratio and the elevator and canard deflections is derived to achieve robust tracking of altitude and velocity references, and regulation of the angle-of-attack to a desired set-point. The controller is based on a combination of robust adaptive dynamic inversion and sequential loop-closure (i.e., backstepping) arguments [17, 29]. Since measurements of the flexible states are not assumed to be available for feedback, the controller developed in this paper makes use of feedback from the rigid- body states only and is designed assuming a perfectly rigid body, by initially keeping the flexible dynamics "frozen" at a nominal trim condition. The stability analysis of the feedback interconnection of the controller and the overall system is then performed using the full control-design model, which does contain the flexible states.

Since the controller *does not* rely on the exact value of the model parameters, the design satisfactorily addresses the issue of robustness with respect to parameter

model uncertainties. In addition, since the proof of stability of the closed-loop system includes the flexible dynamics, robustness with respect to the considered class of dynamic uncertainty is also demonstrated. In contrast to design based on linearized models, the approach of this paper yields a guaranteed domain of attraction for given ranges of parameter variations. A comparative simulation analysis with the approximate dynamic inversion controller of Ref. [28], conducted on the original first-principles model, confirms the validity of the proposed approach.

An important contribution of this work is the complete characterization of the nonlinear internal dynamics of the Bolender and Doman model with respect to velocity, altitude and angle-of-attack as regulated output. The derivation of the internal dynamics, albeit ostensively elaborate, is an indispensable element for the Lyapunov-based stability analysis of the nonlinear closed-loop model, comprehensive with the flexible dynamics, presented in this work. The availability of this analytical tool, in particular, allows the assessment of the gain margins of the closed-loop system and gives precise guidelines for tuning the controller gains. This is a fundamental aspect of the design process, as it is shown in this paper that the admissible range for the controller gains differ dramatically from the range resulting from an analysis based exclusively on the rigid-body dynamics [35, 38, 23, 36, 9, 10].

Although beneficial for controllability, the presence of a canard is problematic for the vehicle structure, as this control surface must withstand a significant thermal stress at hypersonic speed. Therefore, it is of interest to address the case in which the elevator is the only aerodynamic surface available for controlling the vehicle attitude. All the results available in the literature that consider this setup [11, 19] are based on linearized models of air-breathing hypersonic vehicles. So, in the second part of this dissertation, we take a first step in designing a nonlinear adaptive controller for the case in which the elevator is the only aerodynamic surface available. In the following,

the first control design (where the inputs available are the fuel equivalence ratio and the elevator and canard deflections) will be referred to as "*control design with full control authority*", while the second one (where the canard deflection is removed from the control suite) will be referred to as "*control design with reduced control authority*".

Among many challenges encountered in this new framework, one of the most severe is the presence of exponentially unstable zero-dynamics when longitudinal velocity and flight-path angle are selected as regulated output. As discussed in [1], a non-minimum phase behavior arises as a consequence of elevator-to-lift coupling resulting in an instantaneous loss of lift when the elevator is deflected in response to a commanded increase in flight-path angle (FPA). The unstable zero dynamics prevent the application of inversion methods, as the application of a linearizing feedback law generates a hyperbolic saddle equilibrium in the pitch dynamics. It is worth noting that the difficulties encountered in this new setup are not limited to uncompensated non-minimum phase behavior: in the controller derived in the first section, the canard input provided a supplementary stabilizing action and was used to enforce the desired trim condition in steady-state, whereas in the new scenario integral augmentation is required to reconstruct the desired equilibrium.

Here, we present a new control strategy based on a transformation of the vehicle model into the interconnection of systems in feedback and feed-forward form that does not require exact linearization, but employs adaptive dynamic inversion. The approach is based upon a suitable redefinition of the internal dynamics of the system and makes use of a gain-dependent change of coordinates which, by enforcing a time-scale separation between the controlled variables, allows one to manage the peaking phenomenon occurring in the system. Stable adaptation ensures robustness with respect to uncertainty on the model parameters, whereas small-gain arguments are employed in the stability analysis. The proposed approach yields a guaranteed domain

of attraction for given ranges of parameter variations. In these preliminary results the flexible effects are not taken into account in the stability analysis but are considered as a perturbation to the system and are included in the simulation model [2].

Simulation results on the full nonlinear model show the effectiveness of both controllers.

CHAPTER 2

VEHICLE MODEL

Three distinct models of the longitudinal dynamics of the vehicle are considered in this dissertation: a higher-fidelity Simulation Model (SM) is used exclusively for closed-loop simulation, while two reduced-complexity Control-Design Models (CDM1 and CMD2) are employed for control design and for a quantitative stability analysis of the closed-loop system. The model CDM1 will be adopted in the control design with full control authority, while CDM2 will be used in the control design with reduced control authority.

Similar to Parker et al.[28], CDM1 has been derived using curve-fitted approximations of the aerodynamic and propulsive forces. In contrast to Ref. [28], however, this control-oriented model retains the dominant features of the higher fidelity model which are problematic for control design, including non-minimum phase behavior of the flight-path angle dynamics, flexibility effects, and coupling between the propulsion system and the airframe. Since the control design with minimal control authority presents a set of severe challenges, CDM2 is a further simplified control-design model obtained from CDM1 by removing the flexible states, the altitude dynamics and some weak couplings.

2.1 Simulation Model (SM)

The SM adopted in this study is the first principles model developed by Bolender and Doman[2, 37] for the longitudinal dynamics of a flexible air-breathing hypersonic vehicle. The equations of motion, derived using Lagrange's Equations, include flexibility effects by modeling the vehicle as a single flexible structure with mass-normalized mode shapes. This assumed-modes model considers a traditional free beam model [25] of the structure in which the flexible modes are orthogonal to the rigid body modes; therefore, the interaction between rigid and flexible dynamics occurs only through the aerodynamic forces, as opposed to the original "heave-coupling model" of Ref. [2] which was considered in Parker *et al.* [28]. The scramjet engine model is taken from Chavez and Schmidt[4]. Assuming a flat Earth and normalizing by the span of the vehicle to unit depth, the equations of motion of the longitudinal dynamics are written in the stability axes as

$$\begin{aligned}
\dot{V} &= \frac{T\cos\alpha - D}{m} - g\sin\gamma \\
\dot{h} &= V\sin\gamma \\
\dot{\gamma} &= \frac{L + T\sin\alpha}{mV} - \frac{g}{V}\cos\gamma \\
\dot{\alpha} &= -\frac{L + T\sin\alpha}{mV} + Q + \frac{g}{V}\cos\gamma \\
\dot{Q} &= \frac{M}{I_{yy}} \\
\ddot{\eta}_i &= -2\zeta_i\omega_i\dot{\eta}_i - \omega_i^2\eta_i + N_i\,, \qquad i = 1,2,3\,.
\end{aligned} \tag{2.1}$$

This model comprises five rigid-body state variables $x = [V, h, \gamma, \alpha, Q]^T$, six flexible states $\eta = [\eta_1, \dot{\eta}_1, \eta_2, \dot{\eta}_2, \eta_3, \dot{\eta}_3]^T$ and three control inputs $u = [\Phi, \delta_e, \delta_c]^T$. Among the control inputs, the fuel equivalence ratio affects directly the thrust and indirectly the pitching moment and lift by way of coupling between the propulsion system and the airframe. The aerodynamic forces and moment as well as the generalized

elastic forces are influenced by the aerodynamic control surfaces, whose schematic representation is given in Ref [28]. Finally, the structural dynamics are coupled with the rigid-body dynamics as thrust, lift, drag and pitching moment depend upon the modal coordinates, whereas the generalized forces depend on the angle-of-attack. The reader is referred to the cited references for further details.

2.2 Control Design Model 1 (CDM1)

In the SM, the relationships between the control inputs and controlled outputs do not admit a closed-form representation. Following the approach used in Parker *et al.* [28], a simplified model has been derived for control design and stability analysis. This model, referred to as the control-design model, approximates the behavior of the SM by replacing the aerodynamic and generalized forces and moments with curve-fitted functions of the rigid-body states, the control inputs and the elastic modes. The resulting non-linear model, albeit still quite complex, offers the advantage of being analytically tractable, while retaining the relevant dynamical features of the simulation model. The equations of motion of the CDM2 are given by Eq. (2.1), while the approximations of the forces and moments are given as follows

$$
\begin{aligned}
&T \approx \bar{q}S\left[C_{T,\Phi}(\alpha)\Phi + C_T(\alpha) + C_T^{\eta}\eta\right], \qquad L \approx \bar{q}SC_L(\alpha,\delta,\eta) \\
&D \approx \bar{q}SC_D(\alpha,\delta,\eta), \qquad M \approx z_T T + \bar{q}\,\bar{c}\,SC_M(\alpha,\delta,\eta) \\
&N_i \approx \bar{q}S\left[N_i^{\alpha^2}\alpha^2 + N_i^{\alpha}\alpha + N_i^{\delta_e}\delta_e + N_i^{\delta_c}\delta_c + N_i^0 + N_i^{\eta}\eta\right], \qquad i = 1,2,3
\end{aligned}
\tag{2.2}
$$

where $\delta = [\delta_c, \delta_e]^T$, and

$$
\begin{aligned}
C_{T,\Phi}(\alpha) &= C_T^{\Phi\alpha^3}\alpha^3 + C_T^{\Phi\alpha^2}\alpha^2 + C_T^{\Phi\alpha}\alpha + C_T^{\Phi} \\
C_T(\alpha) &= C_T^3\,\alpha^3 + C_T^2\,\alpha^2 + C_T^1\,\alpha + C_T^0 \\
C_M(\alpha,\delta,\eta) &= C_M^{\alpha^2}\alpha^2 + C_M^{\alpha}\alpha + C_M^{\delta_e}\delta_e + C_M^{\delta_c}\delta_c + C_M^0 + C_M^{\eta}\eta \\
C_L(\alpha,\delta,\eta) &= C_L^{\alpha}\alpha + C_L^{\delta_e}\delta_e + C_L^{\delta_c}\delta_c + C_L^0 + C_L^{\eta}\eta \\
C_D(\alpha,\delta,\eta) &= C_D^{\alpha^2}\alpha^2 + C_D^{\alpha}\alpha + C_D^{\delta_e^2}\delta_e^2 + C_D^{\delta_e}\delta_e + C_D^{\delta_c^2}\delta_c^2 + C_D^{\delta_c}\delta_c + C_D^0 + C_D^{\eta}\eta\,. \\
C_j^{\eta} &= [C_j^{\eta_1}\ \ 0\ \ C_j^{\eta_2}\ \ 0\ \ C_j^{\eta_3}\ \ 0]\,, \qquad j = T, M, L, D \\
N_i^{\eta} &= [N_i^{\eta_1}\ \ 0\ \ N_i^{\eta_2}\ \ 0\ \ N_i^{\eta_3}\ \ 0]\,, \qquad i = 1, 2, 3\,.
\end{aligned}
\tag{2.3}
$$

The CDM1 comprises five rigid-body state variables $x = [V, h, \gamma, \alpha, Q]^T$, six flexible states $\eta = [\eta_1, \dot{\eta}_1, \eta_2, \dot{\eta}_2, \eta_3, \dot{\eta}_3]^T$ and three control inputs $u = [\Phi, \delta_e, \delta_c]^T$, whereas the output to be controlled is selected as $y = [V, h]^T$. The values of the vehicle parameters and the curve fit coefficients are reported in Appendix A.1 and A.2. In contrast to Ref. [28], the thrust, lift, drag and moment coefficients of the CDM1 depend explicitly on the elastic modes. Note also that the CDM1 includes lift due to the elevator, and the effect of the thrust on the pitching moment.

Since the CDM1 has been obtained from a curve-fitted approximation of a first-principles model, it is fundamental that the control law provides robustness with respect to uncertainty in the plant model parameters. In developing the controller and assessing its closed-loop performance, it is assumed that all of the coefficients of the CDM1 are subject to uncertainty, apart from obvious parameters corresponding to physically measurable quantities or known constants. The vector of all uncertain parameters, denoted by $p \in \mathbb{R}^m$, includes the vehicle inertial parameters and the coefficients that appear in the force and moment approximations (that is, $C_T^{(\cdot)}$, $C_M^{(\cdot)}$, and so on.) The nominal value of the uncertain parameter vector is denoted by p^0. It

is assumed that $p \in \mathcal{P}$, where $\mathcal{P}$ is a compact convex set that represents the admissible range of variation of p such that p^0 lies in its interior. For simplicity, in this work a maximum uniform variation within 40% of the nominal value has been considered, yielding the parameter set $\mathcal{P} = \{p \in \mathbb{R}^m \mid \quad 0.6\, p_i^0 \;\leq\; p_i \;\leq\; 1.4\, p_i^0\,, \quad i = 1 \ldots m\}$.

The natural frequencies, ω_i, of the flexible dynamics depend on the mass of the vehicle, which decreases as fuel is consumed. Since this variation occurs on a slower time scale than the speed of the references to be tracked, for the purpose of control design the mass has been considered constant during each tracking maneuver. However, both the vehicle mass and the natural frequencies of the flexible dynamics have been considered as uncertain parameters ranging within the intervals given in Ref [32] corresponding to 100% variation in fuel level. Note that these values remain within the assumed 40% uncertainty about the nominal value.

2.3 Control Design Model 2 (CDM2)

The CDM2 has been obtained from CDM1 by removing the flexible states (which are regarded to as a perturbation and their effect is evaluated only in simulation), the altitude dynamics (in this control design the FPA will be selected as regulated output instead of the altitude) and the dependence of the drag on the elevator (this coupling can be neglected since it is a week coupling and by doing that the control design becomes more straightforward). As a result, the equations of motion for the CDM2 read as

$$\begin{aligned} m\dot{V} &= T(\alpha, \Phi)\cos\alpha - D(\alpha) - mg\sin\gamma \\ \dot{\gamma} &= \frac{L(\alpha, \delta_e) + T(\alpha, \Phi)\sin\alpha}{mV} - \frac{g}{V}\cos\gamma \\ \dot{\theta} &= Q \\ I_{yy}\dot{Q} &= M(\alpha, \delta_e) \end{aligned} \tag{2.4}$$

and the expressions of the forces and moments are

$$
\begin{aligned}
T(\alpha, \Phi) &= \bar{q}SC_{T\Phi}(\alpha)\Phi + \bar{q}SC_T(\alpha) \\
D(\alpha) &= \bar{q}SC_D(\alpha)\,, \quad L(\alpha, \delta_e) = \bar{q}S\big[C_L(\alpha) + C_L^{\delta}\delta_e\big] \\
M(\alpha, \delta_e) &= z_T T(\alpha, \Phi) + \bar{q}S\bar{c}\big[C_M(\alpha) + C_M^{\delta}\delta_e\big]
\end{aligned} \tag{2.5}
$$

where

$$
\begin{aligned}
C_{T\Phi}(\alpha) &= C_{T\Phi}^{\alpha^3}\alpha^3 + C_{T\Phi}^{\alpha^2}\alpha^2 + C_{T\Phi}^{\alpha}\alpha + C_{T\Phi}^{0} \\
C_T(\alpha) &= C_T^{\alpha^3}\alpha^3 + C_T^{\alpha^2}\alpha^2 + C_T^{\alpha}\alpha + C_T^{0}) \\
C_M(\alpha) &= C_M^{\alpha^2}\alpha^2 + C_M^{\alpha}\alpha + C_M^{0} \\
C_L(\alpha) &= C_L^{\alpha}\alpha + C_L^{0}\,, \quad C_D(\alpha) = C_D^{\alpha^2}\alpha^2 + C_D^{\alpha}\alpha + C_D^{0}
\end{aligned}
$$

The CMD2 comprises four rigid-body states, $x = [V, \gamma, \theta, Q]^T$, two control inputs $u = [\Phi, \delta_e]^T$ and the output to be controlled is selected as $y = [V, \gamma]^T$. Also in this case, it is assumed that all model parameters are subject to uncertainty and that the vector of uncertain parameters $p \in \mathcal{P} \subset \mathbb{R}^p$.

CHAPTER 3

CONTROL DESIGN WITH FULL CONTROL AUTHORITY

The control design and the stability analysis for the "full control authority" scenario is performed on the control-oriented model CDM1 introduced in section 2.2.

3.1 Control Objectives and Problem Formulation

The goal pursued in this study is to design a dynamic controller of the form

$$\begin{aligned} \dot{\hat{\vartheta}} &= F(\hat{\vartheta}, x, y_{\mathrm{r}}) \,, \qquad \hat{\vartheta} \in \mathbb{R}^{\nu} \\ u &= H(\hat{\vartheta}, x, y_{\mathrm{r}}) \end{aligned} \tag{3.1}$$

using feedback from the rigid-body states only, to steer the output of system (2.1) from a given set of initial values of velocity and altitude to desired trim conditions V^* and h^* along reference trajectories $y_{\mathrm{r}}(t) = [V_{\mathrm{r}}(t),\, h_{\mathrm{r}}(t)]^T$, robustly with respect to the considered model parameter uncertainty. The reference $y_{\mathrm{r}}(t)$ is assumed to be bounded, with bounded derivatives of any order. In addition, the control system should provide asymptotic regulation of the angle-of-attack to a desired trim value, α^*. The control problem considered in this work takes into account only cruise trajectories and does not consider the ascent or the reentry of the vehicle. As a consequence, the velocity and altitude references and the set-point for the angle-of-attack are generated to satisfy the bounds shown in Table 3.1, which determine the flight envelope.

Variable	Min Value	Max Value	Variable	Min Value	Max Value
V	7500 ft/s	11000 ft/s	Φ	0.05	1.5
h	70000 ft	135000 ft	δ_c	-20 deg	20 deg
γ	-5 deg	5 deg	δ_e	-20 deg	20 deg
α	-5 deg	10 deg	$\bar{q}$	500 psf	2000 psf
Q	-10 deg/s	10 deg/s	M	7	12

Table 3.1: Admissible range, $\mathcal{A}$, for states, inputs, dynamic pressure and Mach number

Table 3.1 also shows the admissible range for the control inputs, and the considered range of dynamic pressure. Herein, we denote with $\mathcal{A} \subset \mathbb{R}^{10}$ the admissible range for all variables in Table 3.1. Desired commands $\gamma_{\text{cmd}}(t)$, $\alpha_{\text{cmd}}(t)$ and $Q_{\text{cmd}}(t)$ will be issued by the controller to regulate the corresponding intermediate state variables. The reference and command trajectories are defined such that their asymptotic values yield the desired trim condition of the rigid-body state, $x^* = [V^*, h^*, 0, \alpha^*, 0]^T$, that is, $\lim_{t\to\infty} V_{\text{r}}(t) = V^*$, $\lim_{t\to\infty} h_{\text{r}}(t) = h^*$, $\lim_{t\to\infty} \alpha_{\text{cmd}}(t) = \alpha^*$, whereas $\lim_{t\to\infty} \gamma_{\text{cmd}}(t) = 0$ and $\lim_{t\to\infty} Q_{\text{cmd}}(t) = 0$. Consequently, the tracking error to be regulated to zero is defined as $\tilde{x} = [\tilde{V}, \tilde{h}, \tilde{\gamma}, \tilde{\alpha}, \tilde{Q}]^T := [V - V_{\text{r}}, h - h_{\text{r}}, \gamma - \gamma_{\text{cmd}}, \alpha - \alpha_{\text{cmd}}, Q - Q_{\text{cmd}}]^T$. It should be noted that, once the desired trim condition for the rigid-body state is selected, the corresponding trim values $u^* = [\Phi^*, \delta_e^*, \delta_c^*]^T$ and $\eta^* = [\eta_1^*, 0, \eta_2^*, 0, \eta_3^*, 0]^T$ for the control input and the flexible states, respectively, cannot be determined exactly due to parameter uncertainty. The aim of the stability analysis of the closed-loop system is to prove that all state trajectories remain bounded for all possible values of $p \in \mathcal{P}$, while $\tilde{x}(t)$ and $\tilde{\eta}(t)$ vanish asymptotically.

For the purpose of control design and stability analysis, it is convenient to formulate the specification on the initial conditions of the rigid-body dynamics in terms of the error variables $\tilde{x}(0) = [V_0, h_0, \gamma_0, \alpha_0, Q_0]^T$ rather than in terms of $x(0)$. In particular, it is assumed that $\tilde{x}(0) \in \Xi_0^{\tilde{x}}$, where $\Xi_0^{\tilde{x}} \subset \mathbb{R}^5$ is a *given* compact set. Similarly, for the initial condition of the flexible dynamics and the state of the controller, it is assumed that $\tilde{\eta}(0) \in \Xi_0^{\tilde{\eta}}$ and $\hat{\vartheta}(0) \in \Theta$, for given compact sets $\Xi_0^{\tilde{\eta}} \subset \mathbb{R}^6$ and $\Theta \subset \mathbb{R}^\nu$. First, the controller will be designed to guarantee that for any $[\tilde{x}(0),\, \hat{\vartheta}(0)]^T, \in \Xi_0^{\tilde{x}} \times \Theta$, the trajectory $[\tilde{x}(t),\, \hat{\vartheta}(t)]^T$ of the closed-loop CDM1 remains bounded and $\tilde{x}(t)$ converges to the origin, for all $p \in \mathcal{P}$, when the flexible dynamics are "frozen" at the trim condition $\eta = \eta^*$, i.e., $\tilde{\eta} = 0$. Then, the objective of the stability analysis in Section 3.2 is to give conditions under which, for the same controller, boundedness of all closed-loop trajectories and error regulation continue to hold when $\eta = \tilde{\eta} + \eta^*$, for all initial conditions $[\tilde{x}(0),\, \tilde{\eta}(0),\, \hat{\vartheta}(0)]^T \in \Xi_0^{\tilde{x}} \times \Xi_0^{\tilde{\eta}} \times \Theta$. The performance of the controller is then verified in simulation on the original SM.

3.1.1 Controller Design

The starting point of the proposed methodology is the decomposition of the equations of motion into functional subsystems, namely the horizontal translational dynamics (the velocity subsystem), the vertical translational dynamics outer-loop (the altitude and flight-path angle subsystem) and the vertical translational dynamics inner-loop (the angle-of-attack and pitch rate subsystem). Each subsystem is controlled separately using the available inputs at that level and intermediate virtual control commands, as shown in Fig. 3.1. In particular, a control law with adaptive drag compensation is derived for the velocity subsystem by controlling the thrust from the fuel equivalence ratio input, Φ. The altitude dynamics are controlled through the flight-path angle by means of a suitable command γ_{cmd} derived from the altitude

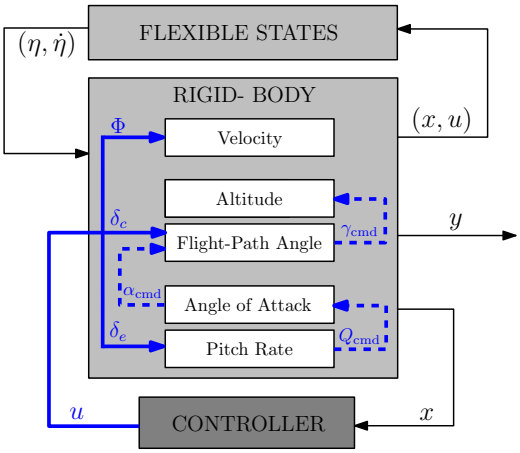

Figure 3.1: Block diagram of the control architecture, showing direct control inputs (bold solid lines) and virtual control inputs (dashed lines).

reference trajectory. The canard deflection, δ_c, and the angle-of-attack serve respectively as a direct and a virtual control input to the flight-path angle dynamics. Due to the fact that the control authority of the canard on the flight-path angle dynamics is significantly smaller than the one of the angle-of-attack, the main control action will be performed by this latter through the command α_{cmd}. The role of the canard is to adaptively decouple lift from elevator commands, rendering the system minimum phase with respect to γ. In addition, the canard is used to enforce the equilibrium at the desired trim condition, and to provide a supplementary stabilizing action. The vertical translational dynamics outer-loop is controlled through the pitch moment by means of the elevator deflection, δ_e.

At each step of the design, a control Lyapunov function candidate is selected and a robust adaptive control law is designed on its basis. The stability of the closed-loop rigid-body dynamics is assessed once the construction of the overall controller has been completed.

Adaptive Controller for the Velocity Subsystem

The controller for the velocity loop is derived by using robust adaptive dynamic inversion. Substituting the expression of T in (2.2) into the first equation of (2.1), the velocity error dynamics become

$$m\dot{\tilde{V}} = \bar{q}S\big[C_{T,\Phi}(\alpha)\,\Phi + C_T(\alpha) + C_T^{\eta}\eta\big]\cos\alpha - D - mg\sin\gamma - m\dot{V}_{\rm r}. \tag{3.2}$$

Defining the vector of uncertain parameters $\vartheta_1 \in \mathbb{R}^{16}$ as

$$\begin{aligned}\vartheta_1 \;=\; \big[&C_T^{\Phi\alpha^3}, C_T^{\Phi\alpha^2}, C_T^{\Phi\alpha}, C_T^{\Phi}, C_T^{3}, C_T^{2}, C_T^{1}, \big(C_T^0 + C_T^{\eta}\eta^*\big),\\ &C_D^{\alpha^2}, C_D^{\alpha}, C_D^{\delta_e^2}, C_D^{\delta_e}, C_D^{\delta_c^2}, C_D^{\delta_c}, \big(C_D^0 + C_D^{\eta}\eta^*\big), m\big]^T\end{aligned}$$

equation (3.2) can be written in the linearly parameterized form

$$m\dot{\tilde{V}} \;=\; \vartheta_1^T\big[B_1(x)\Phi - \Psi_1(x,u,y_{\rm r})\big] + \bar{q}\,S\big[C_T^{\eta}\cos\alpha - C_D^{\eta}\big]\tilde{\eta}$$

where the regressor $\Psi_1(x,u,y_{\rm r})$ and the input matrix $B_1(x)$ are given respectively by

$$\begin{aligned}\Psi_1(x,u,y_{\rm r}) \;&=\; \bar{q}S\big[\,\mathbf{0}_{1\times 4},\, -\alpha^3\cos\alpha,\, -\alpha^2\cos\alpha,\, -\alpha\cos\alpha,\, -\cos\alpha,\, \alpha^2,\, \alpha,\, \delta_e^2,\, \delta_e,\, \delta_c^2,\\ &\qquad \delta_c,\, 1,\, \big(g\sin\gamma + \dot{V}_{\rm r}\big)/(\bar{q}S)\,\big]^T\\ B_1(x) \;&=\; \bar{q}S\big[\,\alpha^3\cos\alpha,\, \alpha^2\cos\alpha,\, \alpha\cos\alpha,\, \cos\alpha,\, \mathbf{0}_{1\times 12}\big]^T.\end{aligned}$$

With considerations analogous to those of Ref. [28], it can be shown that controllability of the model implies that $\vartheta_1^T B_1(x) \neq 0$ for all values of α and $\bar{q}$ within the flight conditions in Table 3.1, and for all possible values assumed by ϑ_1 in the convex compact set $\Theta_1 \subset \mathbb{R}^{16}$ obtained by letting the entries of ϑ_1 vary within the parameter set $\mathcal{P}$. Let $\hat{\vartheta}_1 \in \mathbb{R}^{16}$ be a vector of estimates of the uncertain parameter, ϑ_1, and define $\tilde{\vartheta}_1 := \hat{\vartheta}_1 - \vartheta_1$. The control Lyapunov function candidate for the velocity error dynamics is selected as

$$W_1(\tilde{V},\tilde{\vartheta}_1) \;=\; \frac{\sigma_V}{2}\,\big(m\tilde{V}^2 + \tilde{\vartheta}_1^T\,\Gamma_1^{-1}\,\tilde{\vartheta}_1\big)$$

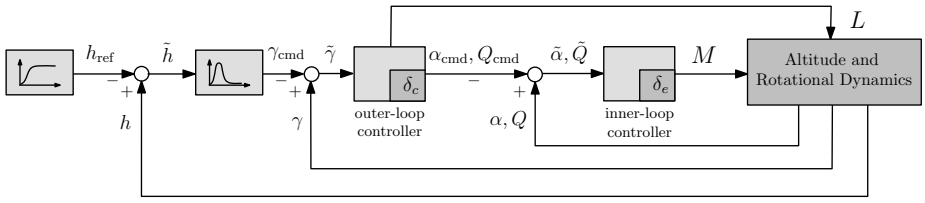

Figure 3.2: Control of the altitude and attitude dynamics

where $\sigma_V > 0$ is a scaling factor, and $\mathit{\Gamma}_1 \in \mathbb{R}^{16\times 16}$ is a diagonal positive definite matrix. Accordingly, the controller for the velocity subsystem is chosen as the dynamical system

$$\begin{aligned} \dot{\hat{\vartheta}}_1 &= \operatorname*{Proj}_{\hat{\vartheta}_1 \in \mathit{\Theta}_1} \left\{ \tilde{V}\, \mathit{\Gamma}_1 \left[B_1(x)\mathit{\Phi} - \mathit{\Psi}_1(x,u,y_{\text{r}}) \right] \right\} \\ \mathit{\Phi} &= \frac{1}{\hat{\vartheta}_1^T B_1(x)} \left[-k_1 \tilde{V} + \mathit{\Psi}_1(x,u,y_{\text{r}})^T\, \hat{\vartheta}_1 \right] \end{aligned} \tag{3.3}$$

with initial conditions $\hat{\vartheta}_1(0) \in \mathit{\Theta}_1$, where $k_1 > 0$ is a gain parameter and $\operatorname*{Proj}_{\hat{\vartheta}_1 \in \mathit{\Theta}_1}(\cdot)$ is a smooth parameter projection[17]. The parameter projection ensures non-singularity of the control law (3.3) over the considered envelope of flight conditions.

Adaptive Controller for the $(\tilde{h}, \tilde{\gamma})$-Subsystem

The outer-loop controller, shown in Figure 3.2, provides the control law for the altitude and flight-path angle dynamics. To begin, the dynamics of the tracking error $\tilde{h}$ is written as

$$\dot{\tilde{h}} = V \sin\gamma - \dot{h}_{\text{r}} \approx V_{\text{r}}\, \gamma - \dot{h}_{\text{r}} + \tilde{V}\gamma$$

using the approximation $\sin\gamma \approx \gamma$, which is valid in the range given in Table 3.1. Choosing the flight-path angle command as $\gamma_{\text{cmd}} = -k_2 \tilde{h} + \dot{h}_{\text{r}}/V_{\text{r}}$, where $k_2 > 0$ is a gain parameter, yields the dynamics of the altitude tracking error as

$$\dot{\tilde{h}} = -k_2\, V_{\text{r}}\, \tilde{h} + V_{\text{r}}\, \tilde{\gamma} + \tilde{V}\gamma.$$

Finally, using equations (2.1) and (2.3), one obtains the dynamics of $\tilde{\gamma}$

$$\dot{\tilde{\gamma}} = \frac{1}{mV}\left[\bar{q}SC_L^{\alpha}\alpha + T\sin\alpha - mg\cos\gamma + \bar{q}S\big(C_L^{\delta_e}\delta_e + C_L^{\delta_c}\delta_c + C_L^0 + C_L^{\eta}\eta\big) - mV\,\dot{\gamma}_{\text{cmd}}\right]. \tag{3.4}$$

The first two terms on the right-hand side of Eq. (3.4) will be used to generate the stabilizing control α_{cmd}. Define the parameterized function of α

$$\Lambda(\alpha, \alpha^*, \bar{q}, \Phi) := \bar{q}SC_L^{\alpha}\,\alpha + T\sin\alpha - \bar{q}SC_L^{\alpha}\,\alpha^* - T^*\sin\alpha^*$$

where $T^* = \bar{q}S\left[C_{T,\Phi}(\alpha^*)\Phi + C_T(\alpha^*) + C_T^{\eta}\eta\right]$. Then the following "sector boundedness" property can be established:

Property 3.1.1. *For all admissible values of α, α^*, $\bar{q}$ and Φ given in Table 3.1, the function $\Lambda(\alpha, \alpha^*, \bar{q}, \Phi)$ can be written as $\Lambda\big(\alpha, \alpha^*, \bar{q}, \Phi\big) = K_{\alpha_1}(x, \Phi)\,V^2\,(\alpha - \alpha^*)$, where $K_{\alpha_1}(x, \Phi)$ is a state-dependent coefficient satisfying $k_m \le K_{\alpha_1}(x, \Phi) \le k_M$ for constants $k_m > 0$, $k_M > 0$.*

Property 3.1.1, sketched in figure 3.3(a), is a consequence of continuous differentiability of $\Lambda(\alpha, \alpha^*, \bar{q}, \Phi)$ with respect to its entries, and can be verified graphically as follows. First, notice that since $\Lambda(\alpha^*, \alpha^*, \bar{q}, \Phi) = 0$, then $\Lambda\big(\alpha, \alpha^*, \bar{q}, \Phi\big) := K(x, \Phi)(\alpha - \alpha^*)$ where $K(x, \Phi)$ is a state-dependent coefficient. For any fixed α^* and $\bar{q}$ within their admissible ranges, the graph of the function $\Lambda(\alpha, \alpha^*, \bar{q}, \Phi)$ versus α can be bounded by two straight lines of appropriate slope for any $\Phi \in \mathcal{A}$, i.e., $k_{min}(\bar{q}) < K(x, \Phi) < k_{max}(\bar{q})$ for two positive functions $k_{min}(\bar{q})$ and $k_{max}(\bar{q})$. Figures 3.3(b)–3.3(c) show two such cases, corresponding to $\alpha^* = 0$ rad and $\bar{q} = 500$ psf, and $\alpha^* = 0.035$ rad and $\bar{q} = 2000$ psf, respectively. Figure 3.3(d) shows the plot of $k_{min}(\bar{q})$ and $k_{max}(\bar{q})$ for some selected values of $\bar{q}$; it is possible to see that these two functions can be approximated by two linear functions. As a result, for $\bar{q} \in \mathcal{A}$, there exist two positive constants k_{min} and k_{max} such that $k_{min}\,\bar{q} < K(x, \Phi) < k_{max}\,\bar{q}$.

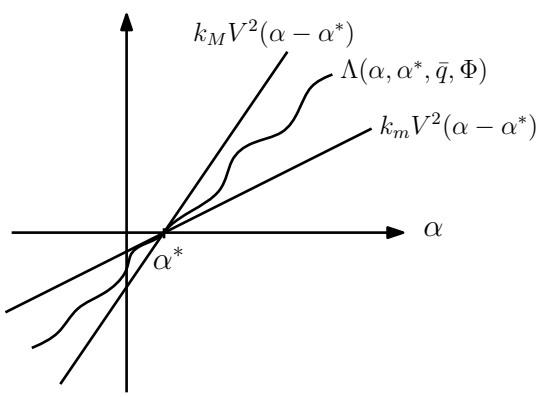

(a) Bounds on $\Lambda(\alpha, \alpha^*, \bar{q}, \Phi)$.

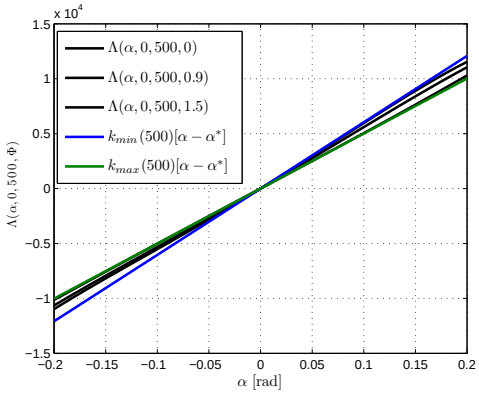

(b) Bounds on $\Lambda(\alpha, 0, 500, \Phi)$.

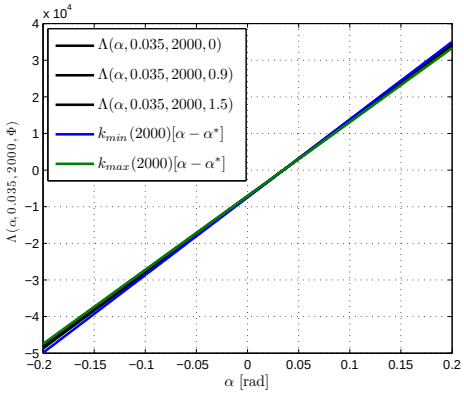

(c) Bounds on $\Lambda(\alpha, 0.035, 2000, \Phi)$.

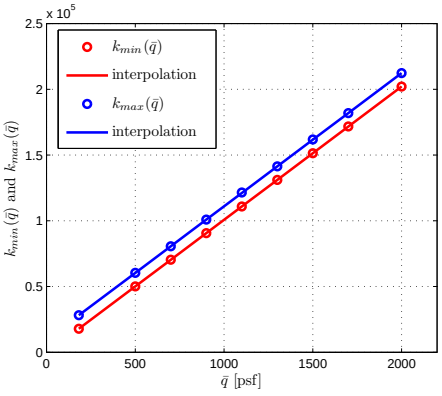

(d) Bounds $k_{\min}\,\bar{q}$ and $k_{\max}\,\bar{q}$.

Figure 3.3: Sector-boundedness property of $\Lambda(\alpha, \alpha^*, \bar{q}_c, \Phi)$

Moreover, since $\bar{q} = 0.5\,\rho\,V^2$ and for the given range of altitude the air density satisfies the bound $0 < \rho_{\min} \leq \rho \leq \rho_{\max}$, it follows that in the range of flight conditions of interest the proposition holds for $K_{\alpha_1}(x, \Phi) = K(x, \Phi)/V^2$, $k_m := 0.5\,k_{\min}\,\rho_{\min}$ and $k_M := 0.5\,k_{\max}\,\rho_{\max}$.

The command trajectory for the angle-of-attack is selected as $\alpha_{\text{cmd}} = \alpha^* - \tilde{\gamma}$, as this choice yields a particularly simple form for the dynamics of the error $\tilde{\alpha}$. Since

$\alpha = \alpha^* - \tilde{\gamma} + \tilde{\alpha}$, using property 3.1.1, one obtains

$$\bar{q}SC_L^{\alpha}\,\alpha\, + T\sin\alpha = K_{\alpha_1}(x,\Phi)\,V^2\,[\tilde{\alpha}-\tilde{\gamma}] + \bar{q}S\,c_1(\alpha^*) + \bar{q}S\,c_2(\alpha^*)\Phi + \bar{q}SC_T^{\eta}\sin\alpha^*\tilde{\eta}$$

where $c_1(\alpha^*) = C_T(\alpha^*)\sin\alpha^* + C_L^{\alpha}\alpha^* + C_T^{\eta}\,\sin\alpha^*\eta^*$ and $c_2(\alpha^*) = C_{T,\Phi}(\alpha^*)\sin\alpha^*$. Letting ϑ_2 and $\Psi_2(x,u,y_{\rm r})$ be defined respectively as

$$\vartheta_2 = \left[\ \frac{C_L^{\delta_e}}{C_L^{\delta_c}}\,,\ \frac{C_L^0 + C_L^{\eta}\,\eta^* + c_1(\alpha^*)}{C_L^{\delta_c}}\,,\ \frac{c_2(\alpha^*)}{C_L^{\delta_c}}\,,\ \frac{m}{S\,C_L^{\delta_c}}\ \right]^T$$

$$\Psi_2(x,u,y_{\rm r}) = \left[\ -\delta_e, -1, -\Phi, \frac{1}{\bar{q}}\big(g\cos\gamma + V\dot{\gamma}_{\rm cmd}\big)\right]^T$$

the dynamics of $\tilde{\gamma}$ is written in the form

$$m\,\dot{\tilde{\gamma}} = \ K_{\alpha_1}(x,\Phi)\,V\,[\tilde{\alpha}-\tilde{\gamma}] + \ \frac{\bar{q}SC_L^{\delta_c}}{V}\big[\,\delta_c - \Psi_2(x,u,y_{\rm r})^T\vartheta_2\big] + \frac{\bar{q}S(C_L^{\eta} + C_T^{\eta}\,\sin\alpha^*)}{V}\,\tilde{\eta} \tag{3.5}$$

Similar to the previous section, we denote with $\Theta_2 \subset \mathbb{R}^4$ the compact convex set obtained by letting the entries of ϑ_2 vary within the parameter set $\mathcal{P}$. Define the vector of estimates $\hat{\vartheta}_2 \in \mathbb{R}^4$, and consider the control Lyapunov function candidate

$$W_2(\tilde{h},\tilde{\gamma},\tilde{\vartheta}_2) = \frac{\sigma_h}{2}\,\tilde{h}^2 + \frac{m}{2}\,\tilde{\gamma}^2 + \frac{SC_L^{\delta_c}}{2}\,\tilde{\vartheta}_2^T\,\Gamma_2^{-1}\,\tilde{\vartheta}_2\,,$$

where $\tilde{\vartheta}_2 = \hat{\vartheta}_2 - \vartheta_2$, $\Gamma_2 \in \mathbb{R}^{4\times 4}$ is a symmetric positive definite diagonal matrix, and $\sigma_h > 0$ is a scaling factor. The controller for the canard is given by the dynamical system

$$\begin{aligned}\dot{\hat{\vartheta}}_2 \ &= \ \underset{\hat{\vartheta}_2\in\Theta_2}{\rm Proj}\left\{-\frac{\bar{q}\,\tilde{\gamma}}{V}\,\Gamma_2\,\Psi_2(x,u,y_{\rm r})\right\}\\ \delta_c \ &= \ \Psi_2(x,u,y_{\rm r})^T\hat{\vartheta}_2 - k_3\tilde{\gamma}\end{aligned} \tag{3.6}$$

with initial conditions $\hat{\vartheta}_2(0) \in \Theta_2$ and gain parameter $k_3 > 0$.

Controller for the (α, Q)-Subsystem

The final steps in our design are to regulate $\tilde{\alpha}(t)$ to zero asymptotically, and provide a comprehensive stability proof for the interconnected system. From the dynamics

for $\tilde{\alpha}$, it is apparent that the command trajectory for the pitch rate should be selected as $Q_{\rm cmd} = \dot{\gamma}_{\rm cmd} - k_4\tilde{\alpha}$, with $k_4 > 0$. Using Eqs. (2.2)–(2.3) the error dynamics can be written as

$$\begin{aligned}\dot{\tilde{\alpha}} &= -k_4\tilde{\alpha} + \tilde{Q} \\ \dot{\tilde{Q}} &= \vartheta_3^T\big[B_3(x)\,\delta_e - \Psi_3(x,u,y_{\rm r})\big] + k_4\tilde{Q} - k_4^2\tilde{\alpha} + \frac{\bar{q}S}{I_{yy}}[z_T C_T^{\eta} + \bar{c}\,C_M^{\eta}]\tilde{\eta} \end{aligned} \tag{3.7}$$

where the vector of uncertain parameters $\vartheta_3 \in \mathbb{R}^{11}$, the regressor $\Psi_3(x,u,y_{\rm r})$ and the input matrix $B_3(x)$ are given respectively by

$$\begin{aligned}\vartheta_3 &= \frac{S}{I_{yy}}\big[\,\bar{c}\,C_M^{\delta_e}, \bar{c}\,C_M^{\delta_c}, z_T\,C_T^{\Phi\alpha^3}, z_T\,C_T^{\Phi\alpha^2}, z_T\,C_T^{\Phi\alpha}, z_T\,C_T^{\Phi}, z_T\,C_T^{3}, (z_T\,C_T^{2} + \bar{c}\,C_M^{\alpha^2}), \\ &\qquad (z_T\,C_T^{1} + \bar{c}\,C_M^{\alpha}), (z_T\,C_T^{0} + \bar{c}\,C_M^{0}) + (z_T\,C_T^{\eta} + \bar{c}\,C_M^{\eta})\,\eta^*,\ I_{yy}/S\,\big]^T \end{aligned}$$

$$\begin{aligned}\Psi_3(x,u,y_{\rm r}) &= -\bar{q}\,\big[\,0,\ \delta_c,\ \alpha^3\Phi,\ \alpha^2\Phi,\ \alpha\ \Phi, \Phi,\ \alpha^3,\ \alpha^2,\ \alpha\,,1\,, -\ddot{\gamma}_{\rm cmd}/\bar{q}\,\big]^T \\ B_3(x) &= \big[\bar{q}, \mathbf{0}_{1\times 10}\big]^T\,. \end{aligned}$$

Finally, denote by $\Theta_3 \subset \mathbb{R}^{11}$ the convex and compact parameter set for ϑ_3, and define the estimate vector $\hat{\vartheta}_3$ and the error $\tilde{\vartheta}_3 = \hat{\vartheta}_3 - \vartheta_3$. The design is completed by selecting

$$W_3(\tilde{\alpha}, \tilde{Q}, \tilde{\vartheta}_3) = \frac{\sigma_\alpha}{2}\,\tilde{\alpha}^2 + \frac{\sigma_Q}{2}\,\tilde{Q}^2 + \frac{\sigma_Q}{2}\,\tilde{\vartheta}_3^T\,\Gamma_3^{-1}\tilde{\vartheta}_3$$

with scaling factors $\sigma_\alpha > 0$, $\sigma_Q > 0$ and positive definite $\Gamma_3 \in \mathbb{R}^{11\times 11}$, yielding the controller

$$\begin{aligned}\dot{\hat{\vartheta}}_3 &= \operatorname*{Proj}_{\vartheta_3\in\Theta_3}\Big\{\Gamma_3\,[B_3(x)\delta_e - \Psi_3(x,u,y_{\rm r})]\,\tilde{Q}\Big\} \\ \delta_e &= \frac{1}{\hat{\vartheta}_3^T B_3(x)}\,[\Psi_3(x,u,y_{\rm r})^T\hat{\vartheta}_3 - k_5\tilde{Q}] \end{aligned} \tag{3.8}$$

where $\hat{\vartheta}_3(0) \in \Theta_3$ and $k_5 > 0$ is a gain parameter.

Stability analysis for the rigid-body dynamics

To prove stability of the overall closed-loop system obtained by interconnecting the rigid-body dynamics in Eqs.(2.1)–(2.2) with the adaptive controller given by Eqs.(3.3), (3.6) and (3.8), consider the Lyapunov function candidate

$$W_{\rm rb}(\tilde{x},\tilde{\vartheta}) = W_1(\tilde{V},\tilde{\vartheta}_1) + W_2(\tilde{h},\tilde{\gamma},\tilde{\vartheta}_2) + W_3(\tilde{\alpha},\tilde{Q},\tilde{\vartheta}_3) \tag{3.9}$$

where $\tilde{\vartheta} = [\tilde{\vartheta}_1^T, \tilde{\vartheta}_2^T, \tilde{\vartheta}_3^T]^T$. The role of the scaling factors in the Lyapunov function $W_{\rm rb}(\tilde{x},\tilde{\vartheta})$ is to allow flexibility in the design by shaping the level sets $\Omega_c(W_{\rm rb}) = \{\tilde{x},\tilde{\vartheta} \,|\, W_{\rm rb}(\tilde{x},\tilde{\vartheta}) \leq c\}$, $c > 0$, to obtain the required estimate of the domain of attraction. In particular, given the compact set $\Xi_0^{\tilde{x}}$ of initial conditions and the parameter set $\Theta = \Theta_1 \times \Theta_2 \times \Theta_3$, it is always possible to determine a constant $c > 0$, and values of the scaling factors $\sigma_\chi, \sigma_V, \sigma_h, \sigma_\alpha, \sigma_Q$ such that, for a given reference $y_{\rm ref}$, the following conditions are verified for all $p \in \mathcal{P}$:

a.1) $\Xi_0^{\tilde{x}} \subset \Omega_c(W_{\rm rb})$;

a.2) $\tilde{x} \in \Omega_c(W_{\rm rb})$ implies $x \in \mathcal{A}$;

a.3) $\hat{\vartheta}$, $\vartheta \in \Theta$ implies $\tilde{\vartheta} \in \Omega_c(W_{\rm rb})$.

The first two conditions ensure that, for the given reference trajectory, the domain of attraction of the equilibrium set at $\tilde{x} = 0$ includes the given compact set $\Xi_0^{\tilde{x}}$, and that the trajectory $x(t)$ remains within the feasible set, $\mathcal{A}$, if the derivative of the Lyapunov function is negative semi-definite on $\Omega_c(W_{\rm rb})$. The third condition implies that the estimates $\hat{\vartheta}(t)$, when projected onto the set Θ, generate an error which remains within the level set $\Omega_c(W_{\rm rb})$.

Proposition 3.1.1. *Consider the closed-loop system*

$$
\begin{aligned}
m\dot{\tilde{V}} &= -k_1\tilde{V} - \big[B_1(x)^T\Phi - \Psi_1(x,u,y_{\rm r})^T\big]\tilde{\vartheta}_1 + \bar{q}S\big[C_T^\eta\cos\alpha - C_D^\eta\big]\tilde{\eta}\\
\dot{\tilde{h}} &= -k_2\,V_{\rm r}\,\tilde{h} + V_{\rm r}\,\tilde{\gamma} + \tilde{V}\gamma\\
m\,\dot{\tilde{\gamma}} &= K_{\alpha_1}(x,\Phi)\,V\,[\tilde{\alpha}-\tilde{\gamma}] + \frac{\bar{q}SC_L^{\delta_c}}{V}\big[-k_3\tilde{\gamma} + \Psi_2(x,u,y_{\rm r})^T\tilde{\vartheta}_2\big] + \frac{\bar{q}S(C_L^\eta + C_T^\eta\,\sin\alpha^*)}{V}\,\tilde{\eta}\\
\dot{\tilde{\alpha}} &= -k_4\tilde{\alpha} + \tilde{Q}\\
\dot{\tilde{Q}} &= -(k_5-k_4)\tilde{Q} - k_4^2\tilde{\alpha} - \big[B_3(x)^T\delta_e - \Psi_3(x,u,y_{\rm r})^T\big]\tilde{\vartheta}_3 + \frac{\bar{q}S}{I_{yy}}[z_TC_T^\eta + \bar{c}\,C_M^\eta]\tilde{\eta}\\
\dot{\tilde{\vartheta}}_1 &= \underset{\hat{\vartheta}_1\in\Theta_1}{\rm Proj}\Big\{\tilde{V}\,\Gamma_1\,\big[\,B_1(x)\Phi - \Psi_1(x,u,y_{\rm r})\big]\Big\}\\
\dot{\tilde{\vartheta}}_2 &= \underset{\hat{\vartheta}_2\in\Theta_2}{\rm Proj}\left\{-\frac{\bar{q}\,\tilde{\gamma}}{V}\,\Gamma_2\,\Psi_2(x,u,y_{\rm r})\right\}\\
\dot{\tilde{\vartheta}}_3 &= \underset{\hat{\vartheta}_3\in\Theta_3}{\rm Proj}\Big\{\Gamma_3\,[B_3(x)\delta_e - \Psi_3(x,u,y_{\rm r})]\,\tilde{Q}\Big\}
\end{aligned}
\tag{3.10}
$$

and the Lyapunov function candidate given in Eq. (3.9)*. Let the level set* $\Omega_c(W_{\rm rb})$ *be chosen to satisfy conditions a.1)–a.3) above. Fix, arbitrarily, the value of the gains* $k_1 > 0$ *and* $k_3 \geq 0$*. Then, there exist positive numbers* $k_i^\star$*,* $i = 2,4,5$*, such that, if* $\tilde{\eta} = 0$*, the trajectories of the closed-loop system* (3.10) *originating within* $\Omega_c(W_{\rm rb})$ *are bounded and satisfy* $\lim_{t\to\infty}\tilde{x}(t) = 0$*, whenever the remaining gains are selected to satisfy* $k_i > k_i^\star$*,* $i = 2,4,5$*.*

Proof. Using standard properties of the projection operator[17] and condition a.3), it can be verified that the derivative of $W_{\rm rb}$ along trajectories of system (3.10) satisfies

$$
\dot{W}_{\rm rb}(\tilde{x},\tilde{\vartheta}) \leq -\,\tilde{x}^T R_{\rm rb}(x,y_{\rm r})\,\tilde{x} + \tilde{x}^T R_{\rm rb,fl}(x)\,\tilde{\eta} \qquad \forall\,(\tilde{x},\tilde{\vartheta}) \in \Omega_c(W_{\rm rb}) \tag{3.11}
$$

where $R_{\rm rb}(x, y_{\rm r})$ is the state-dependent matrix

$$R_{\rm rb}(x, y_{\rm r}) := \begin{bmatrix} k_1\sigma_V & -\frac{\sigma_h\,\gamma}{2} & 0 & 0 & 0 \\ -\frac{\sigma_h\,\gamma}{2} & \sigma_h k_2 V_{\rm r} & -\frac{\sigma_h V_{\rm r}}{2} & 0 & 0 \\ 0 & -\frac{\sigma_h V_{\rm r}}{2} & (K_{\alpha_1} + \frac{\bar{q}SC_L^{\delta_c}}{V^2}k_3)V & -\frac{K_{\alpha_1}V}{2} & 0 \\ 0 & 0 & -\frac{K_{\alpha_1}V}{2} & \sigma_\alpha k_4 & \frac{\sigma_Q k_4^2 - \sigma_\alpha}{2} \\ 0 & 0 & 0 & \frac{\sigma_Q k_4^2 - \sigma_\alpha}{2} & \sigma_Q(k_5 - k_4) \end{bmatrix}$$

and the matrix

$$R_{\rm rb,fl}(x) := \bar{q}S \begin{bmatrix} \sigma_V(C_T^\eta \cos\alpha - C_D^\eta) \\ 0_{1\times 6} \\ \frac{C_L^\eta + C_T^\eta \sin\alpha^*}{V} \\ 0_{1\times 6} \\ \sigma_Q \frac{z_T C_T^\eta + \bar{c} C_M^\eta}{I_{yy}} \end{bmatrix} \in \mathbb{R}^{5\times 6}$$

determines the coupling between the rigid body tracking error and the structural flexibility. Using conditions a.1)–a.2), the lower bound in property 3.1.1 and the fact that $C_L^{\delta_c} > 0$, it is seen that for any $\tilde{x} \in \Omega_c(W_{\rm rb})$ the (3,3)-element of $R_{\rm rb}$ satisfies

$$K_{\alpha_1} + \frac{\bar{q}SC_L^{\delta_c}}{V^2}k_3 \geq k_m + k_c k_3\,, \qquad k_c := \min_{\substack{V,\bar{q}\,\in\,\mathcal{A} \\ p\in\,\mathcal{P}}} \frac{\bar{q}SC_L^{\delta_c}}{V^2} > 0$$

Fix $k_3 \geq 0$, and let Δ_i denote the i-th minor of $R_{\rm rb}(x, y_{\rm r})$. For any $k_1 > 0$, the number

$$k_2^\star := \frac{\sigma_h}{4\,\sigma_V k_1 \min_{V_{\rm r}\in\mathcal{A}} V_{\rm r}} + \frac{\sigma_h \max_{V_{\rm r}\in\mathcal{A}} V_{\rm r}}{4\,(k_m + k_c k_3)\min_{V\in A} V}$$

is such that the minors Δ_1, Δ_2 and Δ_3 are strictly positive for any $k_2 > k_2^*$. Since Δ_1, Δ_2 and Δ_3 do not depend on k_4, there exists $k_4^\star$ (which depend on k_1, k_2 and k_3) such that Δ_4 is positive for any $k_4 > k_4^\star$. Similarly, there exists $k_5^\star$ such that Δ_5 is positive for all $k_5 > k_5^\star$. By Sylvester's criterion it follows that there exist a constant

symmetric positive definite matrix $\bar{R}_{rb}$ such that $R_{\rm rb}(x, y_{\rm r}) \geq \bar{R}_{\rm rb}$. As a result, for all $(\tilde{x}, \tilde{\vartheta}) \in \Omega_c(W_{\rm rb})$ and $\tilde{\eta} = 0$

$$\dot{W}_{\rm rb}(\tilde{x}, \tilde{\vartheta}) \leq -\tilde{x}^T \bar{R}_{\rm rb}\, \tilde{x}$$

and thus the result follows from application of LaSalle-Yoshizawa theorem [16, 17]. □

Notice that a non-zero value of k_3 is not needed for stability of the rigid-body closed-loop system, and that k_1 can be chosen arbitrarily. Once k_1 and k_3 have been fixed, the minimal values of the other gains that ensure closed-loop stability can be determined, and the gains be selected to be any real numbers larger than these values. This result is in sharp contrast with the outcome of the analysis when the structural dynamics are taken into consideration.

3.2 Stability Analysis of the Rigid-Body and Flexible Dynamics

Since the system has vector relative-degree [15] $r = [1, 2, 2]^T$ with respect to the output $[V, h, \alpha]^T$, the CDM1 possesses six-dimensional internal dynamics, related to the structural dynamics. To compute the internal dynamics, we begin by substituting the generalized forces N_i in (2.2) into the last equation of (2.1), obtaining

$$\dot{\eta} \;=\; A_\eta\, \eta + \bar{q} S [A_1\, \alpha + A_2\, \alpha^2 + A_3] + \bar{q} S A_4\, \delta \tag{3.12}$$

where

$$A_\eta = \begin{bmatrix} 0 & 1 & 0 & 0 & 0 & 0 \\ -\omega_1^2 + \bar{q} S N_1^{\eta_1} & -2\zeta_1\omega_1 & \bar{q} S N_1^{\eta_2} & 0 & \bar{q} S N_1^{\eta_3} & 0 \\ 0 & 0 & 0 & 1 & 0 & 0 \\ \bar{q} S N_2^{\eta_1} & 0 & -\omega_2^2 + \bar{q} S N_2^{\eta_2} & -2\zeta_2\omega_2 & \bar{q} S N_2^{\eta_3} & 0 \\ 0 & 0 & 0 & 0 & 0 & 1 \\ \bar{q} S N_3^{\eta_1} & 0 & \bar{q} S N_3^{\eta_2} & 0 & -\omega_3^2 + \bar{q} S N_3^{\eta_3} & -2\zeta_3\omega_3 \end{bmatrix}$$

$$A_1 = \begin{bmatrix} 0 & N_1^{\alpha} & 0 & N_2^{\alpha} & 0 & N_3^{\alpha} \end{bmatrix}^T, \qquad A_2 = \begin{bmatrix} 0 & N_1^{\alpha^2} & 0 & N_2^{\alpha^2} & 0 & N_3^{\alpha^2} \end{bmatrix}^T,$$

$$A_3 = \begin{bmatrix} 0 & N_1^{0} & 0 & N_2^{0} & 0 & N_3^{0} \end{bmatrix}^T, \qquad A_4 = \begin{bmatrix} 0 & N_1^{\delta_c} & 0 & N_2^{\delta_c} & 0 & N_3^{\delta_c} \\ 0 & N_1^{\delta_e} & 0 & N_2^{\delta_e} & 0 & N_3^{\delta_e} \end{bmatrix}^T.$$

Next, we remove the dependence of equation (3.12) on the control inputs. Using the same arguments used in property 3.1.1, one can express the term $\bar{q}SC_L^{\alpha}\alpha + T\sin\alpha$ appearing in the dynamic equation of the angle-of-attack as $\bar{q}SC_L^{\alpha}\,\alpha + T\sin\alpha = \bar{q}S\,K_{\alpha_2}(x,\Phi)\,\alpha$, where the coefficient $K_{\alpha_2}(x,\Phi)$ is bounded in the feasible set $\mathcal{A}$. As a result, using Eqs. (2.3), the (α,Q)-dynamics can be written as

$$\begin{bmatrix} \dot{\alpha} \\ \dot{Q} \end{bmatrix} = \bar{q}S\,G_1(V)\,\delta\, + G_2(x)\,\eta + G_3(x,u) \tag{3.13}$$

where

$$G_1(V) = \begin{bmatrix} -\dfrac{C_L^{\delta_c}}{mV} & -\dfrac{C_L^{\delta_e}}{mV} \\ \dfrac{\bar{c}\,C_M^{\delta_c}}{I_{yy}} & \dfrac{\bar{c}\,C_M^{\delta_e}}{I_{yy}} \end{bmatrix}, \qquad G_2(x) = \bar{q}S \begin{bmatrix} -\dfrac{C_L^{\eta_1}}{mV} & 0 & -\dfrac{C_L^{\eta_2}}{mV} & 0 & -\dfrac{C_L^{\eta_3}}{mV} & 0 \\ \dfrac{\bar{c}\,C_M^{\eta_1}}{I_{yy}} & 0 & \dfrac{\bar{c}\,C_M^{\eta_2}}{I_{yy}} & 0 & \dfrac{\bar{c}\,C_M^{\eta_3}}{I_{yy}} & 0 \end{bmatrix}$$

$$G_3(x,u) = \begin{bmatrix} -\dfrac{\bar{q}S}{mV}\left(K_{\alpha_2}(x,\Phi)\,\alpha + C_L^0\right) + Q + \dfrac{g}{V}\cos\gamma \\ \dfrac{\bar{q}\,S\,\bar{c}}{I_{yy}}\left(C_M^{\alpha^2}\alpha^2 + C_M^{\alpha}\alpha + C_M^0\right) + \dfrac{z_T}{I_{yy}}\,T \end{bmatrix}.$$

The change of coordinates

$$\chi = \eta - B_X\,G_1^{-1}(V_{\mathrm{r}}) \begin{bmatrix} \alpha \\ Q \end{bmatrix} + \frac{m}{\cos\alpha^*}\,D_X\,\tilde{V} \tag{3.14}$$

will be applied to equation (3.12), where

$$B_X = \begin{bmatrix} 0 & B_{X_{11}} & 0 & B_{X_{21}} & 0 & B_{X_{31}} \\ 0 & B_{X_{12}} & 0 & B_{X_{22}} & 0 & B_{X_{32}} \end{bmatrix}^T, \qquad D_X = \begin{bmatrix} 0 & D_{X_1} & 0 & D_{X_2} & 0 & D_{X_3} \end{bmatrix}^T$$

are constant matrices to be determined. In particular, B_X will be chosen to remove the explicit dependence of the flexible states on the aerodynamic control surfaces, while D_X will be selected to suppress the term that depends on thrust (hence, on Φ) that appears in the χ-dynamics by way of the second addendum of (3.14). The special structure of the matrix A_4 dictates the selected structure of the matrices B_X and D_X. Since the transformation (3.14) modifies only the time derivative of the flexible modes, it follows that $\chi_{2i-1} = \eta_i$, $i = 1, 2, 3$. This useful property will be exploited later in the section, when the interconnection with the rigid-body dynamics is considered.

Using equations (2.1)–(2.3) and differentiation (3.14) with respect to time, the χ-dynamics are written as

$$\begin{aligned}
\dot{\chi} = &\left[A_\eta - B_X G_1^{-1}(V_\mathrm{r}) G_2(x) - \frac{\bar{q}S}{\cos\alpha^*} D_X C_D^\eta\right]\chi + \left[A_\eta B_X G_1^{-1}(V_\mathrm{r}) - B_X \frac{\partial G_1^{-1}}{\partial V_\mathrm{r}} \dot{V}_\mathrm{r}\right]\begin{bmatrix}\alpha \\ Q\end{bmatrix} \\
&- \frac{m A_\eta D_X}{\cos\alpha^*}\,\tilde{V} + \bar{q}S\left[\left(A_1 - \frac{C_D^\alpha D_X}{\cos\alpha^*}\right)\alpha + \left(A_2 - \frac{C_D^{\alpha^2} D_X}{\cos\alpha^*}\right)\alpha^2 + \left(A_3 - \frac{C_D^0 D_X}{\cos\alpha^*}\right)\right] \\
&+ \bar{q}S\left[\left[A_4 - B_X G_1^{-1}(V_\mathrm{r}) G_1(V)\right]\,\delta - \frac{D_X}{\cos\alpha^*}\left(C_D^{\delta_e^2}\delta_e^2 + C_D^{\delta_e}\delta_e + C_D^{\delta_c^2}\delta_c^2 + C_D^{\delta_c}\delta_c\right)\right] \\
&- \frac{mg\sin\gamma}{\cos\alpha^*} D_X - \frac{m D_X}{\cos\alpha^*}\dot{V}_\mathrm{r} - B_X G_1^{-1}(V_\mathrm{r})\, G_3(x,u) + \frac{\cos\alpha}{\cos\alpha^*} D_X\, T\,. \qquad (3.15)
\end{aligned}$$

Note that only the last two terms in equation (3.15) depend on T. Defining

$$\begin{aligned}
N_i^{M\delta} &:= C_M^{\delta_e} B_{X_{i1}} - C_M^{\delta_c} B_{X_{i2}}\,, \qquad & N_i^{L\delta} &:= C_L^{\delta_e} B_{X_{i1}} - C_L^{\delta_c} B_{X_{i2}}\,, \quad i = 1,2,3 \\
C_A &:= \frac{1}{C_M^{\delta_c} C_L^{\delta_e} - C_L^{\delta_c} C_M^{\delta_e}}\,, & C_B &:= \frac{C_A z_T}{\bar{c}\,\cos\alpha^*}
\end{aligned}$$

and using the assumption $\cos\alpha \approx \cos\alpha^*$, which is valid within the bounds given in Table 3.1, it is seen that the choice

$$D_X \;=\; \frac{C_A z_T}{\bar{c}}\,\begin{bmatrix}0 & N_1^{L\delta} & 0 & N_2^{L\delta} & 0 & N_3^{L\delta}\end{bmatrix}^T$$

removes the occurrence of T in Eq. (3.15). The terms in Eq. (3.15) which depend on δ, that is,

$$\left[A_4 - B_X G_1^{-1}(V_{\rm r}) G_1(V)\right]\ \delta\ -\ \frac{D_X}{\cos\alpha^*}\left[C_D^{\delta_e^2}\delta_e^2 + C_D^{\delta_e}\delta_e + C_D^{\delta_c^2}\delta_c^2 + C_D^{\delta_c}\delta_c\right]$$

can be gathered into the vector

$$C^\delta\left(\delta_c, \delta_e, \bar{V}\right) = \left[0 \quad C_1^\delta\left(\delta_c, \delta_e, \bar{V}\right) \quad 0 \quad C_2^\delta\left(\delta_c, \delta_e, \bar{V}\right) \quad 0 \quad C_3^\delta\left(\delta_c, \delta_e, \bar{V}\right)\right]^T$$

where $\bar{V} := \tilde{V}/V$, and

$$\begin{aligned} C_i^\delta\left(\delta_c, \delta_e, \bar{V}\right) \ &= \ N_i^{\delta_c}\delta_c + N_i^{\delta_e}\delta_e - C_B N_i^{L\delta}\left[C_D^{\delta_e^2}\delta_e^2 + C_D^{\delta_e}\delta_e + C_D^{\delta_c^2}\delta_c^2 + C_D^{\delta_c}\delta_c\right] \\ &\quad -B_{Xi1}\delta_c - B_{Xi2}\delta_e - C_A N_i^{M\delta}\left(C_L^{\delta_c}\delta_c + C_L^{\delta_e}\delta_e\right)\bar{V} \qquad\qquad i = 1, 2, 3\,. \end{aligned}$$

The task is now to determine B_X so that the functions C_i^δ are identically zero. Due to the quadratic dependence of C_i^δ on δ, and the presence of the term $\bar{V}$, it is not possible to completely eliminate the input δ from the χ-dynamics using a change of coordinates. Notice that had $G_1^{-1}(V)$ been considered in place of $G_1^{-1}(V_{\rm r})$ in (3.14), the terms multiplied by $\bar{V}$ in C_i^δ would have vanished. However, the time derivative of V would appear instead of $\dot{V}_{\rm r}$ in equation (3.15), and the complexity of the transformed system would have significantly increased. As a compromise, the change of coordinate (3.14) has been adopted, with the coefficients of the matrix B_X selected as the solution of the following optimization problem

$$\left(B_{X_{i1}}, B_{X_{i2}}\right) = \underset{(B_{X_{i1}}, B_{X_{i2}})}{\arg\min}\ \frac{1}{N}\sum_{k=1}^{N}\left[\int_{\delta_{c_{min}}}^{\delta_{c_{max}}} |\, C_i^\delta(\delta_c, 0, \bar{V}_k)|\, d\delta_c + \int_{\delta_{e_{min}}}^{\delta_{e_{max}}} |\, C_i^\delta(0, \delta_e, \bar{V}_k)|\, d\delta_e\right] [2mm]$$

where $\bar{V}$ is evaluated on a grid $\{\bar{V}_k\}_{k=1}^N$ of feasible values. Although this choice for $B_{X_{i1}}$ and $B_{X_{i2}}$ does not render the functions C_i^δ identically zero, the effect of the aerodynamic control surfaces on the flexible states is significantly reduced so that the terms C_i^δ can be neglected. This is confirmed by the plots in Figure 3.4, which show a comparison between the influence of the input δ on the generalized elastic

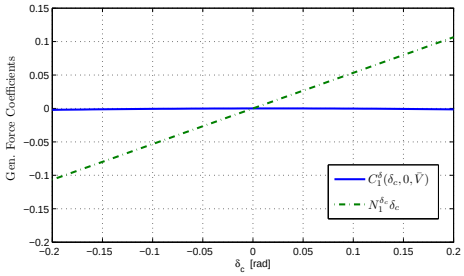

(a) Comparison between $N_1^{\delta_c}\delta_c$ and $C_1^\delta(\delta_c, 0, \bar{V})$.

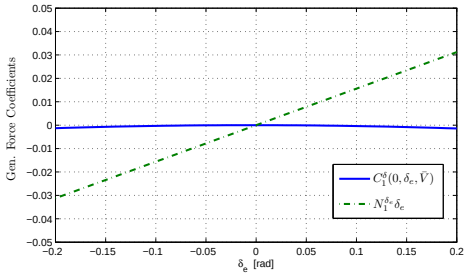

(b) Comparison between $N_1^{\delta_e}\delta_e$ and $C_1^\delta(0, \delta_e, \bar{V})$.

Figure 3.4: Influence of the control surfaces on the original flexible dynamics and after the change of coordinates. In the plots, the representative value $\bar{V} = 6 \times 10^{-3}$ has been selected.

forces before and after the change of coordinates. Letting $\sin\gamma \approx \gamma$, the change of coordinates (3.14) transforms Eq. (3.15) into

$$\dot{\chi} = \left(A_{\rm st} + A_{\rm p} \right) \chi + J_0 + J_1\,\alpha + J_2\,\alpha^2 + J_3\,Q + J_4\,\tilde{V} + J_5\,\gamma \tag{3.16}$$

where the vectors J_i , $0 \le i \le 5$, are given in Appendix B.1, the matrices $A_{\rm st}$ and $A_{\rm p}$ are

$$A_{\rm st} = \begin{bmatrix} 0 & 1 & 0 & 0 & 0 & 0 \\ -\omega_1^2 & -2\zeta_1\omega_1 & 0 & 0 & 0 & 0 \\ 0 & 0 & 0 & 1 & 0 & 0 \\ 0 & 0 & -\omega_2^2 & -2\zeta_2\omega_2 & 0 & 0 \\ 0 & 0 & 0 & 0 & 0 & 1 \\ 0 & 0 & 0 & 0 & -\omega_3^2 & -2\zeta_3\omega_3 \end{bmatrix}, \quad A_{\rm p} = \begin{bmatrix} 0 & 0 & 0 & 0 & 0 & 0 \\ P_{11} & 0 & P_{12} & 0 & P_{13} & 0 \\ 0 & 0 & 0 & 0 & 0 & 0 \\ P_{21} & 0 & P_{22} & 0 & P_{23} & 0 \\ 0 & 0 & 0 & 0 & 0 & 0 \\ P_{31} & 0 & P_{32} & 0 & P_{33} & 0 \end{bmatrix}$$

and

$$P_{jk} = \bar{q}S \left[N_j^{\eta_k} + C_A \left(N_j^{M\delta} C_L^{\eta_k} V_{\rm r}/V - N_j^{L\delta} C_M^{\eta_k} \right) - C_B N_j^{L\delta} C_D^{\eta_k} \right] \qquad 1 \le j,k \le 3\,.$$

Since the damping ratios, ζ_i, are positive and the frequencies ω_i are positive and distinct, the matrix $A_{\rm st}$ is Hurwitz and $A_{\rm p}$ can be seen as a nonlinear perturbation on the asymptotically stable part of the χ-dynamics (notice that the coefficients of $A_{\rm p}$ depend on the rigid-body states and the reference trajectory). By substituting $\gamma = \tilde{\gamma} - k_2\tilde{h} + \dot{h}_{\rm r}/V_{\rm r}$, $\alpha = \alpha^* - \tilde{\gamma} + \tilde{\alpha}$ and $Q = \tilde{Q} - k_4\tilde{\alpha} + k_2^2\, V_{\rm r}\, \tilde{h} - k_2\, V_{\rm r}\, \tilde{\gamma} - k_2\, \tilde{V}\sin\gamma - \dot{V}_{\rm r}\dot{h}_{\rm r}/V_{\rm r}^2 + \ddot{h}_{\rm r}/V_{\rm r}$ in Eq. (3.16), the χ-dynamics is written as

$$\begin{aligned}\dot{\chi} \;=\; (\,A_{\rm st} + A_{\rm p}\,)\,\chi &+ \big(k_2^2\, V_{\rm r}\, J_3 - k_2 J_5\big)\tilde{h} \;-\; \big(J_1 + 2\,J_2\,\alpha^* + k_2 V_{\rm r}\, J_3 - J_5\big)\tilde{\gamma} + J_2\,(\tilde{\alpha} - \tilde{\gamma})^2 \\ &+\big(J_1 + 2\,J_2\,\alpha^* - k_4\,J_3\big)\tilde{\alpha} + J_3\tilde{Q} + \big(J_4 - k_2\,\sin\gamma\,J_3\big)\,\tilde{V} \\ &+J_0 + J_1\alpha^* + J_2{\alpha^*}^2 + \big(\ddot{h}_{\rm r}/V_{\rm r} - \dot{h}_{\rm r}\dot{V}_{\rm r}/V_{\rm r}^2\big)J_3 + J_5\,\dot{h}_{\rm r}/V_{\rm r} \qquad (3.17)\end{aligned}$$

A closer look at the terms on the right-hand side of Eq. (3.17) reveals that $(\ddot{h}_{\rm r}/V_{\rm r} - \dot{h}_{\rm r}\dot{V}_{\rm r}/V_{\rm r}^2)J_3 + J_5\,\dot{h}_{\rm r}/V_{\rm r}$ is a bounded perturbation vanishing at trim, whereas $J_0 + J_1\alpha^* + J_2{\alpha^*}^2$ is a non-vanishing term that determines the steady-state value χ^* of $\chi(t)$. As a result, the analysis of the stability properties of the equilibrium point $\chi = \chi^*$ of (3.17) is reduced to studying the stability properties of the origin of the nonlinear system

$$\dot{\tilde{\chi}} \;=\; [\,A_{\rm st} + A_{\rm p}(x, y_{\rm r})\,]\,\tilde{\chi} + B(x, y_{\rm r})\tilde{x} \qquad (3.18)$$

where $\tilde{\chi} = \chi - \chi^*$ and

$$\begin{aligned}B(x, y_{\rm r}) \;=\; \big[\; & J_4 - k_2\,\sin\gamma\,J_3 \quad k_2^2\, V_{\rm r}\, J_3 - k_2 J_5 \quad J_2\tilde{\gamma} - 2J_2\tilde{\alpha} - J_1 - 2J_2\,\alpha^* - k_2 V_{\rm r}\, J_3 + J_5 \\ & J_2\tilde{\alpha} + J_1 + 2J_2\,\alpha^* - k_4\,J_3 \quad J_3\,\big]\end{aligned}$$

System (3.18) is the required representation of the internal dynamics of the closed-loop system which arises when the structural flexibilities are taken into consideration.

3.2.1 Stability Analysis of the Zero-dynamics

A necessary step towards the analysis of the interconnection of systems (3.10) and (3.18) is the investigation of the stability of its zero-dynamics, that is, the system

$$\dot{\tilde{\chi}} = \big[\, A_{\rm st} + A_{\rm p}(x, y_{\rm r}) \,\big]\, \tilde{\chi} \tag{3.19}$$

obtained by setting $\tilde{x} = 0$ in Eq. (3.18). A Lyapunov function candidate for (3.19) is obtained from the Lyapunov equation for the Hurwitz matrix $A_{\rm st}$. Specifically, the matrices

$$A_i = \begin{bmatrix} 0 & 1 \\ -\omega_i^2 & -2\zeta_i\omega_i \end{bmatrix}, \qquad P_i = \begin{bmatrix} \dfrac{1+\omega_i^2+4\zeta_i^2}{4\,\zeta_i\,\omega_i} & \dfrac{1}{2\,\omega_i^2} \\ \dfrac{1}{2\,\omega_i^2} & \dfrac{1+\omega_i^2}{4\,\zeta_i\,\omega_i^3} \end{bmatrix}, \qquad i = 1, 2, 3$$

satisfy the Lyapunov equation $P_i A_i + A_i^T P_i = -I_{2\times 2}$, and P_i is positive definite since $\zeta_i > 0$. Recalling that $A_{\rm st} = \mathrm{diag}\{A_1, A_2, A_3\}$, the Lyapunov function candidate for system (3.19) is selected as

$$W_{\rm f}(\tilde{\chi}) = \sigma_\chi\, \tilde{\chi}^T P \tilde{\chi} \tag{3.20}$$

where $P := \mathrm{diag}\{P_1, P_2, P_3\}$ and σ_χ is a positive scaling factor. By construction, the derivative of $W_{\rm f}$ along the vector field of system (3.19) satisfies

$$\dot{W}_{\rm f}(\tilde{\chi}) = -\sigma_\chi\, \tilde{\chi}^T \big[\, I_{6\times 6} - (\, P A_{\rm p}^T + A_{\rm p} P) \big] \tilde{\chi}$$

therefore the origin of system (3.19) is asymptotically stable if the perturbation $A_{\rm p}$ is small enough so as to satisfy $P A_{\rm p}^T + A_{\rm p} P < I_{6\times 6}$. Note that the entries of $A_{\rm p}$ depend on the model parameters, $\bar{q}$, V and $V_{\rm r}$. Thus, the Lyapunov equation above gives a method to ascertain the stability of the internal dynamics in terms of current and desired flight conditions.

For the model under investigation, it has been verified numerically that the above stability condition on the matrix $A_{\rm p}$ holds in the feasible set $\mathcal{A}$, and for all $p \in \mathcal{P}$.

Consequently, the origin of system (3.19) is robustly asymptotically stable, and there exists a constant symmetric and positive definite matrix $\bar{R}_{\rm f}$ such that, for any $x \in \mathcal{A}$ and $p \in \mathcal{P}$, the derivative of $W_{\rm f}(\tilde{\chi})$ along trajectories of system (3.18) satisfies

$$\dot{W}_{\rm f}(\tilde{\chi}) \leq -\sigma_\chi \tilde{\chi}^T \bar{R}_{\rm f}\, \tilde{\chi} + \tilde{\chi}^T R_{\rm fl,rb}(x, y_{\rm ref})\, \tilde{x} \tag{3.21}$$

where $R_{\rm fl,rb}(x, y_{\rm r}) := 2\sigma_\chi P B(x, y_{\rm r})$.

3.2.2 Stability Analysis of the Overall Closed-loop System

The last step of the stability analysis is to consider explicitly the overall system (3.10)–(3.18), since the stability of the internal dynamics and the rigid-body closed-loop system alone does not guarantee stability of the interconnection. Unsurprisingly, the analysis is carried out by using $W(\tilde{x}, \tilde{\chi}, \tilde{\vartheta}) = W_{\rm rb}(\tilde{x}, \tilde{\vartheta}) + W_{\rm f}(\tilde{\chi})$ as a Lyapunov function candidate.

Let $\Omega_c(W) = \{\tilde{x}, \tilde{\chi}, \tilde{\vartheta} \,|\, W(\tilde{x}, \tilde{\chi}, \tilde{\vartheta}) \leq c\}$ be the level set corresponding to the value $c > 0$ defined in Section 3.1.1, so that properties a.1)–a.3) continue to hold with W replacing $W_{\rm rb}$, and choose $\sigma_\chi > 0$ small enough so that $\Xi_0^{\tilde{\eta}} \subset \Omega_c(W)$. As a result, property a.1) is replaced by

b.1) $\Xi_0^{\tilde{x}} \times \Xi_0^{\tilde{\eta}} \subset \Omega_c(W)$, for all $x \in \mathcal{A}$, $p \in \mathcal{P}$.

As mentioned, the particular structure of the matrices B_X and D_X employed in the transformation (3.14) plays an important role. Looking at the definition of the vectors C_i^η, $i = T, M, L, D$, in Eq. (2.3), it is immediately concluded that $C_i^\eta B_X = 0$ and $C_i^\eta D_X = 0$. This, in turn, implies that $C_i^\eta \eta = C_i^\eta \chi$, and, since the trim value $\chi^* = \eta^* - B_X G_1^{-1}(V^*)[\alpha^*\ 0]^T$ satisfies $\chi^*_{2i-1} = \eta_i^*$, $i = 1, 2, 3$, this also implies $C_i^\eta \tilde{\eta} = C_i^\eta \tilde{\chi}$, $i = T, M, L, D$. As a result, the derivative of W along trajectories of system (3.10)–(3.18) satisfies

$$\dot{W}(\tilde{x}, \tilde{\chi}, \tilde{\vartheta}) \leq -[\tilde{\chi}^T\, \tilde{x}^T]\, R(x, y_{\rm r})\, [\tilde{\chi}^T\, \tilde{x}^T]^T \tag{3.22}$$

where

$$R(x, y_{\rm r}) = \begin{bmatrix} \sigma_\chi \bar{R}_f & -\frac{1}{2}R_{\rm fl,rb}(x, y_{\rm r}) - \frac{1}{2}R_{\rm rb,fl}(x)^T \\ -\frac{1}{2}R_{\rm fl,rb}(x, y_{\rm r})^T - \frac{1}{2}R_{\rm rb,fl}(x) & R_{\rm rb}(x) \end{bmatrix}$$

It is important to notice that the off-diagonal terms of the matrix $R(x, y_{\rm r})$ depend on the controller gains k_2 and k_4 relative to the altitude and angle-of-attack loops. Consequently, the influence of these gains on the stability of the closed-loop system is fundamentally different from the case analyzed in Proposition 3.1.1, when the internal dynamics was ignored. The following proposition constitutes the main result of the paper:

Proposition 3.2.1. *Consider the closed-loop system given by Eqs.* (3.10) *and* (3.18)*, and the Lyapunov function candidate* $W(\tilde{x}, \tilde{\chi}, \tilde{\vartheta})$*. Let the level set* $\Omega_c(W)$ *and the scaling factors of* W *be chosen to satisfy conditions b.1), a.2) and a.3). Then, there exist constants* $k_1^\star > 0$*,* $k_2^\star > 0$*,* $k_3^\star > 0$*,* $k_5^\star > 0$ *and* $0 < \underline{k}_4^\star < \overline{k}_4^\star$ *such that for any* $k_1 > k_1^\star$*,* $0 < k_2 < k_2^\star$*,* $k_3 > k_3^\star$*,* $\underline{k}_4^\star < k_4 < \overline{k}_4^\star$ *and* $k_5 > k_5^\star$*, the trajectories of the closed-loop system originating within* $\Omega_c(W)$ *are bounded and satisfy* $\lim_{t\to\infty} \tilde{x}(t) = 0$*,* $\lim_{t\to\infty} \tilde{\eta}(t) = 0$*.*

Proof. To proceed with the analysis, we define upper bounds on the off-diagonal terms of R as follows:

$$\begin{aligned}
R_V(k_2) &:= \max_{x\in\mathcal{A},\, p\in\mathcal{P}} \left\{ \sigma_\chi \|P\| \, \|J_4 - k_2 \sin\gamma \, J_3\| + (\bar{q}S\sigma_V/2)\|C_T^\eta \cos\alpha - C_D^\eta\| \right\} \\
R_h(k_2) &:= \sigma_\chi \, k_2 \max_{x\in\mathcal{A},\, p\in\mathcal{P}} \left\{ \|PJ_5\| + V_{\rm r} \, \|PJ_3\| \, k_2 \right\} \\
R_\gamma(k_2) &:= \max_{x\in\mathcal{A},\, p\in\mathcal{P}} \left\{ \sigma_\chi \|P\| \, \|J_1 + (2\tilde{\alpha} + 2\alpha^* - \tilde{\gamma}) \, J_2 + k_2 V_{\rm r} \, J_3 - J_5 \| \right. \\
&\qquad \left. + \bar{q}S \, \|C_T^\eta \sin\alpha^* + C_L^\eta\| \, /(2V) \right\} \\
R_\alpha(k_4) &:= \max_{x\in\mathcal{A},\, p\in\mathcal{P}} \left\{ \sigma_\chi \|P\| \, \|J_1 + (\tilde{\alpha} + 2\alpha^*) \, J_2\| + \sigma_\chi \, \| \, PJ_3\| k_4 \right\} \\
R_Q &:= \max_{x\in\mathcal{A},\, p\in\mathcal{P}} \left\{ \sigma_\chi \|PJ_3\| + \bar{q}S\sigma_Q \, \|z_T C_T^\eta + \bar{c} \, C_M^\eta\| / (2I_{yy}) \right\}
\end{aligned}$$

and let for notational convenience $V_{\min} := \min_{\mathcal{A}} V = \min_{\mathcal{A}} V_{\mathrm{r}}$, and

$$R_h(k_2) := \sigma_\chi \, k_2 \big(R_{\gamma_0} + \, R_{\gamma_1} k_2 \big) \,, \qquad R_\alpha(k_4) := \big(\sigma_\chi \, R_{\alpha_0} + \sigma_\chi \, R_{\alpha_1} k_4 \big) \,.$$

Rearranging the elements of the vector $\tilde{x}$ and considering norms term by term, inequality (3.22) can be further bounded as

$$\dot{W}(\tilde{x}, \tilde{\chi}, \tilde{\vartheta}) \leq - \big[\, \|\tilde{\chi}\| \;\; |\tilde{h}| \;\; |\tilde{\alpha}| \;\; |\tilde{\gamma}| \;\; |\tilde{Q}| \;\; |\tilde{V}| \, \big] \, \bar{R} \, \big[\, \|\tilde{\chi}\| \;\; |\tilde{h}| \;\; |\tilde{\alpha}| \;\; |\tilde{\gamma}| \;\; |\tilde{Q}| \;\; |\tilde{V}| \, \big]^T$$

where

$$\bar{R} = \left[\begin{array}{c|ccccc} \sigma_\chi \lambda_{\mathrm{f}} & -R_h(k_2) & -R_\alpha(k_4) & -R_\gamma(k_2) & -R_Q & -R_V(k_2) \\ \hline -R_h(k_2) & k_2 \sigma_h V_{\min} & 0 & -R_{13}^{\mathrm{rb}} & 0 & -R_{15}^{\mathrm{rb}} \\ -R_\alpha(k_4) & 0 & \sigma_\alpha k_4 & -R_{23}^{\mathrm{rb}} & -R_{24}^{\mathrm{rb}}(k_4) & 0 \\ -R_\gamma(k_2) & -R_{13}^{\mathrm{rb}} & -R_{23}^{\mathrm{rb}} & (k_m + k_c k_3) V_{\min} & 0 & 0 \\ -R_Q & 0 & -R_{24}^{\mathrm{rb}}(k_4) & 0 & \sigma_Q (k_5 - k_4) & 0 \\ -R_V(k_2) & -R_{15}^{\mathrm{rb}} & 0 & 0 & 0 & k_1 \sigma_V \end{array}\right]$$

$$R_{13}^{\mathrm{rb}} = \frac{\sigma_h \, \max_{\mathcal{A}} V_{\mathrm{r}}}{2} \qquad\qquad R_{15}^{\mathrm{rb}} = \frac{\sigma_h \, \max_{\mathcal{A}} |\gamma \,|}{2}$$

$$R_{23}^{\mathrm{rb}} = \frac{k_M \, \max_{\mathcal{A}} V}{2} \qquad\qquad R_{24}^{\mathrm{rb}}(k_4) = \frac{|\sigma_\alpha - \sigma_Q k_4^2|}{2}$$

and $\lambda_{\mathrm{f}} > 0$ denotes the smallest eigenvalue of $\bar{R}_{\mathrm{f}}$. As before, let Δ_i denote the determinant associated with i-th order upper-left sub-matrix of $\bar{R}$. Clearly, $\Delta_1 = \sigma_\chi \lambda_{\mathrm{f}} > 0$. Since

$$\Delta_2 = \sigma_\chi \sigma_h \lambda_{\mathrm{f}} \, k_2 V_{\min} - R_h^2(k_2) = \sigma_\chi \sigma_h \lambda_{\mathrm{f}} \, k_2 \, V_{\min} - \sigma_\chi^2 \, k_2^2 \, \left(R_{\gamma_0} + \, R_{\gamma_1} k_2 \right)^2 \,,$$

it follows that for any $\lambda_{\mathrm{f}}, \sigma_h, \sigma_\chi > 0$ there exists $k_2^\star > 0$ such that $\sigma_\chi k_2^\star \, (R_{\gamma_0} + \, R_{\gamma_1} k_2^\star)^2 <$

$\sigma_h \lambda_{\rm f} V_{\rm min}$. Therefore, Δ_2 is positive for any $0 < k_2 < k_2^\star$. On the other hand, the determinant Δ_3, given by

$$\begin{aligned}\Delta_3 &= \Delta_2\, \sigma_\alpha k_4 - k_2\, \sigma_h V_{\rm min} R_\alpha^2(k_4) \\ &= \Big[\sigma_\chi \sigma_h \lambda_{\rm f}\, k_2\, V_{\rm min} - \sigma_\chi^2\, k_2^2 \big(R_{\gamma_0} + R_{\gamma_1} k_2\big)^2\Big]\, \sigma_\alpha k_4 - k_2\, \sigma_h V_{\rm min} \sigma_\chi^2\, (\, R_{\alpha_0} + R_{\alpha_1} k_4)^2\end{aligned}$$

is strictly positive if and only if the quadratic function of k_4, defined as,

$$\begin{aligned}f(k_4) \;:=\; & \sigma_h \sigma_\chi V_{\rm min} R_{\alpha_1}^2 k_4^2 + \Big[2\sigma_h \sigma_\chi V_{\rm min} R_{\alpha_0} R_{\alpha_1} + \sigma_\chi \sigma_\alpha k_2 \big(R_{\gamma_0} + R_{\gamma_1} k_2\big)^2 \\ & - \sigma_h \sigma_\alpha \lambda_{\rm f} V_{\rm min}\Big]\, k_4 + \sigma_h \sigma_\chi V_{\rm min} R_{\alpha_0}^2\end{aligned}$$

is strictly negative. This condition, differently from the ones found so far, cannot be satisfied simply by increasing or decreasing k_4. In particular, it is necessary to analyze the function $f(k_4)$ to verify an interval $(\underline{k}_4^\star, \overline{k}_4^\star)$ where $f(k_4)$ is negative exists, and consequently Δ_3 can be made positive. Since the leading coefficient of k_4 is positive, $f(k_4)$ is a concave upward parabola whose intersection with the vertical axis is $\sigma_h \sigma_\chi R_{\alpha_0}^2 > 0$. As a result, the required interval $(\underline{k}_4^\star, \overline{k}_4^\star)$ exists if and only if the following two conditions are satisfied

$$\begin{aligned}&\Big[2\sigma_h \sigma_\chi V_{\rm min} R_{\alpha_0} R_{\alpha_1} + \sigma_\chi \sigma_\alpha k_2 \big(R_{\gamma_0} + R_{\gamma_1} k_2\big)^2 - \sigma_h \sigma_\alpha \lambda_{\rm f} V_{\rm min}\Big]^2 - 4\sigma_h^2 \sigma_\chi^2 R_{\alpha_1}^2 R_{\alpha_0}^2 V_{\rm min}^2 > 0 \\ &2\sigma_h \sigma_\chi V_{\rm min} R_{\alpha_0} R_{\alpha_1} + \sigma_\chi \sigma_\alpha k_2 \big(R_{\gamma_0} + R_{\gamma_1} k_2\big)^2 - \sigma_h \sigma_\alpha \lambda_{\rm f} V_{\rm min} < 0 \qquad (3.23)\end{aligned}$$

It is easy to see that, given any fixed positive value of $\sigma_h, \sigma_\alpha, \lambda_{\rm f}$ and k_2, there exists $\sigma_\chi^\star > 0$ such that conditions (3.23) are met for any $0 < \sigma_\chi < \sigma_\chi^\star$. This implies that there exists an interval for values of k_4 which render Δ_3 strictly positive only if σ_χ is chosen small enough. The crucial thing to notice is that the original value of the scaling factor σ_χ can always be lowered to be made smaller than $\sigma_\chi^\star$ without shrinking the domain of attraction, that is, without affecting the property b.1), and thus the interval $(\underline{k}_4^\star, \overline{k}_4^\star)$ is guaranteed to exist. Finally, notice that the determinants (Δ_1,

Δ_2, Δ_3) do not depend on k_3, (Δ_1, Δ_2, Δ_3, Δ_4) do not depend on k_5, and (Δ_1, Δ_2, Δ_3, Δ_4,Δ_5) do not depend on k_1. Consequently, for any fixed $k_2, k_4 > 0$ there exist $k_3^\star > 0$, $k_5^\star > 0$ and $k_1^\star > 0$ such that, for any $k_3 > k_3^\star$, $k_5 > k_5^\star$ and $k_1 > k_1^\star$, Δ_4, Δ_5 and Δ_6 are strictly positive. By Sylvester's criterion it follows that matrix $\bar{R}$ can be made positive definite by choice of the controller gains. Arguments similar to those invoked in the proof of Proposition 3.1.1 imply that all trajectories of the closed-loop system are bounded, and that the error trajectories $\tilde{x}(t)$, $\tilde{\chi}(t)$ are regulated to zero asymptotically. By virtue of Eq. (3.14) and the fact that $\chi^* = \eta^* - B_X G_1^{-1}(V^*)[\alpha^*\ 0]^T$, this also implies that $\tilde{\eta}(t)$ converges to zero asymptotically. □

The existence of a finite interval for the stabilizing values of k_4 (i.e., conditional stability) and the finite stability margin for k_2 are both consequence of the peaking phenomenon[16] exhibited by the internal dynamics, which is due to the simultaneous appearance of α and Q in Eq. (3.16). Thus, the overall closed-loop system can not be stabilized by purely low-gain or high-gain feedback [15]. Had the peaking phenomenon not occurred, the term R_{α_0} would have been zero and therefore Δ_3 could have been rendered positive simply by lowering the value of the gain k_4. The difference with the case in which only the rigid-body dynamics is considered in the closed-loop system is very significant, especially regarding the role of k_2. For the sake of comparison, a schematic representation of the gain stability margins for k_2 and k_4 is depicted in Figure 3.5, for the results or Propositions 3.1.1 and 3.2.1, respectively. Since a non-zero value of the gain k_3 is required for stability, it is seen that the canard input plays a fundamental role for robust stabilization in presence of structural flexibilities.

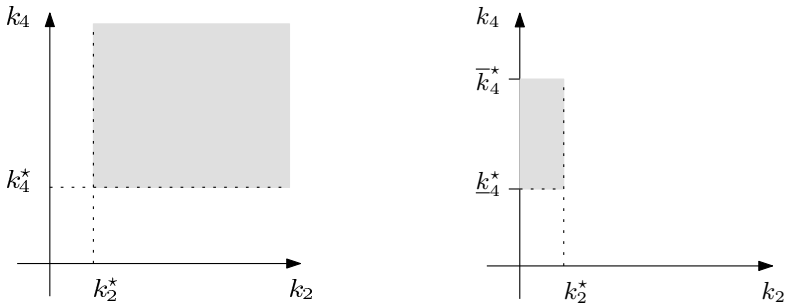

(a) Rigid-body dynamics

(b) Flexible-body dynamics

Figure 3.5: Representation of the region of stability for the gains k_2 and k_4, resulting from the analysis without flexible dynamics (a) and after incorporation of the flexible dynamics (b).

3.3 Simulations

The performance of the controller derived in the previous section has been tested in simulation using the full SM implemented in SIMULINK®. Two representative case studies will be presented here, corresponding respectively to a climbing maneuver at constant dynamic pressure, and a climbing maneuver with longitudinal acceleration using separate reference commands for altitude and velocity. The initial and final trim conditions for each case study are reported in Table 3.2. In both cases, the reference commands have been generated by filtering step reference commands by a second-order pre-filter with natural frequency $\omega_f = 0.03$ rad/s and damping factor $\zeta_f = 0.95$. The SM includes appropriate saturation blocks at the plant input, set respectively at the corresponding values in Table 3.1. In this study, the constraints are dealt with indirectly by tuning the controller gains, including the parameters of the pre-filter of the reference model. The controller gains used in all simulations are shown in Table 3.3. To take into further account the parameter uncertainty of the

CDM1, the initial condition of the controller parameter vector $\hat{\vartheta}$ has been selected randomly within a 40% variation of the nominal value of the parameter vector ϑ.

In the first simulation study, the vehicle is initially at trim. The reference $h_{\mathrm{r}}(t)$ is generated to let the vehicle climb 13000 ft in about 350 s, whereas the velocity reference is computed according to the relation $V_{\mathrm{r}}(t) = \left[2\bar{q}\exp((h_{\mathrm{r}}(t) - h_0)/h_s)/\rho_0\right]^{1/2}$ to maintain constant dynamic pressure at $\bar{q} = 1982$ psf throughout the maneuver. The results of the simulation confirm that the controller provides stable tracking of the reference trajectories and convergence to the desired trim condition. More specifically, the tracking performance for the velocity and altitude is shown in Figures 3.6(a)–3.6(b), where it is seen that the tracking error remains remarkably small during the entire maneuver and vanishes asymptotically. Figure 3.6(c) shows the tracking performance of the flight-path angle command, whereas the behavior of the angle-of-attack is given in the top plot of Figure 3.6(d). As a representative of the state variables of the adaptive controller, the bottom plot shows the time history of the crucial parameter estimate $\hat{\vartheta}_{2,1}(t)$, corresponding to the coefficient $\vartheta_{2,1} = C_L^{\delta_e}/C_L^{\delta_c}$ which provides

	Case study 1		Case study 2	
Variable	Initial condition (trim)	Final trim	Initial condition	Final trim
V	7850 ft/s	10640 ft/s	7850 ft/s	10500 ft/s
h	86000 ft	99000 ft	86000 ft	111000 ft
α	1.36 deg	1.71 deg	2 deg	1.5 deg
$\bar{q}$	1982 psf	1982 psf	1982 psf	1153 psf

Table 3.2: Initial and desired final conditions for the regulated output and dynamic pressure

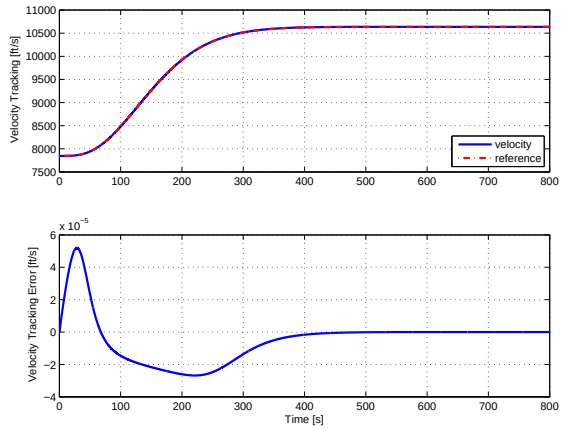

(a) $V(t)$ and $V_{\mathrm{r}}(t)$ (top), and $\tilde{V}(t)$ (bottom)

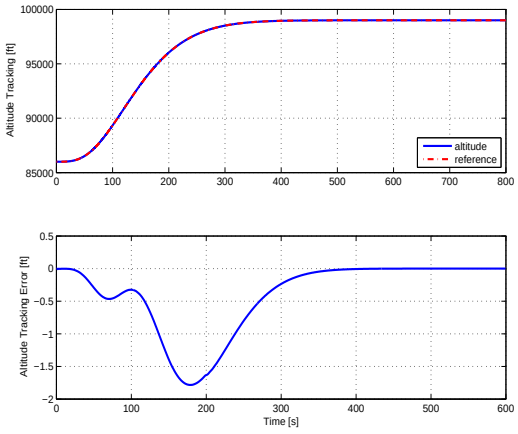

(b) $h(t)$ and $h_{\mathrm{r}}(t)$ (top), and $\tilde{h}(t)$ (bottom)

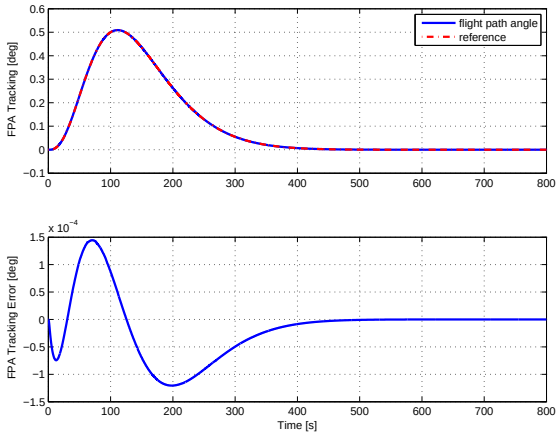

(c) $\gamma(t)$ and $\gamma_{\mathrm{cmd}}(t)$ (top), and $\tilde{\gamma}(t)$ (bottom)

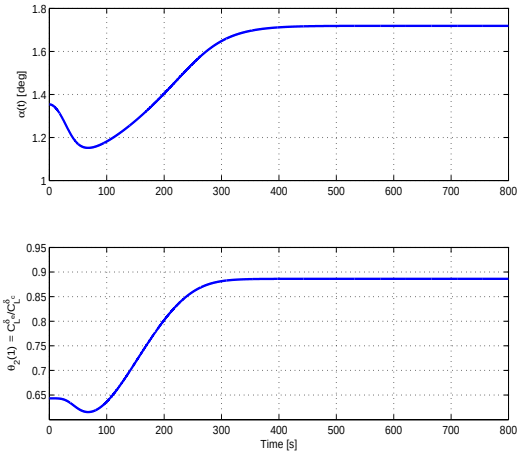

(d) $\alpha(t)$ (top) and $\hat{\vartheta}_{2,1}(t)$ (bottom)

Figure 3.6: Case study 1: Climb at constant dynamic pressure, $\bar{q} = 1982$ psf. (a) Velocity, (b) altitude and (c) flight-path angle tracking performance. (d) Angle-of-attack and parameter estimate $\hat{\vartheta}_{1,2}$.

cancellation of the elevator-to-lift coupling. The flexible modes $\eta(t)$, shown in Figure 3.7(a), remain damped throughout the maneuver. Finally, Figure 3.7(b) shows that the control inputs range within their bounds.

The second case study considers a more aggressive maneuver, where the altitude and velocity reference trajectories are defined independently. In particular, $h_{\mathrm{r}}(t)$ is

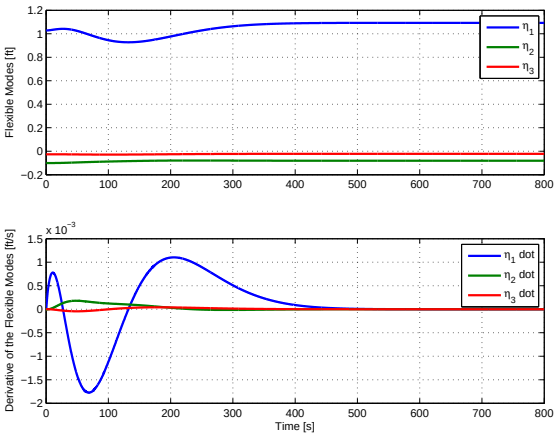

(a) $\eta(t)$ (top) and $\dot{\eta}(t)$ (bottom)

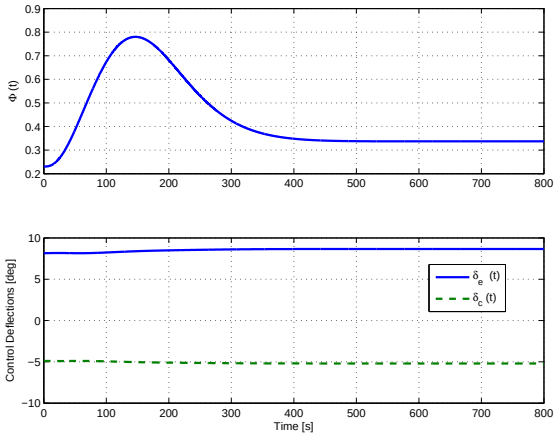

(b) $\Phi(t)$ (top) and $\delta_c(t)$, $\delta_e(t)$ (bottom)

Figure 3.7: Case study 1: Climb at constant dynamic pressure, $\bar{q} = 1982$ psf. (a) Flexible modes, (b) control inputs.

generated to let the vehicle climb 25000 ft in about $250s$, corresponding to a climb rate approximately three times faster than the previous case. At the same time, $V_{\mathrm{r}}(t)$ provides a longitudinal acceleration of about 10 ft/s^2, which corresponds to having the dynamic pressure decreasing from $\bar{q} = 1982$ psf at $t = 0$ to $\bar{q} = 1153$ psf at $t = 300$. To make the test more demanding, the initial condition is selected at an off-trim condition, obtained by changing the initial value of the angle-of-attack to

Gain	Value	Gain	Value	Gain Matrix	Value
k_1	200	k_4	50	Γ_1	$0.1 \times I_{16\times16}$
k_2	1×10^{-4}	k_5	60	Γ_2	$0.1 \times I_{5\times5}$
k_3	10			Γ_3	$0.1 \times I_{13\times13}$

Table 3.3: Controller Gains

$\alpha(0) = 2$ deg while keeping the remaining values of $x(0)$ and $u(0)$ unchanged from the previous case study. The desired steady-state value for the angle-of-attack has also been decreased to $\alpha^* = 1.5$ deg. The trim condition reached at the end of the maneuver is shown in the last column of Table 3.2. As in the previous case study, the results of the simulation are shown in Figure 3.8. The performance in closed-loop remain excellent, although the tracking error exhibits a slightly worse transient behavior. This is to be expected due to the more demanding control objective and the fact that the initial condition is not at an equilibrium. In particular, note that the flexible states remain well-behaved despite a larger excitation (see Fig.3.8(e)).

Finally, the performance of the adaptive controller in these two case studies has been compared with results obtained using the approximate feedback linearization controller developed in Parker et al.[28]. For this scheme, the control law is comprised of a fixed-structure dynamic inversion inner-loop and an outer-loop LQG controller with integral error augmentation. The canard is ganged to the elevator to provide cancelation of the elevator-to-lift coupling, computed on the basis of the nominal values of the parameters of the CDM1. For case study 1, simulation results obtained with the approximate dynamic inversion controller are comparable to those obtained with the adaptive controller, although the former exhibit a larger error during transient, and the altitude error takes substantially longer to converge (see Fig. 3.9(a)). On the other hand, for the more demanding control objective in case study 2, the fixed linearization scheme is not capable of providing enough robustness to maintain stable tracking of the reference, as it is visible from Fig. 3.9(b), showing the onset of instability. The simulation stops at about $t = 3.5$ s due to the fact that the engine reaches a condition that does no longer sustain scramjet propulsion. The reason for closed-loop instability can be attributed to the effect of model uncertainty leading to imperfect compensation of the non-minimum phase behavior of the FPA

dynamics, and to the resulting interaction of the pitch dynamics with the structural dynamics. The domain of attraction provided by the fixed controller is reduced as a consequence of residual undesired coupling. This phenomenon was also observed in Ref. [28], where a fine tuning of the gain of the canard input for a given reference trajectory was required to obtain a stable closed-loop behavior. The adaptive controller presented in this work avoids the necessity of such gain scheduling, as it compensates automatically for the model mismatch.

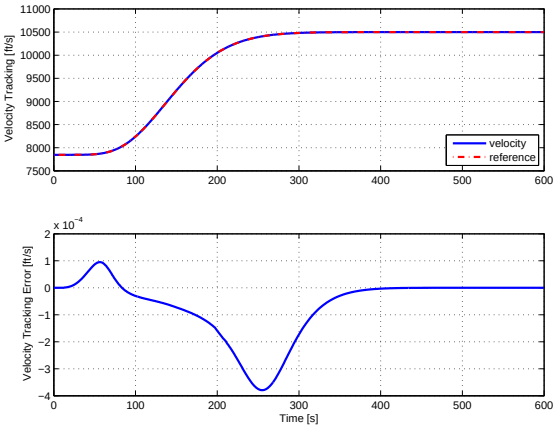

(a) $V(t)$ and $V_{\mathrm{r}}(t)$ (top), and $\tilde{V}(t)$ (bottom)

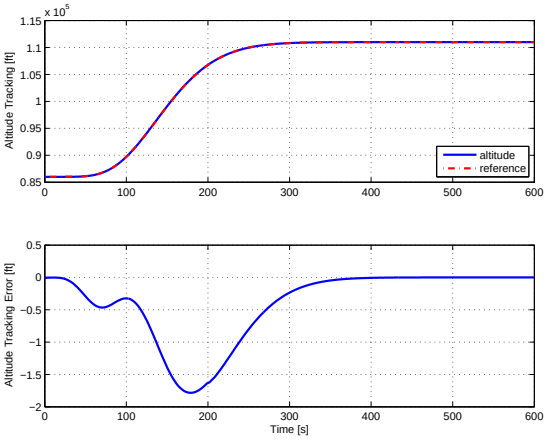

(b) $h(t)$ and $h_{\mathrm{r}}(t)$ (top), and $\tilde{h}(t)$ (bottom)

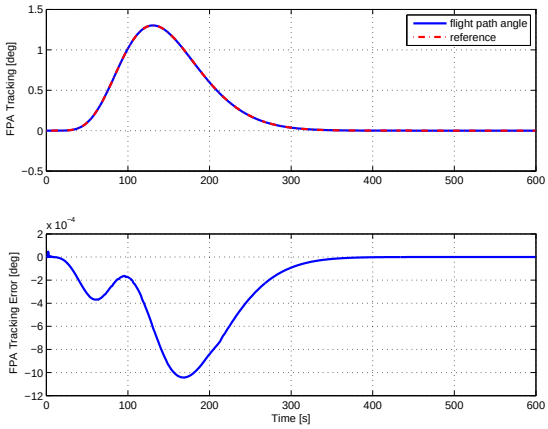

(c) $\gamma(t)$ and $\gamma_{\mathrm{cmd}}(t)$ (top), and $\tilde{\gamma}(t)$ (bottom)

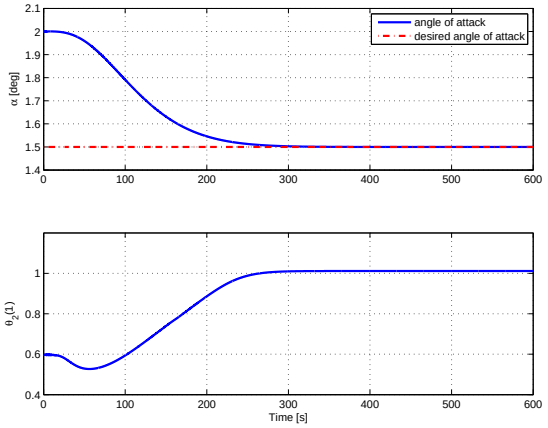

(d) $\alpha(t)$ (top) and $\hat{\vartheta}_{2,1}(t)$ (bottom)

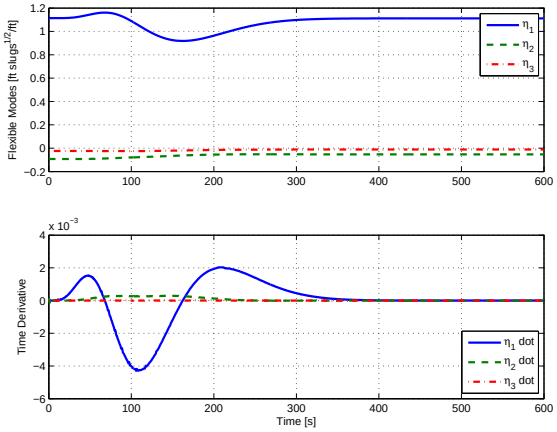

(e) $\eta(t)$ (top) and $\dot{\eta}(t)$ (bottom)

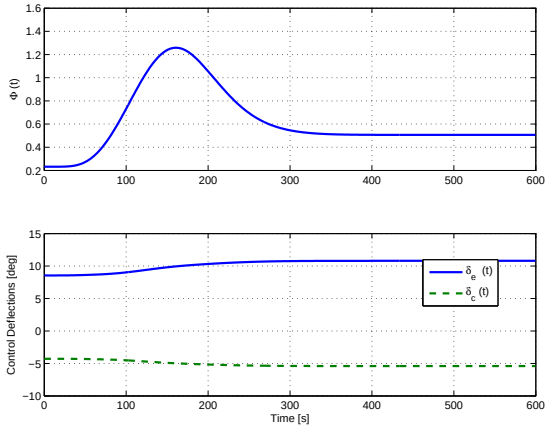

(f) $\Phi(t)$ (top) and $\delta_c(t)$, $\delta_e(t)$ (bottom)

Figure 3.8: Case study 2: Climb and acceleration at varying dynamic pressure. (a) Velocity, (b) altitude and (c) flight-path angle tracking performance. (d) Angle-of-attack and parameter estimate $\hat{\vartheta}_{1,2}$. (e) Flexible modes and (f) control inputs.

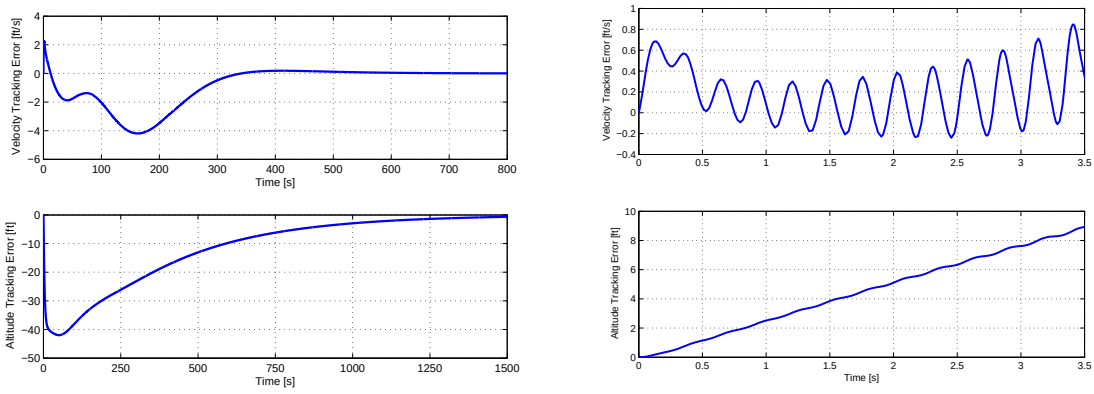

(a) $\tilde{V}(t)$ (top) and $\tilde{h}(t)$ (bottom), case study 1 (b) $\tilde{V}(t)$ (top) and $\tilde{h}(t)$ (bottom), case study 2

Figure 3.9: Approximate feedback linearization controller (Parker et al., 2007). Tracking error $\tilde{V}(t)$ and and $\tilde{h}(t)$; (a) case study 1, (b) case study 2.

3.4 Conclusions

The first control design has been performed using the control design model CDM1 which is derived from the Bolender and Doman model[2, 37] by replacing the aerodynamic and generalized forces and moments with curve-fitted functions of the rigid-body states, the control inputs and the elastic modes. This control design is referred to as control design with "*full control authority*" since all the actuators (i.e. the fuel equivalence ratio and the elevator and canard deflections) are used by the controller. A dynamic state-feedback controller has been derived combining robust adaptive dynamic inversion with backstepping arguments to obtain a control architecture that uses the natural decomposition of the longitudinal vehicle dynamics into velocity, altitude/flight-path angle, and angle-of-attack/pitch rate subsystems. Stable adaptation in the controller parameters allows to satisfactorily address the issue of model mismatch when performing dynamic inversion. The important contribution of this work is the complete characterization of the nonlinear internal dynamics of the Bolender and Doman model with respect to velocity, altitude and angle-of-attack as regulated output. The result of the rigorous stability analysis performed on the overall system is in sharp contrast with the one performed on the rigid body only; in particular, it has highlighted that the interaction of the rigid and flexible dynamics results in conditional stability.

Although beneficial for controllability, the presence of a canard is problematic for the vehicle structure, therefore we decide to tackle the much more challenging problem of controlling the vehicle when the only two available inputs are the fuel equivalence ration and the elevator deflection.

CHAPTER 4

CONTROL DESIGN WITH REDUCED CONTROL AUTHORITY

The control design and the stability analysis for the "reduced control authority" scenario is performed on the control-oriented model CDM2 introduced in section 2.3.

4.1 Control Objectives

As in the previous design, only hypersonic cruising regimes are considered. As a consequence of the physical constraints that characterize hypersonic flight, the bounds shown in Table 3.1 must be satisfied. In particular, the state trajectory $x(t)$ is bound to remain within a *feasible set*, defined in this study by the following hypercube

$$\begin{aligned}\Xi_x = \big\{ & 7500 \leq V \leq 11000 \text{ [ft/s]}; \quad -5 \leq \gamma \leq 5 \text{ [deg]}; \\ & -5 \leq \alpha \leq 10 \text{ [deg]}; \ -10 \leq Q \leq 10 \text{ [deg/s]} \big\} \end{aligned} \tag{4.1}$$

Output reference trajectories and their derivatives, $\eta_r = [V_r, \dot{V}_r, \gamma_r, \dot{\gamma}_r]^T$ shall evolve in a compact set $\Xi_\eta \subset \mathbb{R}^4$, to be defined. Furthermore, $y_r := [V_r, \gamma_r]^T$ shall satisfy $y_r(t) \in \overset{\circ}{\Xi}_x$ for all $t \geq 0$ and $\lim_{t\to\infty} y_r(t) = [V^\star, 0]^T$, where $V^\star$ is a desired velocity setpoint.[1] The goal is to design a dynamic state-feedback controller and to determine

[1]Note that the setpoint $\gamma^\star = 0$ and the trim value $Q^\star = 0$ of the pitch rate are required to obtain level flight in steady-state.

appropriately a set Ξ_η and a compact set $\Xi_0 \subset \Xi_x$ such that the state of system (2.4) is steered from any initial condition $x_0 = [V_0, \gamma_0, \theta_0, Q_0]^T \in \Xi_0$ to the equilibrium point $x^\star = [V^\star, 0, \theta^\star, 0]^T \in \Xi_x$ along the reference $y_r(t)$, in such a way that $x(t) \in \Xi_x$ for $\forall t \geq 0$. It should be noted that neither the trim value of the pitch angle, $\theta^\star$, nor the trim value of the control input, $u^\star = [\Phi^\star, \delta_e^\star]^T$, can be determined a priori due to parameter uncertainty.

4.2 Zero-dynamics of the Model

As is well known, the zero-dynamics of a system with respect to the regulated output play a crucial role in the solvability of a robust tracking problem. In this section, the properties of the zero-dynamics of the considered model will be investigated to determine the appropriate control strategy to be pursued. For the sake of simplicity (and without loss of generality) we will restrict our attention to the set-point regulation error, whereas the general tracking problem will be dealt with in the sequel. The system (2.4) has vector relative degree $r = [1, 1]$ and a two-dimensional zero-dynamics with respect to the set-point error $e_s = [V - V^\star, \gamma]^T$. Applying the decoupling inputs

$$\begin{aligned} \bar{\Phi} &= \frac{D(\alpha) + mg\sin\gamma}{\bar{q}SC_{T\Phi}(\alpha)\cos\alpha} - \frac{C_T(\alpha)}{C_{T\Phi}(\alpha)} \\ \bar{\delta}_e^\gamma &= -\frac{C_L(\alpha)}{C_L^\delta} - \frac{T(\alpha,\Phi)\sin\alpha}{\bar{q}SC_L^\delta} + \frac{mg\cos\gamma}{\bar{q}SC_L^\delta} \end{aligned} \tag{4.2}$$

and choosing the initial condition $\gamma_0 = 0$, one obtains the zero dynamics of the system (2.4) with respect to the output e_s

$$\begin{aligned} \dot{\theta} &= Q \\ I_{yy}\dot{Q} &= \bar{M}(\theta, \bar{\Phi}) \end{aligned} \tag{4.3}$$

where we have made use of the fact that $\gamma = 0 \iff \alpha = \theta$. The *effective moment*, $\bar{M}$, is defined as

$$\begin{aligned}\bar{M}(\alpha, \Phi) &= \bar{q}S\bar{c}\left[C_M^{\alpha}(\alpha) - \frac{C_M^{\delta}}{C_L^{\delta}}C_L^{\alpha}(\alpha) + \frac{mg}{\bar{q}S}\frac{C_M^{\delta}}{C_L^{\delta}}\cos\gamma\right] \\ &\quad + \Big(z_T - \bar{c}\,\frac{C_M^{\delta}}{C_L^{\delta}}\sin\alpha\Big)T(\alpha, \Phi)\end{aligned}$$

System (4.3) has an equilibrium at $(\theta, Q) = (\theta^\star, 0)$ and $\bar{\Phi} = \Phi^\star$, where the constants $\theta^\star$ and $\Phi^\star$ are determined by the trim condition at $V^\star$, namely

$$T(\theta^\star, \Phi^\star)\cos\theta^\star - D\big(\theta^\star\big) = 0\,, \quad \bar{M}(\theta^\star, \Phi^\star) = 0$$

For the model under consideration [2, 28], it can be verified that $\partial\bar{M}(\alpha, \Phi)/\partial\alpha > 0$ at $(\alpha, \Phi) = (\theta^\star, \Phi^\star)$, for all $V^\star \in \Xi_x$ and all $p \in \mathcal{P}$; hence the equilibrium $(\theta^\star, 0)$ of (4.3) is a hyperbolic saddle. Any attempt to apply a standard feedback linearization control results in unstable internal dynamics. The following observation is key: by redefining the setpoint error (hence the regulated output) as $e_s' = [V - V^\star, \theta - \theta^\star\,]^T$, the second decoupling input in (4.2) is replaced by

$$\bar{\delta}_e^{\theta} = -\frac{C_M^{\alpha}(\alpha)}{C_M^{\delta}} - \frac{z_T T(\alpha, \Phi)}{\bar{q}S\bar{c}C_M^{\delta}}$$

With this choice, the system has now vector relative degree $r' = [1, 2]$ and 1-dimensional zero dynamics given by

$$\dot{\gamma} = \frac{\bar{L}(\theta^\star - \gamma, \Phi^\star) - mg\cos\gamma}{mV^\star} \tag{4.4}$$

where the *effective lift* is defined as $\bar{L}(\alpha, \Phi) = L(\alpha, \bar{\delta}_e^{\theta}) + T(\alpha, \Phi)\sin\alpha$, which satisfies $\bar{L}(\theta^\star, \Phi^\star) = mg$ by definition. This time, the fact that $\partial\bar{L}(\alpha, \Phi)/\partial\alpha > 0$ at $(\alpha, \Phi) = (\theta^\star, \Phi^\star)$ for all $V^\star \in \Xi_x$ and all $p \in \mathcal{P}$ implies that the equilibrium $\gamma = 0$ of (4.4) is asymptotically stable (recall that $\alpha = \theta - \gamma$). This observation suggests to *trade the flight-path angle for the pitch angle* as the regulated output for the flight path dynamics; since the setpoint $\theta^\star$ is not known, it must be reconstructed by the controller.

4.3 Control Design

The design of the controller is approached by considering separately the velocity and the flight-path angle dynamics. The strategy for the velocity subsystem is borrowed from the previous design, where a control law with adaptive drag compensation is employed using Φ as the main control effector for the engine thrust. On the other hand, the design philosophy for the flight-path dynamics (γ, θ, Q) is novel: the CDM1 had full relative degree, hence adaptive dynamic inversion was allowed. Here, a preliminary change of coordinates is applied to the FPA dynamics in order to represent the internal dynamics of the system. Integral control is applied to reconstruct asymptotically the unknown trim value $\theta^\star$, and a suitable command θ_{cmd} for the pitch angle is selected to stabilize the augmented internal dynamics. Finally, the pitch angle is adaptively controlled through the pitch moment by means of the elevator deflection. In particular, the properties of the redefined internal dynamics enable the application of small-gain techniques.

4.3.1 Translational dynamics

The design of the velocity loop is routine, and we will dispose of it rather quickly. In the error coordinate, $\tilde{V} = V - V_r$, the first equation of (2.4) reads as

$$m\dot{\tilde{V}} = T(\alpha, \Phi)\cos\alpha - D(\alpha) - mg\sin\gamma - m\dot{V}_r \tag{4.5}$$

Using the definitions given in Appendix B.2, system (4.5) is written in parametrized form as

$$m\dot{\tilde{V}} = \vartheta_1^T\left[G_1(x)\Phi - F_1(x, \eta_r)\right] \tag{4.6}$$

Let $\hat{\vartheta}_1$ be a vector of estimates of the parameter vector ϑ_1, define $\tilde{\vartheta}_1 := \hat{\vartheta}_1 - \vartheta_1$ and let Θ_1 be the compact set in which ϑ_1 is assumed to range, obtained by letting the

entries of ϑ_1 vary within the set $\mathcal{P}$. The control law for Φ is chosen as

$$\Phi = \frac{1}{\hat{\vartheta}_1^T G_1(x)} \left[-k_V \tilde{V} + F_1^T(x, \eta_r)\, \hat{\vartheta}_1 \right] \tag{4.7}$$

where $k_V > 0$ is a gain parameter, whereas the update law is selected as

$$\dot{\hat{\vartheta}}_1 = \underset{\hat{\vartheta}_1 \in \Theta_1}{\text{Proj}} \left\{ \tilde{V}\, \Gamma_1 \left[G_1(x)\Phi - F_1(x, \eta_r) \right] \right\} \tag{4.8}$$

where $\Gamma_1 \in \mathbb{R}^{12\times 12}$ is a symmetric positive definite matrix of adaptation gains. The smooth projection operator $\underset{\hat{\vartheta}_1 \in \Theta_1}{\text{Proj}}(\cdot)$ [16] is necessary to ensure non-singularity of the control. The resulting velocity error dynamics reads as

$$\dot{\tilde{V}} = -k_V \tilde{V} + \tilde{\vartheta}_1^T \left[F_1(x, \eta_r) - G_1(x)\Phi \right] \tag{4.9}$$

The stability analysis is postponed to Section 4.4.

4.3.2 Redefinition of the internal dynamics

Using the error coordinate $\tilde{\gamma} = \gamma - \gamma_r$, the first equation of the flight-path dynamics is written as

$$\dot{\tilde{\gamma}} \;=\; \frac{L(\alpha, \delta_e) + T(\alpha, \Phi)\sin\alpha}{mV} - \frac{g}{V}\cos\gamma - \dot{\gamma}_r \tag{4.10}$$

The exact form of the internal dynamics of (4.10) with respect to the new output θ is rather involved and difficult to manipulate. A simpler expression can be obtained by applying the following change of coordinates

$$\xi_2 = \tilde{\gamma} + \mu_1(V_r)Q + \mu_2(V_r, \alpha_r)\tilde{V} \tag{4.11}$$

where

$$\mu_1(V_r) := -\frac{1}{V_r}\, \frac{I_{yy}\, C_L^\delta}{\bar{c}\, m\, C_M^\delta} > 0$$

$$\mu_2(V_r, \alpha_r) := \frac{1}{V_r} \left[\frac{z_T\, C_L^\delta}{\bar{c}\, C_M^\delta} \frac{1}{\cos\alpha_r} - \tan\alpha_r \right] =: \frac{\bar{\mu}_2(\alpha_r)}{V_r}$$

The function $\alpha_r = \alpha_r(y_r)$ defines the equilibrium value of α when y is "frozen" at y_r; hence $\alpha_r = \theta^\star$ when $y_r = [V^\star, 0]^T$. The change of coordinates (4.11) has the effect of removing from (4.10) the appearance of the inputs δ_e and Φ. Since μ_1 and μ_2 are not known, the state ξ_2 is not available and a partial-state feedback problem is presented. Differentiating (4.11) one obtains[2]

$$\begin{aligned}\dot{\xi}_2 &= f_1(x, y_r) + \Lambda_2(x, y_r)\xi_2 + [\dot{\mu}_1 - \mu_1\Lambda_2(x, y_r)]Q \\ &\quad + [f_2(x, y_r, \eta_r) - \mu_2\Lambda_2(x, y_r)]\tilde{V} - \mu_2\dot{V}_r - \dot{\gamma}_r \end{aligned} \tag{4.12}$$

where the functions f_1, f_2 and Λ_2 are defined in Appendix B.2. Since the desired equilibrium entails $\tilde{V} = 0$ and $Q = 0$, from equation (4.11) it is seen that at trim $\tilde{\gamma} = 0 \iff \xi_2 = 0$. Imposing the equilibrium condition to (4.12) yields the following algebraic equation in the unknown α_r

$$\begin{aligned}&-\left(\frac{C_L^\delta C_M^{\alpha^2}}{C_M^\delta} + \bar{\mu}_2 C_D^{\alpha^2}\right)\alpha_r^2 - \left(\frac{C_L^\delta C_M^\alpha}{C_M^\delta} + \bar{\mu}_2 C_D^\alpha - C_L^\alpha\right)\alpha_r \\ &+ C_L^0 - \frac{C_L^\delta C_M^0}{C_M^\delta} - \bar{\mu}_2 C_D^0 - \frac{2mg}{\rho S V_r^2}\big(\cos\gamma_r + \bar{\mu}_2 \sin\gamma_r\big) = 0\end{aligned}$$

The small angle approximation $\cos\alpha_r \approx 1$, $\tan\alpha_r \approx \alpha_r$ yields the simplified cubic equation for α_r

$$a_{\alpha 3}\alpha_r^3 + a_{\alpha 2}\alpha_r^2 + a_{\alpha 1}\alpha_r + a_{\alpha 0} = 0 \tag{4.13}$$

where

$$\begin{aligned}a_{\alpha 0} &= C_L^0 - \frac{C_L^\delta C_M^0}{C_M^\delta} - \frac{z_T C_L^\delta C_D^0}{\bar{c}\, C_M^\delta} - \frac{2mg}{\rho S V_r^2}\left(1 + \frac{z_T C_L^\delta \gamma_r}{\bar{c}\, C_M^\delta}\right) \\ a_{\alpha 1} &= C_L^\alpha - \frac{C_L^\delta C_M^\alpha}{C_M^\delta} - \frac{z_T C_L^\delta C_D^\alpha}{\bar{c}\, C_M^\delta} + C_D^0 + \frac{2mg\gamma_r}{\rho S V_r^2} \\ a_{\alpha 2} &= C_D^\alpha - \frac{C_L^\delta C_M^{\alpha^2}}{C_M^\delta} - \frac{z_T C_L^\delta C_D^{\alpha^2}}{\bar{c}\, C_M^\delta}, \quad a_{\alpha 3} = C_D^{\alpha^2}\end{aligned}$$

[2]For simplicity, arguments of functions will often be omitted.

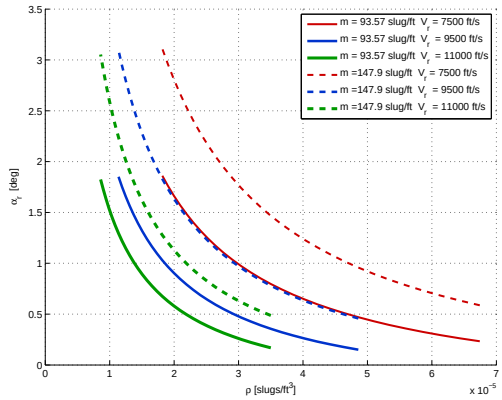

(a) $m = 93.57$ slug/ft and $m = 147.9$ slug/ft

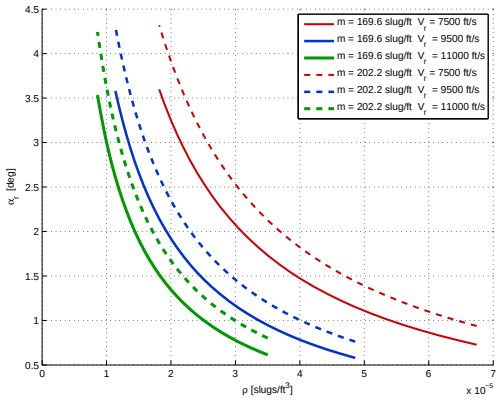

(b) $m = 169.6$ slug/ft and $m = 202.2$ slug/ft

Figure 4.1: Plots of $\alpha^\star(\rho)$ for different values of $V_{\rm r}$ and m.

For the model under consideration, it has been verified that the discriminant of the cubic equation (4.13) is negative for all $y_r \in \Xi_x$ and for all $p \in \mathcal{P}$. Applying *Cardano's method*, it follows that (4.13) has one real root and a pair of complex conjugate roots; hence the equilibrium is uniquely determined. With a slight abuse of notation, the real root is identified with α_r. Figure 4.1 shows sample plots of α_r versus ρ, obtained by considering nominal values of the parameters, values of the mass corresponding to 70% and 100% fuel level, $\gamma_r = 0$ and some feasible values of V_r.

Finally, using arguments similar to Property 3.1.1, it is possible to show that $f_1(x, y_r)$ satisfies a "sector boundedness" condition with respect to $\alpha - \alpha_r$. This is formally stated as follows:

Property 4.3.1. *There exists a smooth function $\Lambda_1(x, y_r)$ such that*

$$f_1(x, y_r) := \Lambda_1(x, y_r)[\alpha - \alpha_r].$$

Furthermore, for all $x, y_r \in \Xi_x$, and $p \in \mathcal{P}$, the function $\Lambda_1(x, y_r)$ satisfies

$$\lambda_1^m \leq \Lambda_1(x, y_r) \leq \lambda_1^M \tag{4.14}$$

for some positive constants $\lambda_1^m < \lambda_1^M$.

4.3.3 Controller design for the pitch dynamics

As mentioned, to deal with uncertainty on the value of $\theta^\star$, the system is augmented with the integral error

$$\dot{\xi}_1 = \tilde{\gamma} = \xi_2 - \mu_1 Q - \mu_2 \tilde{V}$$

The zero-dynamics of the augmented system, i.e., the subsystem in the coordinates (ξ_1, ξ_2), no longer possesses a Locally Asymptotically Stable (LAS) equilibrium. This prompts a further redefinition of the regulated output as $\tilde{\theta} = \theta - \theta_{\text{cmd}}$, where θ_{cmd} is a function of the available states, to be designed to enforce a LAS zero-dynamics and to achieve $\lim_{t\to\infty} \theta_{\text{cmd}}(t) = \theta^\star$. To this end, let $k_1 > 0$ be a gain parameter and change coordinate as

$$\chi_1 = k_1 \xi_1 + \alpha_r, \qquad \chi_2 = \xi_2 + \chi_1 \tag{4.15}$$

To compute $\dot{\chi}_1$, we make use of the typical expression of the air density $\rho \approx \rho_0 \exp(-(h - h_0)/h_s)$. Using the kinematic relation $\dot{h} = V \sin\gamma$, one obtains

$$\dot{\alpha}_r = \frac{\partial \alpha_r}{\partial V_r}\dot{V}_r + \frac{\partial \alpha_r}{\partial \gamma_r}\dot{\gamma}_r - \frac{\partial \alpha_r}{\partial \rho}\frac{\rho}{h_S}\frac{\sin\gamma}{\gamma} V\gamma \tag{4.16}$$

where the last addendum is the perturbation due to the time-varying nature of ρ. Note that the graphical analysis on Figure 4.1 confirms that $\partial\alpha_r/\partial\rho$ is strictly negative in the flight envelope. Therefore, by continuity, there exists $\lambda_3^m > 0$ such that for all $x, y_r \in \Xi_x$ and $p \in \mathcal{P}$

$$\Lambda_3(x, y_r) := -\frac{\partial \alpha_r}{\partial \rho}\frac{\rho}{h_S}\frac{\sin\gamma}{\gamma} V > \lambda_3^m \tag{4.17}$$

Using (4.15)–(4.17), the internal dynamics is written as

$$\begin{aligned}
\dot{\chi}_1 &= -a_1(x, y_r, k_1)\big[\chi_1 - \chi_2 + \mu_1 Q + \mu_2 \tilde{V}\big] + d_1(x, \eta_r) \\
\dot{\chi}_2 &= -a_2(x, y_r, k_1)\chi_1 - a_3(x, y_r, k_1)\chi_2 + \Lambda_1(x, y_r)\,\tilde{\theta} + b_2(x, \eta_r, k_1) Q \\
&\quad + b_3(x, \eta_r, k_1)\tilde{V} + d_2(x, \eta_r) + \Lambda_1(x, y_r)[\theta_{\text{cmd}} + \chi_1 - \gamma_r - \alpha_r]
\end{aligned} \tag{4.18}$$

where, respectively,

$$
\begin{aligned}
a_1(x, y_r, k_1) &:= k_1 + \Lambda_3(x, y_r) \\
a_2(x, y_r, k_1) &:= \Lambda_2(x, y_r) + a_1(x, y_r, k_1) \\
a_3(x, y_r, k_1) &:= \Lambda_1(x, y_r) - a_2(x, y_r, k_1) \\
b_2(x, \eta_r, k_1) &:= \dot{\mu}_1 + \mu_1 a_3(x, y_r, k_1) \\
b_3(x, \eta_r, k_1) &:= f_2(x, \eta_r, k_1) + \mu_2 a_3(x, y_r, k_1) \\
d_1(x, \eta_r) &:= \frac{\partial \alpha_r}{\partial V_r}\dot{V}_r + \frac{\partial \alpha_r}{\partial \gamma_r}\dot{\gamma}_r + \Lambda_3(x, y_r)\gamma_r \\
d_2(x, \eta_r) &:= d_1(x, \eta_r) - \dot{\gamma}_r - \mu_2 \dot{V}_r
\end{aligned}
$$

By removing the last addendum in (4.18), the selection

$$
\theta_{\text{cmd}} := -k_1\xi_1 + \gamma_r = -\chi_1 + \gamma_r + \alpha_r
$$

will be shown in the sequel to enforce asymptotic stability of the origin of the zero dynamics via small-gain arguments. The change of coordinates $[\theta, Q]^T \mapsto z = [\tilde{\theta}, \tilde{Q}]^T$, where

$$
\tilde{\theta} = \theta + k_1\xi_1 - \gamma_r, \qquad \tilde{Q} = Q + k_1\tilde{\gamma} - \dot{\gamma}_r
$$

yields the pitch error dynamics

$$
\dot{z} = A_z z + B_z\big[\vartheta^T G_2(x)\delta_e - \vartheta^T F_2(x, \Phi) - k_1 g V^{-1}\cos\gamma - k_1\dot{\gamma}_r - \ddot{\gamma}_r\big] \tag{4.19}
$$

where the pair $(A_z, B_z) \in \mathbb{R}^{2\times 2} \times \mathbb{R}^{2\times 1}$ is in Brunovsky form and the parameter vector ϑ_2, the regressor $F_2(x, \Phi)$ and the input matrix $G_2(x)$ are defined in Appendix B.2. Let $\hat{\vartheta}_2$ be a vector of estimates of ϑ_2 with estimation error $\tilde{\vartheta}_2 = \hat{\vartheta}_2 - \vartheta_2$, and let Θ_2 be the compact set for θ_2 obtained by letting the entries of θ_2 vary within $\mathcal{P}$. Letting $K_z \in \mathbb{R}^{1\times 2}$ be such that $A_z + B_z K_z$ is Hurwitz, the control law for the elevator deflection is selected as

$$
\delta_e \;=\; \frac{K_z z + F_2^T(x, \Phi)\hat{\vartheta}_2 + k_1 g V^{-1}\cos\gamma + k_1\dot{\gamma}_r + \ddot{\gamma}_r}{\hat{\vartheta}_2^T G_2(x)}
$$

with update law for $\hat{\vartheta}_2$ given by

$$\dot{\hat{\vartheta}}_2 = \underset{\hat{\vartheta}_2 \in \Theta_2}{\text{Proj}} \left\{ z^T P_z B_z \Gamma_2 \left[G_2(x)\delta_e - F_2(x,\Phi) \right] \right\} \tag{4.20}$$

where $\Gamma_2 \in \mathbb{R}^{23\times 23}$ is a symmetric positive definite gain matrix and $P_z = P_z^T > 0$ solves the Lyapunov equation $P_z(A_z + B_z K_z) + (A_z + B_z K_z)^T P_z = -k_z I$ where k_z is a positive constant. Let $k_{1a} := 1/\max_{V_r \in \Xi_\eta} \mu_1(V_r) > 0$. Since k_1 is a small gain, then by choosing $k_1 < k_{1a}$, the variable $\mu_3(y_r, k_1) := (1 - k_1\mu_1(V_r))^{-1}$ is well defined and $\mu_3 \geq 1$. As a result, the pitch-error dynamics reads as

$$\dot{z} = \big(A_z + B_z K_z\big) z + B_z \big[F_2^T(x,\Phi) - G_2^T(x)\delta_e\big]\tilde{\vartheta}_2 \tag{4.21}$$

whereas the final form of the internal dynamics is given by

$$\begin{aligned}
\dot{\chi}_1 &= -A_1(x,\eta_r,k_1)\big[\chi_1 - \chi_2 + \mu_1\tilde{Q} + \mu_2\tilde{V}\big] + D_1(x,\eta_r) \\
\dot{\chi}_2 &= -A_2(x,\eta_r,k_1)\chi_1 - A_3(x,\eta_r,k_1)\chi_2 + B_1(x,y_r)\tilde{\theta} \\
&\quad + B_2(x,\eta_r)\tilde{Q} + B_3(x,\eta_r)\tilde{V} + D_2(x,\eta_r)
\end{aligned} \tag{4.22}$$

where

$$\begin{aligned}
A_1(x,y_r,k_1) &:= \mu_3(y_r,k_1)\, a_1(x,y_r,k_1) \\
A_2(x,\eta_r,k_1) &:= \mu_3(y_r,k_1)\, a_2(x,y_r,k_1) - k_1\mu_3(\dot{\mu}_1 + \mu_1\Lambda_1) \\
A_3(x,\eta_r,k_1) &:= \mu_3(y_r,k_1)\, a_3(x,y_r,k_1) + k_1\mu_3\dot{\mu}_1 \\
B_1(x,y_r) &:= \Lambda_1(x,y_r) \\
B_2(x,y_r) &:= \mu_3(y_r,k_1)\, b_2(x,\eta_r,k_1) \\
B_3(x,\eta_r) &:= f_2 + \mu_2\mu_3(a_3 + k_1\dot{\mu}_1) \\
D_1(x,\eta_r) &:= d_1(x,\eta_r) - \mu_1\mu_3(y_r,k_1)\, a_1(x,y_r,k_1)\dot{\gamma}_r \\
D_2(x,\eta_r) &:= d_2(x,\eta_r) + \mu_3(y_r,k_1)\, b_2(x,\eta_r,k_1)\dot{\gamma}_r
\end{aligned}$$

Note that, in the interest of conciseness, we have omitted the argument k_1 in the functions $B_i(\cdot)$ and $D_i(\cdot)$.

4.4 Closed-loop Stability Analysis

The stability analysis will be carried out using $\mathcal{L}_\infty$ small-gain arguments and their asymptotic generalization [34]. In doing so, we will exploit the "quasi-cascade" structure [22] enforced by the passivity-based adaptive control between the $(\tilde{V}, z, \tilde{\vartheta})$-dynamics and the χ-dynamics. Given an initial instant of time $t_0 \in \mathbb{R}_{\geq 0}$ and an initial condition $x_0 = x(t_0) \in \Xi_0$, let $\tau = \inf\{t : x(t, t_0, x_0) \in \partial\Xi_x\}$. Let x_τ represent the truncation of the signal x at time τ. Since $\Xi_0 \subset \Xi_x$, then $\tau > 0$ and since the vector field (2.4) is locally Lipschitz and the set Ξ_x is compact, the trajectories of the system are defined in the interval $[0, \tau]$ and hence x_τ is well defined.

The first step in the stability analysis will be to compute the $\mathcal{L}_\infty$ bounds of the truncated error signals $\tilde{V}_\tau$ and z_τ. Then, after having derived the $\mathcal{L}_\infty$ bounds of the signals χ_{1_τ}, χ_{2_τ}, the interconnection of the χ_1 and χ_2 dynamics will be analyzed first, and finally the interconnection of the (χ_1, χ_2)-system and the $(\tilde{V}, z, \tilde{\vartheta})$-system will be considered. The following propositions hold for the $\tilde{V}$ and z subsystems.

Proposition 4.4.1. *Let $\vartheta_{10}, \vartheta_{20}, \hat{\vartheta}_{10}$ and $\hat{\vartheta}_{20}$ be the initial conditions of the parameter vectors ϑ_1 and ϑ_2 and their estimates $\hat{\vartheta}_1$ and $\hat{\vartheta}_2$. Let $\lambda_P^m > 0$ and $\lambda_P^M > 0$ be the minimum and maximum eigenvalue of the matrix P_z and let $\Delta\vartheta_1$ and $\Delta\vartheta_2$ be a arbitrary positive constants. Then there exist symmetric positive definite matrices $\Gamma_1 \in \mathbb{R}^{12\times 12}$ and $\Gamma_2 \in \mathbb{R}^{23\times 23}$ such that*

$$\begin{aligned} \|\tilde{V}_\tau\|_\infty &< \sqrt{\tilde{V}_0^2 + \Delta\vartheta_1} \\ \|\tilde{\theta}_\tau\|_\infty &< \sqrt{\frac{\lambda_P^M}{\lambda_P^m}|z_0|^2 + \frac{\lambda_P^M}{\lambda_P^m}\Delta\vartheta_2} \\ \|\tilde{Q}_\tau\|_\infty &< \sqrt{\frac{\lambda_P^M}{\lambda_P^m}|z_0|^2 + \frac{\lambda_P^M}{\lambda_P^m}\Delta\vartheta_2} \end{aligned}$$

Morevoer, if $\tau = +\infty$, then

$$\|\tilde{V}\|_a = 0, \quad \|\tilde{\theta}\|_a = 0 \quad \|\tilde{Q}\|_a = 0$$

Proof. Choose $\Gamma_1 \in \mathbb{R}^{12\times 12}$ and $\Gamma_2 \in \mathbb{R}^{23\times 23}$ such that, for all $\vartheta_{10}, \hat{\vartheta}_{10} \in \Theta_1$ and all $\vartheta_{20}, \hat{\vartheta}_{20} \in \Theta_2$

$$\tilde{\vartheta}_{10}^T \Gamma_1^{-1} \tilde{\vartheta}_{10} \leq \Delta\vartheta_1$$
$$\tilde{\vartheta}_{20}^T \Gamma_2^{-1} \tilde{\vartheta}_{20} \leq \Delta\vartheta_2$$

and consider the Lyapunov functions candidate $W_V(\tilde{V}, \tilde{\vartheta}_1) = \tilde{V}^2 + \tilde{\vartheta}_1^T \Gamma_1^{-1} \tilde{\vartheta}_1$ and $W_z(z, \tilde{\vartheta}_2) = z^T P_z z + \tilde{\vartheta}_2^T \Gamma_2^{-1} \tilde{\vartheta}_2$. Since as long as the trajectories of the overall system are defined the Lie derivatives of W_V and W_z along the closed-loop trajectories defined by (4.8)-(4.9) satisfy

$$\dot{W}_V \leq -2k_V \tilde{V}^2 \quad \text{and} \quad \dot{W}_z \leq -k_z |z|^2 ,$$

then the first part of the proposition follows from the following inequalities

$$\tilde{V}^2 \leq W_V \leq \tilde{V}_0^2 + \tilde{\vartheta}_{10}^T \Gamma_1^{-1} \tilde{\vartheta}_{10} \leq \tilde{V}_0^2 + \Delta\vartheta_1$$
$$\lambda_P^m |z|^2 \leq W_z \leq \lambda_P^M |z_0|^2 + \tilde{\vartheta}_{20}^T \Gamma_2^{-1} \tilde{\vartheta}_{20} \leq \lambda_P^M |z_0|^2 + \Delta\vartheta_2$$

Finally, if, as it will be shown in the sequel, no finite escape time occurs in the system (i.e. $\tau = \infty$), the second result follows by applying the LaSalle-Yoshizawa Theorem [16]. □

This proposition tells us that as long as the trajectories of the overall system are defined, the velocity, pitch angle and pitch rate tracking errors remain bounded and converge asymptotically to zero while the parameter estimates remain bounded. This is a consequence of the "nearly cascade" structure enforced in the system by the adaptive control strategy adopted in the design of the control laws for Φ and δ_e . In fact, looking at the closed-loop dynamics, defined by (4.8)-(4.9) and (4.20)-(4.22), it is possible to notice that χ_1 and χ_2 affect the $(\tilde{V}, z)$-dynamics only through the regressors $F_1(x, \eta_r)$ and $F_2(x, \Phi)$.

Let ε be a design parameter such that $0<\varepsilon<1$, define $\mu_1^M = \max_{V_r} |\mu_1(V_r)|$, $\mu_2^M = \max_{V_r,\alpha_r} |\mu_2(V_r,\alpha_r)|$, $\dot{\mu}_1^M = \max_{\eta_r} |\dot{\mu}_1(\eta_r)|$ and let $d := [D_1(x,\eta_r), D_2(x,\eta_r)]^T$. In what follows, extremal values of functions are assumed to be evaluated by considering the involved variables in their feasible set, although we often omit referencing the set to avoid clutter. The following propositions establish the infinity bounds on the $\chi_{1\tau}$ and $\chi_{2\tau}$ signals.

Proposition 4.4.2. *For all $k_1 < k_{1a}$ the signal χ_{1_τ} satisfies the following bound*

$$\|\chi_{1_\tau}\|_\infty \;<\; \max\left\{|\chi_{1_0}|,\, \frac{1}{1-\varepsilon}\|\chi_{2_\tau}\|_\infty,\, \frac{3\mu_1^M}{\varepsilon}\|\tilde{Q}_\tau\|_\infty,\, \frac{3\mu_2^M}{\varepsilon}\|\tilde{V}_\tau\|_\infty,\, \frac{3}{\varepsilon\lambda_3^m}\|d_\tau\|_\infty\right\}.$$

Proof. Consider the Lyapunov function candidate $W_1(\chi_1) = \frac{1}{2}\chi_1^2$ whose derivative along trajectories of system (4.22) satisfies, in the time interval $[t_0,\tau]$,

$$\dot{W}_1 \;\leq\; -A_1|\chi_1|\left\{\left[(1-\varepsilon)|\chi_1| - |\chi_2|\right] + \left[\varepsilon|\chi_1| - 3\max\left\{\mu_1^M|\tilde{Q}|,\, \mu_2^M|\tilde{V}|,\, \frac{|d|}{|A_1|}\right\}\right]\right\}.$$

Since $x_\tau \in \Xi_x$ implies that condition (4.17) holds, it follows that for $\forall t \in [t_0,\tau]$, $|A_1| > 0$, so the previous inequality is well defined, and in particular

$$|\chi_1| \;>\; \max\left\{\frac{|\chi_2|}{1-\varepsilon}, \frac{3\mu_1^M|\tilde{Q}|}{\varepsilon}, \frac{3\mu_2^M|\tilde{V}|}{\varepsilon}, \frac{3|d|}{\varepsilon\lambda_3}\right\} \;\Rightarrow\; \dot{W}_1 < 0$$

which yields the bound for χ_{1_τ} [34, Lemma 3.3]. □

Proposition 4.4.3. *Assume that for $\forall x \in \Xi_x$ and $\eta_r \in \Xi_\eta$*

$$\exists \Lambda_{S1} > 0 : \quad \min_{x,y_r}\{\Lambda_1 - \Lambda_2 - \Lambda_3\} \geq \Lambda_{S1}\,. \tag{4.23}$$

Then there exists $k_{1b} > 0$ such that for all $k_1 < k_{1b}$ the following bound holds

$$\|\chi_{2_\tau}\|_\infty \;<\; \max\left\{|\chi_{2_0}|,\, \frac{c_1(k_1)}{1-\varepsilon}\|\chi_{1_\tau}\|_\infty,\, c_2\|\tilde{\theta}_\tau\|_\infty, c_3\|\tilde{Q}_\tau\|_\infty,\, c_4\|\tilde{V}_\tau\|_\infty,\, c_5\|\tilde{d}_\tau\|_\infty\right\}$$

where $c_1(k_1)$ is a positive functions of k_1 and c_i, for $i = 2,\ldots,5$, are positive constants.

Proof. Consider the Lyapunov function candidate $W_2(\chi_2) = \frac{1}{2}\chi_2^2$ whose derivative along trajectories of (4.22) for $\forall t \in [t_0, \tau]$ satisfies

$$\begin{aligned}\dot{W}_2 \;\leq\; & -|\chi_2|\left\{\left[(1-\varepsilon)A_3|\chi_2| - |A_2||\chi_1|\right] + \left[\varepsilon A_3|\chi_2|\right.\right. \\ & \left.\left. -4\max\{\,|B_1||\tilde{\theta}|,\,|B_2||\tilde{Q}|,\,|B_3||\tilde{V}|,|d|\}\right]\right\}.\end{aligned}$$

Let $k_{1S} = \tau\Lambda_{S1}/(1+\dot{\mu}_1^M)$, where $0 < \tau < 1$, and select $k_1 < k_{1b} := \min\{k_{1a}, k_{1S}\}$. Then for $\forall t \in [t_0, \tau]$

$$c_1(k_1) \;:=\; \max_{x,\eta_r}\frac{|A_2|}{A_3} \;=\; \max_{x,\eta_r}\frac{|\Lambda_2+\Lambda_3+k_1(1-\dot{\mu}_1+\mu_1\Lambda_1)|}{\Lambda_1-[\Lambda_2+\Lambda_3+k_1(1-\dot{\mu}_1)]}$$

is well defined and positive. Therefore, for $\forall t \in [t_0, \tau]$

$$|\chi_2| \;>\; \max\left\{\frac{c_1(k_1)}{1-\varepsilon}|\chi_1|,\, c_2|\tilde{\theta}|,\, c_3|\tilde{Q}|,\, c_4|\tilde{V}|,\, c_5|d|\right\} \;\Rightarrow\; \dot{W}_2 < 0$$

where

$$c_2 := \max_{\substack{x,\eta_r\\ k_1=k_{1b}}}\left|\frac{4B_1}{\varepsilon A_3}\right|, \qquad c_3 := \max_{\substack{x,\eta_r\\ k_1=k_{1b}}}\left|\frac{4B_2}{\varepsilon A_3}\right|$$

$$c_4 := \max_{\substack{x,\eta_r\\ k_1=k_{1b}}}\left|\frac{4B_3}{\varepsilon A_3}\right|, \qquad c_5 := \max_{\substack{x,\eta_r\\ k_1=k_{1b}}}\left|\frac{4}{\varepsilon A_3}\right|$$

and hence the infinity bound for χ_{2_τ} is proved to hold. □

Note that the Assumption (4.23) depends on the vehicle geometries. Using the same arguments used to show the sector boundedness property of the function $f_1(x, y_r)$, it is possible to show that this assumption is indeed satisfied for the vehicle model considered in this work [2]. Since a stronger condition on the function Λ_1 will be required in the sequel, a graphical proof that (4.23) is satisfied will be shown later in the paper.

Proposition 4.4.4. *Assume that for* $\forall x \in \Xi_x$ *and* $\eta_r \in \Xi_\eta$

$$\exists \Lambda_{S2} > 0 : \quad \min_{x,y_r}\{\Lambda_1 - 2|\Lambda_2 - \Lambda_3|\} \geq \Lambda_{S2}\,. \tag{4.24}$$

Then there exists $k_{1c} > 0$ such that for all $k_1 < k_{1c}$ the following bounds hold

$$\begin{aligned}
\|\chi_{1_\tau}\|_\infty &< \max\left\{|\chi_{1_0}|, \frac{|\chi_{2_0}|}{1-\varepsilon}, \frac{c_2}{1-\varepsilon}\|\tilde{\theta}_\tau\|_\infty, c_6\|\tilde{Q}_\tau\|_\infty, c_7\|\tilde{V}_\tau\|_\infty, c_8\|d_\tau\|_\infty\right\} \\
\|\chi_{2_\tau}\|_\infty &< \max\left\{|\chi_{2_0}|, \frac{|\chi_{1_0}|}{1-\varepsilon}, c_2\|\tilde{\theta}_\tau\|_\infty, c_9\|\tilde{Q}_\tau\|_\infty, c_{10}\|\tilde{V}_\tau\|_\infty, c_{11}\|\tilde{d}_\tau\|_\infty\right\}
\end{aligned}$$

where c_i, for $i = 6, \ldots, 11$, are positive constants.

Proof. Let $k_1 < k_{1b}$; then, since Propositions 4.4.2 and 4.4.3 hold, the result follows [34] for

$$\begin{aligned}
c_6 &= \max\left\{\frac{c_3}{1-\varepsilon}, \frac{3\mu_1^M}{\varepsilon}\right\}, \quad c_7 = \max\left\{\frac{c_4}{1-\varepsilon}, \frac{3\mu_2^M}{\varepsilon}\right\} \\
c_8 &= \max\left\{\frac{c_5}{1-\varepsilon}, \frac{3}{\varepsilon\lambda_3^m}\right\}, \quad c_9 = \max\left\{\frac{3\mu_1^M c_1(k_{1b})}{\varepsilon(1-\varepsilon)}, c_3\right\} \\
c_{10} &= \max\left\{\frac{3\mu_2^M c_1(k_{1b})}{\varepsilon(1-\varepsilon)}, c_4\right\}, \quad c_{11} = \max\left\{\frac{3c_1(k_{1b})}{\varepsilon(1-\varepsilon)}, c_5\right\}
\end{aligned}$$

if, for $\forall t \in [t_0, \tau]$, the following small-gain condition is satisfied

$$\frac{c_1(k_1)}{(1-\varepsilon)^2} < 1\,. \tag{4.25}$$

Since $c_1(k_1)$ is a continuous positive and increasing functions of k_1 for $0 < k_1 < k_{1b}$, using Assumption (4.24), by continuity, there exist $k_1^* > 0$ and ε^*, $0 < \varepsilon^* < 1$, such that (4.25) is satisfied for any $\varepsilon < \varepsilon^*$ and $k_1 < k_1^*$. As a result the proposition holds for any $k_1 < k_{1c} := \min\{k_{1b}, k_1^*\}$. □

Note that, as before, Assumption (4.24) depends on the vehicle geometries. Recalling the definition of the function Λ_1, it is possible to see that that (4.24) is satisfied, and hence also (4.23), if

$$f_1(x, y_r)|_{\alpha=\alpha+\alpha_r} - 2|\Lambda_2 + \Lambda_3|\alpha \begin{cases} > 0 & \alpha > 0 \\ = 0 & \alpha = 0 \\ < 0 & \alpha < 0 \end{cases}. \tag{4.26}$$

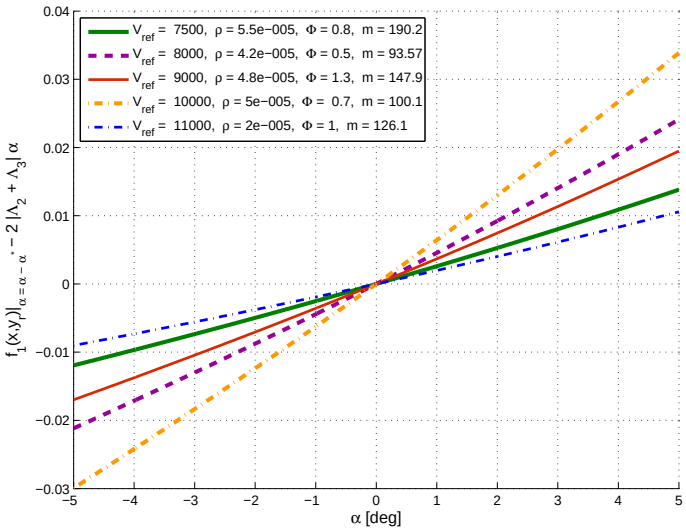

Figure 4.2: Plot of the function $f_1(x, y_r)|_{\alpha=\alpha+\alpha_r} - 2|\Lambda_2 + \Lambda_3|\alpha$.

For the vehicle model considered in this work [2], it has been verified numerically that condition (4.26) indeed holds for all admissible flight conditions and some case studies are shown in Figure 4.2, which shows that in the considered control problem Assumptions (4.23) and (4.24) are satisfied.

Before proceeding to the final step of the stability analysis, appropriate feasible sets for the state in the new coordinates need to be defined. Select $k_1 < k_{1c}$ and denote the augmented state by $x^a := [V, \xi_1, \gamma, \theta, Q]^T$, with initial condition[3] $x^a(0) = x_0^a$ and feasible set Ξ_x^a defined as

$$\Xi_x^a := \{x^a \in \mathbb{R}^5 : \, x \in \Xi_x, \; -5 \leq k_1 \xi_1 \leq 10 \; [\text{deg}]\}$$

The tracking error for the augmented system is defined as $e := [\tilde{V}, \chi^T, z^T]^T$, where $\chi := [\chi_1, \chi_2]^T$, whereas d is regarded (for the time being) as an external disturbance

[3]Recall that it is always possible to choose $\xi_1(0)$ arbitrarily.

signal. Given $y_r \in \Xi_\eta$, consider the following inequalities

$$
\begin{aligned}
& 7500 - \min V_r < \tilde{V} < 11000 - \max V_r \ \text{[ft/s]} \\
& \max_{V_r,\alpha_r} \mu_3 \left|\chi_2 - \chi_1 - \mu_1\tilde{Q} - \mu_2\tilde{V} - \mu_1\dot{\gamma}_r\right| < 5 - \max_t|\gamma_r(t)| \ \text{[deg]} \\
& \max_{V_r,\alpha_r} |\tilde{\theta} + k_1\mu_1\mu_3\chi_1 - \mu_3(\chi_2 - \mu_1\tilde{Q} - \mu_2\tilde{V} - \mu_1\dot{\gamma}_r)| < 5 \ \text{[deg]} \\
& |\mu_3\tilde{Q} + k_1\mu_3(\chi_1 - \chi_2 + \mu_2\tilde{V}) + \mu_3\dot{\gamma}_r| < 10 \ \text{[deg/s]} \\
& -5 < \chi_1 < 5 \ \text{[deg]}
\end{aligned} \tag{4.27}
$$

and let $\mathcal{E} = \{e \in \mathbb{R}^5 |$ the inequalities (4.27) are satisfied$\}$. Since

$$
\begin{aligned}
V &= \tilde{V} + V_r \\
k_1\xi_1 &= \chi_1 - \alpha_r \\
\gamma &= \mu_3(\chi_2 - \chi_1 - \mu_1\tilde{Q} - \mu_2\tilde{V} - \mu_1\dot{\gamma}_r) + \gamma_r \\
\alpha &= \alpha_r + \tilde{\theta} + k_1\mu_1\mu_3\chi_1 - \mu_3(\chi_2 - \mu_1\tilde{Q} - \mu_2\tilde{V} - \mu_1\dot{\gamma}_r) \\
Q &= \mu_3\tilde{Q} + k_1\mu_3(\chi_1 - \chi_2 + \mu_2\tilde{V}) + \mu_3\dot{\gamma}_r
\end{aligned}
$$

and $0\,\text{deg} < \alpha_r < 5\,\text{deg}$, it follows that there exists an open set $\mathcal{D}$, $\mathcal{D} \subseteq \overset{\circ}{\Xi}{}^a_x$, such that :

$$
e \in \mathcal{E} \Rightarrow x^a \in \mathcal{D}. \tag{4.28}
$$

By similar arguments, given a set $\mathcal{E}_0 \subset \mathcal{E}$ of initial conditions for e, there exist a set $\Xi^a_0 \subset \mathcal{D}$ such that

$$
x^a_0 \in \Xi^a_0 \Rightarrow e_0 \in \mathcal{E}_0. \tag{4.29}
$$

A graphical representation of the sets of interest is given in Figure 4.3. In this final part of the stability analysis it will be shown that there exist a compact set $\Xi^a_0 \subset \Xi^a_x$ and a positive number $\Delta > 0$ such that, for any $x^a_0 \in \Xi^a_0$ and any signal d such that $\|d\|_\infty < \Delta$:

(a) $x^a(t) \in \Xi^a_x$ for $\forall t \geq 0$ and therefore no finite escape time occurs in the system;

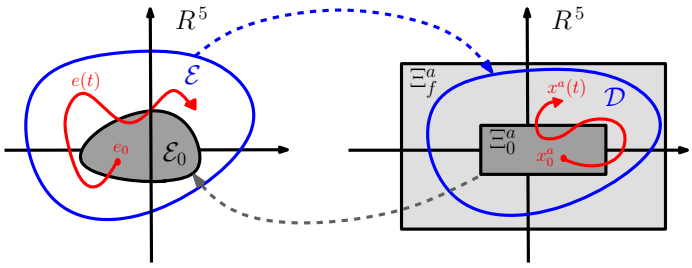

Figure 4.3: Schematics of the sets $\mathcal{E}_0$, $\mathcal{E}$, Ξ_0, $\mathcal{D}$ and Ξ_x.

(b) $\lim_{t\to\infty} e(t) = \underline{0}$.

Note that the infinity norm of the disturbance signal d can be rendered smaller than any arbitrary number Δ by properly choosing the climbing rate and acceleration profile of the reference trajectories (i.e. by choosing Ξ_η).

By combining Propositions 4.4.1 and 4.4.4, it follows that there exist positive real numbers $\Delta\vartheta_1, \Delta\vartheta_2$ and Δ and a set $\mathcal{E}_0$ such that if $(\tilde{V}_0, \chi_0, \tilde{\theta}_0, \tilde{Q}_0) \in \mathcal{E}_0$ and $\|d\|_\infty < \Delta$, then $e_\tau \in \mathcal{E}$. This in turn implies that, for the same $\Delta\vartheta_1, \Delta\vartheta_2$ and Δ there exists a compact set $\Xi_0^a \subset \mathcal{D}$ such that for any $x_0^a \in \Xi_0^a$, $x^a(t) \in \mathcal{D}$ for $\forall t \geq 0$ and therefore $\tau = \infty$ and (a) is satisfied. Since no finite escape time can occur in the system, from Proposition (4.4.1) it follows that $\|\tilde{V}\|_a = 0$ and $\|z\|_a = 0$. Finally, since $\|d\|_a = 0$, it is possible to conclude [34] that

$$\begin{aligned} \|\chi_1\|_a &< \max\left\{\frac{c_2\|\tilde{\theta}\|_a}{1-\varepsilon}, c_6\|\tilde{Q}\|_a, c_7\|\tilde{V}\|_a, c_8\|d\|_a\right\} = 0 \\ \|\tilde{\theta}\|_a &< \max\left\{c_2\|\tilde{\theta}\|_a, c_9\|\tilde{Q}\|_a, c_{10}\|\tilde{V}\|_a, c_{11}\|d\|_a\right\} = 0 \end{aligned}$$

which shows that condition (b) is satisfied as well.

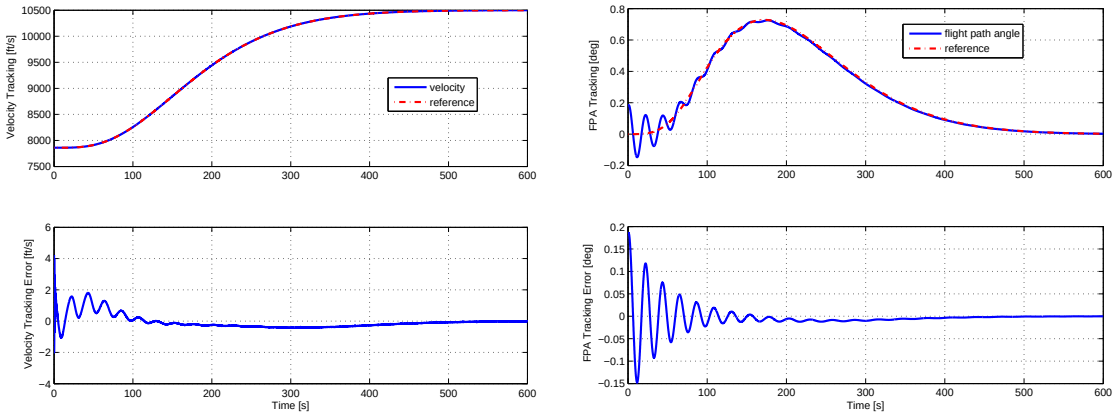

(a) Velocity Tracking and Tracking Error

(b) Flight Path Angle Tracking and Tracking Error

Figure 4.4: Simulation 1: tracking and tracking errors.

4.5 Simulations

To test the performance of the controller derived in the previous section, simulations have been performed on the full nonlinear vehicle model described in [2], which includes structural flexibility. It must be kept in mind that the model used here for control design approximates the behavior of the full nonlinear model with reduced complexity, and thus a significant discrepancy between the two models is expected. While this is far from a comprehensive robustness analysis, the simulations provide a qualitative assessment of the ability of the proposed scheme to deal with model uncertainty, including dynamic perturbations. For reasons of space limitation, only two representative case studies will be presented here: in the first case study the vehicle is not initially trimmed while in the second one it is. The velocity reference trajectory is generated by filtering the signal

$$s_1(t) = \begin{cases} 7860\,\text{ft/s} & t \geq 0\,\text{s} \\ 10500\,\text{ft/s} & \text{otherwise} \end{cases}$$

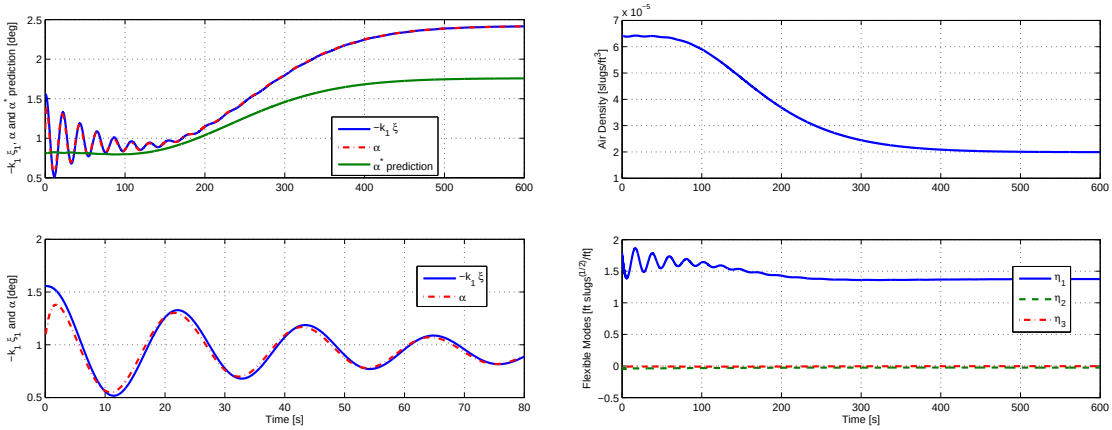

(a) Integrator, Angle-of-Attack and α_r prediction

(b) Air Density and Flexible Modes

Figure 4.5: Simulation 1: integrator, angle-of-attack, α_r, air density and flexible modes.

with a first-order prefilter with natural frequency $\omega_f = 0.02$ rad/s and damping factor $\zeta_f = 0.95$, while the flight path angle reference trajectory is generated by filtering the signal

$$s_2(t) = \begin{cases} 3.5\,\text{deg} & 0 < t < 45\,\text{s} \\ 0 & \text{otherwise} \end{cases}$$

with the same first-order prefilter. The controller gains have been chosen as $k_V = 120$, $k_z = 4$ and $k_1 = 0.1$ moreover $K_z = [-2, -1]$. With this choice of gains and references and using the nominal values of the parameters, it is possible to show that if

$$\begin{aligned} &\|\tilde{V}\|_\infty \leq 60\,\text{ft/s}\,, && \|\chi\|_\infty \leq 2\,\text{deg} \\ &\|\tilde{\theta}\|_\infty \leq 2.8\,\text{deg}\,, && \|\tilde{Q}\|_\infty \leq 4\,\text{deg/s} \end{aligned} \tag{4.30}$$

then bounds (4.27) are satisfied. The initial condition of the vectors $\hat{\vartheta}_1$ and $\hat{\vartheta}_2$, the

gain matrices Γ_1 and Γ_2 and the parameter ε have been chosen using Propositions 4.4.1 and 4.4.4 in such a way that, if

$$\begin{aligned} &|\tilde{V}_0| \leq 30\,\text{ft/s}\,, && |\chi_0| \leq 1.6\,\text{deg} \\ &|\tilde{\theta}_0| \leq 1.5\,\text{deg}\,, && |\tilde{Q}_0| \leq 2.2\,\text{deg/s}\,, \end{aligned} \tag{4.31}$$

then bounds (4.30) are met. As a consequence, to satisfy (4.31), the initial conditions for the state variables and control inputs have been chosen as

$$\begin{aligned} &V_0 = 7864\ \text{ft/s} && Q_0 = -0.1\ \text{deg/s} && \delta_{e,0} = 11.5\ \text{deg} \\ &\gamma_0 = 0.2\ \text{deg} && k_1\xi_{1,0} = -1.55\ \text{deg} && \Phi_0 = 0.3 \\ &\theta_0 = 1.2\ \text{deg} && \rho_0 = 6.4\cdot 10^{-5}\,\text{slugs/ft}^3. \end{aligned}$$

The tracking performance for the velocity and FPA is shown in Figs. 4.4a and 4.4b, in which it is seen that even if at $t = 0$ the vehicle is not trimmed and the tracking errors are not zero, the tracking errors remain small and converge asymptotically to zero. Plots of the integrator, angle-of-attack and the prediction of α_r obtained by solving at each step Eq. (4.13) are given in the top part of Fig 4.5a. It is possible to see how, although the general behavior of α_r is captured by Eq. (4.13), due to parametric and model uncertainty, $\lim_{t\to\infty} \alpha(t) \neq \alpha_r$. This emphasizes the necessity of adopting robust techniques, like adaptive control, and the importance of testing the control scheme on the high fidelity model and not only on the model used to design the controller as it is often done in the literature. The bottom part of Fig 4.5a shows how the integrator is capable of reconstructing the steady-state value of the angle-of-attack so that $\lim_{t\to\infty} \xi_1(t) = -\lim_{t\to\infty} \alpha(t)/k_1$ and therefore $\lim_{t\to\infty} \chi_1(t) = 0$ and $\lim_{t\to\infty} \chi_2(t) = 0$. Fig 4.5b shows that the air density remains inside the desirable range and that the flexible modes are damped throughout the maneuver; in particular it is possible to see how the first bending mode is excited when the vehicle is trimming.

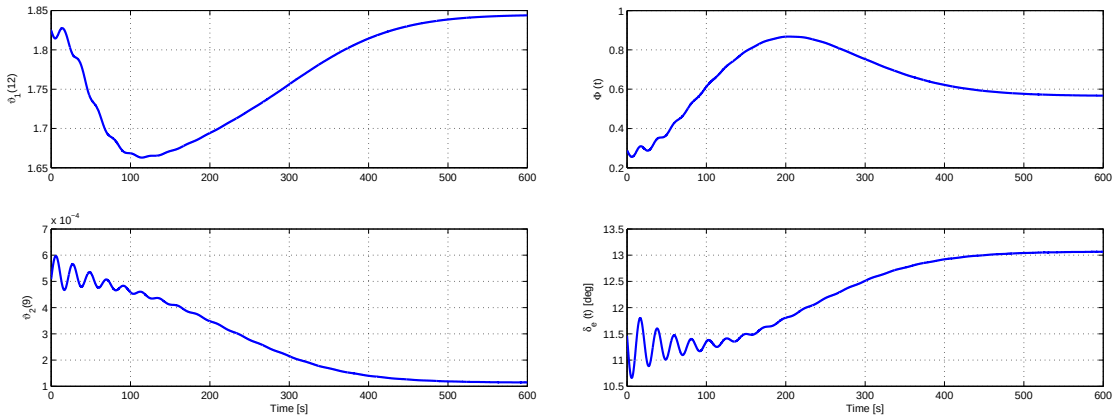

(a) Parameter Estimates (b) Control Inputs

Figure 4.6: Simulation 1: parameter estimates and control inputs.

Two parameter estimates are reported in Fig 4.6a and even though they do not converge to their true values, they are well-behaved and settle to constant values. Finally Fig 4.6b shows that the control inputs range within their bounds and it is possible to see the initial control effort spent to trim the vehicle.

The second case study considers the same initial condition for the velocity and air density, but the vehicle is initially trimmed so the other initial conditions are given as

$$\begin{array}{llllll} \gamma & = & 0 \text{ deg} & Q & = & 0 \text{ deg/s} \qquad \delta_e = 11.3 \text{ deg} \\ \theta & = & 0.97 \text{ deg} & k_1\xi_1 & = & -0.97 \text{ deg} \qquad \Phi = 0.28\,. \end{array}$$

The same reference trajectories, the same gains and initial conditions for the parameter estimates of the previous case study have been considered. To highlight the key role played by the gain k_1, the same simulation has been performed considering also $k_1 = 0.01$ and $k_1 = 0.001$. Fig. 4.7a shows how the velocity tracking error remains remarkably small when the vehicle is initially trimmed. Since the gain k_1 does not affect the velocity subsystem, only the case $k_1 = 0.1$ has been reported here. On the

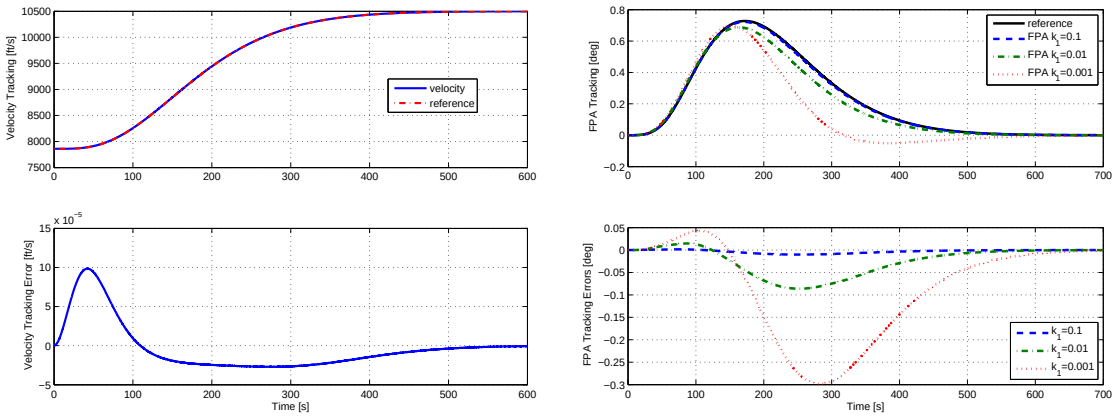

(a) Velocity Tracking and Tracking Error

(b) Flight Path Angle Tracking Varying k_1

Figure 4.7: Simulation 2: Tracking and Tracking Errors.

other hand, Fig. 4.7b shows how the tracking performance for the FPA changes considerably varying the value of k_1. This tells us that there is a trade-off.. For reasons of space limitations the other plots have not been reported here; they are very close to the ones obtained in the previous case study except that they do not exhibit the initial oscillation behavior due to the fact that the vehicle is already trimmed. So we can conclude that the results of the simulations confirm that the controller provides stable tracking of the reference trajectories.

4.6 Conclusions

The second control design has been performed using the control design model CDM2 which is derived from the CDM1 by removing the flexible states, the altitude dynamics and some weak couplings. This control design is referred to as control design with "*reduced control authority*" since the canard deflection is removed from the control suite. Among many challenges encountered in this new framework, one of the most severe is the presence of exponentially unstable zero-dynamics when longitudinal velocity and flight-path angle are selected as regulated output. This non-minimum phase behavior has been counteracted by redefining the internal dynamics of the system. Integral augmentation was necessary to impose the desired equilibrium at trim and the stable adaptation employed by the controller ensures robustness with respect to uncertainty on the model parameters. The proposed approach yields a guaranteed domain of attraction for given ranges of parameter variations.

The important fact highlighted by the stability analysis is that there exists a performance limitation: by removing the canard from the control suite, bounds on the acceleration profile and climbing rate must be imposed whilst in the previous control design arbitrary reference trajectories could be tracked. Those bounds are not too strict, so the main obstacle in the tracking of aggressive manoeuver is still represented by the thermal chocking of the engine.

CHAPTER 5

CONCLUSIONS

In this dissertation, we have presented the design of two nonlinear robust controllers for an air-breathing hypersonic vehicle model capable of providing stable tracking of velocity and altitude (or flight-path angle) reference trajectories. To overcome the analytical intractability of a dynamical model derived from first principles, two simplified control-oriented models have been used for control design.

The first control design considers as control inputs the fuel equivalence ratio and the elevator and canard deflections. Robustness against parameter and dynamic uncertainty is a fundamental issue when adopting a reduced-order or a reduced-complexity model for control systems design. For the hypersonic vehicle model considered in this study, this aspect has been fully addressed by developing an analytical control-oriented model that can be used for both nonlinear control design and quantitative stability analysis. For controller design, we have followed an approach that combines robust adaptive dynamic inversion with backstepping arguments to obtain a control architecture that uses the natural decomposition of the longitudinal vehicle dynamics into velocity, altitude/flight-path angle, and angle-of-attack/pitch rate subsystems.

The important contribution of this work is the complete characterization of the nonlinear internal dynamics of the Bolender and Doman model with respect to velocity, altitude and angle-of-attack as regulated output. The controller uses feedback

from the rigid-body only, but the availability of the internal dynamics has allowed to perform two stability analysis: one on the rigid body only and one on the overall system (rigid body and flexible dynamics). The results of these two analysis are in sharp contrast and in particular it has been highlighted that the interaction of the rigid and flexible dynamics results in conditional stability.

Although beneficial for controllability, the presence of a canard is problematic for the vehicle structure, therefore we decide to tackle the much more challenging problem of controlling the vehicle when the only two available inputs are the fuel equivalence ration and the elevator deflection. The main focus of this work is on counteracting the exponentially non-minimum phase behavior of the rigid-body FPA dynamics. The method reposes upon the redefinition of the internal dynamics of the systems and upon a gain-dependent change of coordinates which enforces a time-scale separation between the controlled variables. Model uncertainties are dealt with by adaptive control and small-gain arguments are employed for stability analysis. The important fact highlighted by the stability analysis is that there exists a performance limitation: by removing the canard from the control suite bounds on the acceleration profile and climbing rate must be imposed whilst in the previous control design arbitrary reference trajectories could be tracked. Those bounds are not too strict, so the main obstacle in the tracking of aggressive manoeuver is still represented by the thermal chocking of the engine.

Simulations, which are performed and the full nonlinear model considering meaningful reference trajectories, validate the proposed methodologies.

Current work is extending the results obtained in the second control design by considering tracking of altitude reference trajectories instead of flight-path angle reference trajectories. It will also be of interest to analyze what happens when flexible

effects are included in the closed loop system stability analysis. Finally, we are currently working on developing a general framework to combine ISS stability arguments with adaptive control.

BIBLIOGRAPHY

[1] M. A. Bolender and D. B. Doman. Flight path angle dynamics of air-breathing hypersonic vehicles. AIAA Paper 2006-6692, 2006.

[2] M. A. Bolender and D. B. Doman. A nonlinear longitudinal dynamical model of an air-breathing hypersonic vehicle. *Journal of Spacecraft and Rockets*, 44(2):374–387, 2007.

[3] H. Buschek and A. J. Calise. Uncertainty modeling and fixed-order controller design for a hypersonic vehicle model. *Journal of Guidance, Control, and Dynamics*, 20(1):42–8, 1997.

[4] F. R. Chavez and D. K. Schmidt. Analytical aeropropulsive/aeroelastic hypersonic-vehicle model with dynamic analysis. *Journal of Guidance, Control, and Dynamics*, 17(6):1308–19, 1994.

[5] F. R. Chavez and D. K. Schmidt. Uncertainty modeling for multivariable-control robustness analysis of elastic high-speed vehicles. *Journal of Guidance, Control, and Dynamics*, 22(1):87–95, 1999.

[6] C.E. Cockrell Jr, W.C. Engelund, R.D. Bittner, T.N. Jentink, A.D. Dilley, and A. Frendi. Integrated Aeropropulsive Computational Fluid Dynamics Methodology for the Hyper-X Flight Experiment. *Journal of Spacecraft and Rockets*, 38(6):836–843, 2001.

[7] J. Davidson, F. Lallman, J. D. McMinn, J. Martin, J. Pahle, M. Stephenson, J. Selmon, and D. Bose. Flight control laws for NASA's Hyper-X research vehicle. AIAA paper 1999-4124, 1999.

[8] W.C. Engelund, S.D. Holland, C.E. Cockrell Jr, and R.D. Bittner. Integrated Aeropropulsive Computational Fluid Dynamics Methodology for the Hyper-X Flight Experiment. *Journal of Spacecraft and Rockets*, 38(6):803–810, 2001.

[9] L. Fiorentini, A. Serrani, M. Bolender, and D. Doman. Nonlinear robust/adaptive controller design for an air-breathing hypersonic vehicle model. AIAA Paper 2007-6329, 2007.

[10] L. Fiorentini, A. Serrani, M. A. Bolender, and D. B. Doman. Robust nonlinear sequential loop closure control design for an air-breathing hypersonic vehicle model. In *Proceedings of the 2008 American Control Conference*, Seattle, WA, 2008.

[11] T. Gibson, L. Crespo, and A. Annaswamy. Adaptive control of hypersonic vehicles in the presence of modeling uncertainties. In *Proceedings of the 2009 American Control Conference*, 2009.

[12] K. P. Groves, A. Serrani, S. Yurkovich, M. A. Bolender, and D. B. Doman. Anti-windup control for an air-breathing hypersonic vehicle model. AIAA Paper 2006-6557, 2006.

[13] K. P. Groves, D. O. Sigthorsson, A. Serrani, S. Yurkovich, M. A. Bolender, and D. B. Doman. Reference command tracking for a linearized model of an air-breathing hypersonic vechicle. AIAA Paper 2005-6144, 2005.

[14] Jennifer Heeg, Michael G. Gilbert, and Anthony S. Pototzky. Active control of aerothermoelastic effects for a conceptual hypersonic aircraft. *Journal of Aircraft*, 30(4):453–458, 1993.

[15] A. Isidori. *Nonlinear Control Systems*. Springer-Verlag, Berlin, Germany, third edition, 1995. pp. 219–241, 293–312.

[16] H. K. Khalil. *Nonlinear systems*. Prentice Hall, Upper Saddle River, N.J., third edition, 2002. pp. 322–325, 534.

[17] M. Krstic, P.V. Kokotovic, and I. Kanellakopoulos. *Nonlinear and Adaptive Control Design*. John Wiley & Sons, Inc., New York, NY, 1995. pp. 489–492, 511–514.

[18] M. Kuipers, M. Mirmirani, P. Ioannou, and Y. Huo. Adaptive control of an aeroelastic airbreathing hypersonic cruise vehicle. AIAA Paper 2007-6326, 2007.

[19] Y. Lei, C. Cao, E. Cliff, N. Hovakimyan, A. Kurdila, and K. Wise. L1 adaptive controller for air-breathing hypersonic vehicle with flexible body dynamics. In *Proceedings of the 2009 American Control Conference*, 2009.

[20] R. Lind. Linear parameter-varying modeling and control of structural dynamics with aerothermoelastic effects. *Journal of Guidance, Control, and Dynamics*, 25(4):733–9, 2002.

[21] R. Lind, J.L. Buffington, and A.K. Sparks. Multi-loop aeroservoelastic control of a hypersonic vehicle. AIAA Paper 1999-4123, 1999.

[22] A. Loria. From feedback to cascade-interconnected systems: Breaking the loop. In *Proceedings of the 47th IEEE Conference on Decision and Control*, pages 4109–14, Cancun, MX, 2008.

[23] C.I. Marrison and R.F. Stengel. Design of robust control systems for a hypersonic aircraft. *Journal of Guidance, Control, and Dynamics*, 21(1):58–63, 1998.

[24] J. McNamara and P. Friedmann. Aeroelastic and aerothermoelastic analysis of hypersonic vehicles: Current status and future trends. AIAA Paper 2007-2013, 2007.

[25] L. Meirovitch. *Analytical Methods in Vibration*. McMillan Publishing Co., New York, 1967. pages 135-143,161-163.

[26] M. Mirmirani, C. Wu, A. Clark, S. Choi, and R. Colgren. Modeling for control of a generic airbreathing hypersonic vehicle. AIAA Paper 2005-6256, 2005.

[27] E. Mooij. Numerical investigation of model reference adaptive control for hypersonic aircraft. *Journal of Guidance, Control, and Dynamics*, 24(2):315–23, 2001.

[28] J. T. Parker, A. Serrani, S. Yurkovich, M. A. Bolender, and D. B. Doman. Control-oriented modeling of an air-breathing hypersonic vehicle. *Journal of Guidance, Control, and Dynamics*, 30(3):856–869, 2007.

[29] J.D. Schierman, D.G. Ward, J.R. Hull, N. Gandhi, M.W. Oppenheimer, and D.B. Doman. Integrated adaptive guidance and control for re-entry vehicles with flight-test results. *Journal of Guidance, Control, and Dynamics*, 27(6):975–88, 2004.

[30] D. K. Schmidt. Dynamics and control of hypersonic aeropropulsive/aeroelastic vehicles. In *AIAA Guidance, Navigation and Control Conference*, Hilton Head, SC, 1992.

[31] D. K. Schmidt. Optimum mission performance and multivariable flight guidance for airbreathing launch vehicles. *Journal of Guidance, Control, and Dynamics*, 20(6):1157–64, 1997.

[32] D. Sigthorsson, P. Jankovsky, A. Serrani, S. Yurkovich, M. A. Bolender, and D. B. Doman. Robust linear output feedback control of an airbreathing hypersonic vehicle. *Journal of Guidance, Control, and Dynamics*, 31(4):1052–1066, JulyAugust 2008.

[33] D. O. Sigthorsson, A. Serrani, S. Yurkovich, M. A. Bolender, and D. B. Doman. Tracking control for an overactuated hypersonic air-breathing vehicle with steady state constraints. AIAA Paper 2006-6558, 2006.

[34] A. R. Teel. A nonlinear small gain theorem for the analysis of control systems with saturation. *IEEE Transactions on Automatic Control*, 41(9):1256–70, 1996.

[35] C. Tournes, D. B. Landrum, Y. Shtessel, and C. W. Hawk. Ramjet-powered reusable launch vehicle control by sliding modes. *Journal of Guidance, Control, and Dynamics*, 21(3):409–15, 1998.

[36] Qian Wang and R.E. Stengel. Robust nonlinear control of a hypersonic aircraft. *Journal of Guidance, Control, and Dynamics*, 23(4):577–85, 2000.

[37] T. Williams, M. A. Bolender, D. B. Doman, and O. Morataya. An aerothermal flexible mode analysis of a hypersonic vehicle. AIAA Paper 2006-6647, 2006.

[38] Haojian Xu, M.D. Mirmirani, and P.A. Ioannou. Adaptive sliding mode control design for a hypersonic flight vehicle. *Journal of Guidance, Control, and Dynamics*, 27(5):829–38, 2004.

Appendix A

VEHICLE PARAMETERS AND COM COEFFICIENTS

A.1 Vehicle Parameters

Symbol	Value	Unit
g	32.17	ft/s^2
I_{yy}	86722.54	slug·ft^2/rad
S	17	ft^2
$\bar{c}$	17	ft
z_T	8.36	ft
ρ_0	6.7429e-5	slugs/ft^3
h_s	21358.8	ft
h_0	85000	ft

Table A.1: Vehicle Parameters

A.2 Curve Fit Model Coefficients

Coefficient	Value	Units	Coefficient	Value	Units
C_L^{α}	5.9598×10^{0}	rad^{-1}	$C_M^{\alpha^2}$	6.8888×10^{0}	rad^{-2}
$C_L^{\delta_e}$	7.3408×10^{-1}	rad^{-1}	C_M^{α}	5.1390×10^{0}	rad^{-1}
$C_L^{\delta_c}$	9.2176×10^{-1}	rad^{-1}	C_M^{0}	1.6277×10^{-1}	
C_L^{0}	-2.4377×10^{-2}		$C_M^{\delta_e}$	-1.3642×10^{0}	rad^{-1}
$C_L^{\eta_1}$	-3.4102×10^{-2}	ft^{-1}	$C_M^{\delta_c}$	2.7326×10^{0}	rad^{-1}
$C_L^{\eta_2}$	-3.1737×10^{-2}	ft^{-1}	$C_M^{\eta_1}$	-7.1776×10^{-3}	ft^{-1}
$C_L^{\eta_3}$	-6.7580×10^{-2}	ft^{-1}	$C_M^{\eta_2}$	-3.0220×10^{-2}	ft^{-1}
$C_D^{\alpha^2}$	7.9641×10^{0}	rad^{-2}	$C_M^{\eta_3}$	-1.0666×10^{-2}	ft^{-1}
C_D^{α}	-7.4020×10^{-2}	rad^{-1}	$C_T^{\Phi\alpha^3}$	-1.4038×10^{1}	rad^{-3}
$C_D^{\delta_e^2}$	9.1021×10^{-1}	rad^{-2}	$C_T^{\Phi\alpha^2}$	-1.5839×10^{0}	rad^{-2}
$C_D^{\delta_e}$	1.0840×10^{-6}	rad^{-1}	$C_T^{\Phi\alpha}$	6.9341×10^{-1}	rad^{-1}
$C_D^{\delta_c^2}$	1.1859×10^{0}	rad^{-2}	C_T^{Φ}	1.9904×10^{-1}	
$C_D^{\delta_c}$	-2.2416×10^{-16}	rad^{-1}	C_T^{3}	1.0929×10^{0}	rad^{-3}
C_D^{0}	-1.9880×10^{-2}		C_T^{2}	9.7141×10^{-1}	rad^{-2}
$C_D^{\eta_1}$	1.2934×10^{-3}	ft^{-1}	C_T^{1}	3.7275×10^{-2}	rad^{-1}
$C_D^{\eta_2}$	2.5523×10^{-4}	ft^{-1}	C_T^{0}	-2.1635×10^{-2}	
$C_D^{\eta_3}$	2.7066×10^{-3}	ft^{-1}	$C_T^{\eta_1}$	-2.7609×10^{-3}	ft^{-1}
			$C_T^{\eta_2}$	-3.4979×10^{-3}	ft^{-1}
			$C_T^{\eta_3}$	-5.3310×10^{-3}	ft^{-1}

Table A.2: Nominal Values of Lift, Drag, Moment and Thrust Coefficients

Coefficient	Value	Units
$N_1^{\alpha^2}$	-8.9274×10^{-2}	$\text{lb} \times \text{ft}^{-1} \times \text{slug}^{-0.5} \times \text{rad}^{-2}$
N_1^{α}	3.4971×10^{-1}	$\text{lb} \times \text{ft}^{-1} \times \text{slug}^{-0.5} \times \text{rad}^{-1}$
N_1^{0}	2.7562×10^{-3}	$\text{lb} \times \text{ft}^{-1} \times \text{slug}^{-0.5}$
$N_1^{\delta_e}$	3.9029×10^{-2}	
$N_1^{\delta_c}$	1.3314×10^{-1}	
$N_1^{\eta_1}$	-9.3415×10^{-4}	
$N_1^{\eta_2}$	-6.7015×10^{-4}	
$N_1^{\eta_3}$	-1.8813×10^{-3}	
$N_2^{\alpha^2}$	8.8374×10^{-2}	$\text{lb} \times \text{ft}^{-1} \times \text{slug}^{-0.5} \times \text{rad}^{-2}$
N_2^{α}	9.5685×10^{-2}	$\text{lb} \times \text{ft}^{-1} \times \text{slug}^{-0.5} \times \text{rad}^{-1}$
N_2^{0}	1.3834×10^{-3}	$\text{lb} \times \text{ft}^{-1} \times \text{slug}^{-0.5}$
$N_2^{\delta_e}$	-2.4875×10^{-2}	
$N_2^{\delta_c}$	8.7965×10^{-2}	
$N_2^{\eta_1}$	4.1120×10^{-4}	
$N_2^{\eta_2}$	1.0924×10^{-4}	
$N_2^{\eta_3}$	8.5621×10^{-4}	
$N_3^{\alpha^2}$	-7.4826×10^{-2}	$\text{lb} \times \text{ft}^{-1} \times \text{slug}^{-0.5} \times \text{rad}^{-2}$
N_3^{α}	1.0299×10^{-1}	$\text{lb} \times \text{ft}^{-1} \times \text{slug}^{-0.5} \times \text{rad}^{-1}$
N_3^{0}	-1.9277×10^{-3}	$\text{lb} \times \text{ft}^{-1} \times \text{slug}^{-0.5}$
$N_3^{\delta_e}$	-4.2624×10^{-3}	
$N_3^{\delta_c}$	7.4550×10^{-2}	
$N_3^{\eta_1}$	3.2963×10^{-4}	
$N_3^{\eta_2}$	3.0022×10^{-4}	
$N_3^{\eta_3}$	6.5423×10^{-4}	

Appendix B

VECTORS AND FUNCTIONS

B.1 Flexible Dynamics Vectors

The expression of the vectors in equation (3.16) are given by

$$\boldsymbol{J}_0 = \begin{bmatrix} 0 \\ \bar{q}S\left[N_1^0 - C_B C_D^0 N_1^{L\delta}\right] - \bar{q}SC_A\left[N_1^{L\delta}C_M^0 - \frac{V_{\text{ref}}}{V}N_1^{M\delta}C_L^0\right] - C_A mg\frac{V_{\text{ref}}}{V}N_1^{M\delta}\cos\gamma - mC_B N_1^{L\delta}\dot{V}_{\text{ref}} \\ 0 \\ \bar{q}S\left[N_2^0 - C_B C_D^0 N_2^{L\delta}\right] - \bar{q}SC_A\left[N_2^{L\delta}C_M^0 - \frac{V_{\text{ref}}}{V}N_2^{M\delta}C_L^0\right] - C_A mg\frac{V_{\text{ref}}}{V}N_2^{M\delta}\cos\gamma - mC_B N_2^{L\delta}\dot{V}_{\text{ref}} \\ 0 \\ \bar{q}S\left[N_3^0 - C_B C_D^0 N_3^{L\delta}\right] - \bar{q}SC_A\left[N_3^{L\delta}C_M^0 - \frac{V_{\text{ref}}}{V}N_3^{M\delta}C_L^0\right] - C_A mg\frac{V_{\text{ref}}}{V}N_3^{M\delta}\cos\gamma - mC_B N_3^{L\delta}\dot{V}_{\text{ref}} \end{bmatrix}$$

$$\boldsymbol{J}_1 = \begin{bmatrix} C_A m V_{\text{ref}} N_1^{M\delta} \\ \bar{q}S\left[N_1^{\alpha} - C_B C_D^{\alpha} N_1^{L\delta}\right] - \bar{q}SC_A\left[N_1^{L\delta}C_M^{\alpha} - \frac{V_{\text{ref}}}{V}N_1^{M\delta}K_{\alpha_2}\right] - C_A m N_1^{M\delta}\left[2\omega_1\zeta_1 V_{\text{ref}} + \dot{V}_{\text{ref}}\right] \\ C_A m V_{\text{ref}} N_2^{M\delta} \\ \bar{q}S\left[N_2^{\alpha} - C_B C_D^{\alpha} N_2^{L\delta}\right] - \bar{q}SC_A\left[N_2^{L\delta}C_M^{\alpha} - \frac{V_{\text{ref}}}{V}N_2^{M\delta}K_{\alpha_2}\right] - C_A m N_2^{M\delta}\left[2\omega_2\zeta_2 V_{\text{ref}} + \dot{V}_{\text{ref}}\right] \\ C_A m V_{\text{ref}} N_3^{M\delta} \\ \bar{q}S\left[N_3^{\alpha} - C_B C_D^{\alpha} N_3^{L\delta}\right] - \bar{q}SC_A\left[N_3^{L\delta}C_M^{\alpha} - \frac{V_{\text{ref}}}{V}N_3^{M\delta}K_{\alpha_2}\right] - C_A m N_3^{M\delta}\left[2\omega_3\zeta_3 V_{\text{ref}} + \dot{V}_{\text{ref}}\right] \end{bmatrix}$$

$$\boldsymbol{J}_2 = \bar{q}S\begin{bmatrix} 0 \\ N_1^{\alpha^2} - C_B C_D^{\alpha^2} N_1^{L\delta} - C_A N_1^{L\delta} C_M^{\alpha^2} \\ 0 \\ N_2^{\alpha^2} - C_B C_D^{\alpha^2} N_2^{L\delta} - C_A N_2^{L\delta} C_M^{\alpha^2} \\ 0 \\ N_3^{\alpha^2} - C_B C_D^{\alpha^2} N_3^{L\delta} - C_A N_3^{L\delta} C_M^{\alpha^2} \end{bmatrix} \qquad \boldsymbol{J}_3 = C_A\begin{bmatrix} \frac{I_{yy}}{\bar{c}}N_1^{L\delta} \\ -mV_{\text{ref}}N_1^{M\delta} - 2\omega_1\zeta_1\frac{I_{yy}}{\bar{c}}N_1^{L\delta} \\ \frac{I_{yy}}{\bar{c}}N_2^{L\delta} \\ -mV_{\text{ref}}N_2^{M\delta} - 2\omega_2\zeta_2\frac{I_{yy}}{\bar{c}}N_2^{L\delta} \\ \frac{I_{yy}}{\bar{c}}N_3^{L\delta} \\ -mV_{\text{ref}}N_3^{M\delta} - 2\omega_3\zeta_3\frac{I_{yy}}{\bar{c}}N_3^{L\delta} \end{bmatrix}$$

$$\boldsymbol{J}_4 = m\,C_B \begin{bmatrix} -N_1^{L\delta} \\ 2\,\omega_1\zeta_1\,N_1^{L\delta} \\ -N_2^{L\delta} \\ 2\,\omega_2\zeta_2\,N_2^{L\delta} \\ -N_3^{L\delta} \\ 2\,\omega_3\zeta_3\,N_3^{L\delta} \end{bmatrix} \qquad \boldsymbol{J}_5 = -mg\,C_B \begin{bmatrix} 0 \\ N_1^{L\delta} \\ 0 \\ N_2^{L\delta} \\ 0 \\ N_3^{L\delta} \end{bmatrix}$$

B.2 Vectors and Functions Defined in the Second Control Design

Eq. (4.6) is obtained by defining the parameter vector ϑ_1 as

$$\vartheta_1 = S\,[C_{T\Phi}^{\alpha^3}, C_{T\Phi}^{\alpha^2}, C_{T\Phi}^{\alpha}, C_{T\Phi}^{0},\, C_T^{\alpha^3}\,,\, C_T^{\alpha^2}\,,\, C_T^{\alpha},\, C_T^{0}, C_D^{\alpha^2}, C_D^{\alpha}, C_D^{0}, m/S]^T$$

and by defining regressors $G_1(x)$ and $F_1(x,\eta_r)$ as

$$G_1(x) = \bar{q}\,\cos\alpha\,[\alpha^3, \alpha^2, \alpha, 1, 0_{1\times 8},]^T$$

$$F_1(x,\eta_r) = [0_{1\times 4}, -\bar{q}\alpha^3\cos\alpha, -\bar{q}\alpha^2\cos\alpha, -\bar{q}\alpha\cos\alpha, -\bar{q}\cos\alpha, \bar{q}\alpha^2, \bar{q}\alpha\,, \bar{q}\,, g\sin\gamma + \dot{V}_r]^T$$

Eq. (4.19) is obtained by defining the parameter vector ϑ_2 as

$$\begin{aligned}\vartheta_2 = [&S\bar{c}C_M^{\delta}/Iyy, SC_L^{\delta}/m, z_T C_{T\Phi}^{\alpha^3}/I_{yy}, z_T C_{T\Phi}^{\alpha^2}/I_{yy}, z_T C_{T\Phi}^{\alpha}/I_{yy}, z_T C_{T\Phi}^{0}/I_{yy}, C_{T\Phi}^{\alpha^3}/m,\\ &C_{T\Phi}^{\alpha^2}/m, C_{T\Phi}^{\alpha}/m, C_{T\Phi}^{0}/m, z_T C_T^{\alpha^3}/I_{yy}, z_T C_T^{\alpha^2}/I_{yy}, z_T C_T^{\alpha}/I_{yy}, z_T C_T^{0}/I_{yy},\\ &C_T^{\alpha^2}/m, C_T^{\alpha}/m, C_T^{0}/m, S\bar{c}C_M^{\alpha^2}/I_{yy}, S\bar{c}C_M^{\alpha}/I_{yy}, C_T^{\alpha^3}/m, S\bar{c}C_M^{0}/I_{yy}, SC_L^{\alpha}/m, sC_L^{0}/m]^T\end{aligned}$$

and by defining regressors $G_2(x)$ and $F_2(x,\Phi)$ as

$$G_2(x) = \bar{q}\,[1, k_1/V, 0_{1\times 21},]^T$$

$$\begin{aligned}F_2(x,\Phi) = [&0_{1\times 2}, \alpha^3\Phi, \alpha^2\Phi, \alpha\Phi, \Phi, \alpha^3\Phi k_1\sin\alpha/V, \alpha^2\Phi k_1\sin\alpha/V, \alpha\Phi k_1\sin\alpha/V,\\ &\Phi k_1\sin\alpha/V, \alpha^3, \alpha^2, \alpha, 1, \alpha^3 k_1\sin\alpha/V, \alpha^2 k_1\sin\alpha/V, \alpha k_1\sin\alpha/V,\\ &k_1\sin\alpha/V, \bar{q}\alpha^2, \bar{q}\alpha, \bar{q}, \bar{q}k_1\alpha/V, \bar{q}k_1/V]^T\end{aligned}$$

$$f_1(x,y_r) := \frac{\rho S V_r}{2\,m}\Bigg[-\bigg(\frac{C_L^\delta C_M^{\alpha^2}}{C_M^\delta}+\bar\mu_2 C_D^{\alpha^2}\bigg)\alpha^2-\bigg(\frac{C_L^\delta C_M^\alpha}{C_M^\delta}+\bar\mu_2 C_D^\alpha - C_L^\alpha\bigg)\alpha + C_L^0$$
$$-\frac{C_L^\delta C_M^0}{C_M^\delta}-\bar\mu_2 C_D^0-\frac{2mg}{\rho S V_r^2}\bigg(\cos\gamma_r+\bar\mu_2\sin\gamma_r\bigg)\Bigg]$$
$$+\frac{T}{mV_r}\Bigg[\sin\alpha-\sin\alpha_r+\frac{\cos\alpha-\cos\alpha_r}{\cos\alpha_r}\bigg(\frac{z_T C_L^\delta}{\bar c\, C_M^\delta}-\sin\alpha_r\bigg)\Bigg]$$

$$f_2(x,y_r,\eta_r) := \dot\mu_2-\bigg(\frac{L+T\sin\alpha-mg\cos\gamma}{mVV_r}\bigg)+\frac{\rho S(\tilde V+2V_r)}{2mV_r}$$
$$\Bigg[-\bigg(\frac{C_L^\delta C_M^{\alpha^2}}{C_M^\delta}+\bar\mu_2 C_D^{\alpha^2}\bigg)\alpha^2-\bigg(\frac{C_L^\delta C_M^\alpha}{C_M^\delta}+\bar\mu_2 C_D^\alpha - C_L^\alpha\bigg)\alpha$$
$$+C_L^0-\frac{C_L^\delta C_M^0}{C_M^\delta}-\bar\mu_2 C_D^0\Bigg]$$

$$\Lambda_2(x,y_r)\tilde\gamma := -\frac{g}{V_r}\big[\cos\gamma-\cos\gamma_r+\bar\mu_2(\sin\gamma-\sin\gamma_r)\big]$$